Friedrich-Schiedel Institut für Neurowissenschaften

Technische Universität München

Quantitative single-cell RT-PCR analysis of the TRPC channel subunits expression patterns in cerebellar Purkinje neurons

Elena Dragicevic

Vollständiger Abdruck der von der Fakultät für Medizin der Technischen Universität München zur Erlangung des akademischen Grades eines

Doctor of Philosophy (Ph.D.)

genehmigten Dissertation.

Vorsitzender: apl. Prof. Dr. Helmuth Adelsberger

Prüfer der Dissertation:

1. Univ.-Prof. Dr. Arthur Konnerth
2. Univ.-Prof. Dr. Michael Schemann

Die Dissertation wurde am 20.12.2007 beim Studienausschuss des Ph.D. Studiengangs Medical Life Science and Technology an der Fakultät für Medizin der Technischen Universität München eingereicht und durch die Fakultät für Medizin am 31.03.2008 angenommen.

Table of Contents

Glossary:

AMPA	α-amino-3-hydroxy-5-methyl-4-isoxazolepropionic acid
AMPA-R	AMPA receptor
ATP	adenosine triphosphate
BDNF	brain-derived neurotrophic factor
bp	base pair
°C	degree Centigrade
c-	centi-
Ca^{2+}	calcium ions
cDNA	complementary DNA
DAG	diacylglycerol
dATP	2'-deoxyadenosine 5'-triphosphate
dCTP	2'-deoxycytidine 5'-triphosphate
dGTP	2'-deoxyguanosine 5'-triphosphate
DNA	deoxyribonucleic acid
DNase	deoxyribonuclease
dNTP	2´- Deoxyribonucleotide -5´-triphosphate
ds	double stranded
DTT	dithiothreitol
dTTP	2'-deoxythymidine 5'-triphosphate
E.coli	*Escherichia Coli*
EDTA	ethylenediaminetetraacetic acid
for	forward (primer)
FSGS	focal segmental glomerulosclerosis
g	gram
X g	acceleration of gravity
GABA	gamma-aminobutyric acid
GAPDH	glyceraldehyde-3-phosphate dehydrogenase
GluR	glutamate receptor
h	hour
H_2O	water
I	current
EPSC	mGluR dependent current
IP_3	inositol triphosphate
IP_3R	IP_3 receptor
K^+	potassium ions
l	liter
LB	Luria-Bertani broth
LTD	long term depression

µ	micro
-m	meter
m-	milli
-M	molar solution
min	minute
M-MLV	*Moloney murine leukemia virus*
mRNA	messenger RNA
Mw	molecular weight
n-	nano
Na^+	sodium ions
NMDA	N-Methyl-D-Aspartate
OAG	oleylacetyl glycerol
OD	optical density
OD_{260}	optical density at 260nm
p-	pico
PAM	point accepted mutation
PCR	polymerase chain reaction
pH	inverse logarithmic representation of proton concentration
PIP_2	phosphatidylinositol 4,5-bisphosphate
PLC	phospholipase C
rev	reverse (primer)
RNA	ribonucleic acid
RNase	ribonuclease
RNasin	inhibitor of ribonucleases
rpm	rounds per minute (centrifugation)
RT	reverse transcription
RT-PCR	reverse transcription-polymerase chain reaction
s	second
SMOC	second messenger-operated channel
SOCE	store operated calcium entry
ss	single stranded
T	temperature
t	time
TAE	Tris/Acetate buffer
Taq	*Thermus Aquaticus* (DNA polymerase)
TBE	Tris/Boric acid buffer
Tris	Tris-(hydroxymethyl)-aminomethan
TRP	transient receptor potential (channel)
U	units; uracil
UV	ultra violet
V	volt
v/v	volume per volume ratio
VNO	vomeronasal organ
w/v	weight per volume ratio

Abbreviations for the DNA/RNA base pairs:

Base	Code
adenine	A
cytosine	C
guanine	G
thymine	T
uracil	U

Abbreviations for the amino acids:

Amino acid	Code	Amino acid	Code
alanine	A	leucine	L
arginine	R	lysine	K
asparagine	N	methionine	M
aspartic acid	D	phenylalanine	F
cysteine	C	proline	P
glutamic acid	E	serine	S
glutamine	Q	threonine	T
glycine	G	tryptophan	W
histidine	H	tyrosine	Y
isoleucine	I	valine	V

1. Introduction

The cerebellum has an essential role in motor coordination, implicit learning of automated movements, timing of conditioned reflexes as well as the acquirement of a number of cognitive skills which is thought to be critical for the formation of motor learning. Purkinje neurons as one of the cerebellar cell types play a major role in the cerebellar signaling machinery. Specific receptor expressed in these neurons, mGluR1, is crucial for cerebellar function and mice lacking this receptor suffer from ataxia and also completely lack cerebellar long term depression (LTD). Recently, a group of diverse and evolutionary conserved ion channels, called classical transient receptor potential (TRPC) channels were implicated into Purkinje neurons receptor signaling through mGluR1 receptor. TRPC channel family members have a crucial role in sensory physiology and they take part in neurite outgrowth and receptor signaling in the central nervous system. But their exact role in Purkinje neurons still remains a mystery. This study gives an insight in the quantitative expression pattern of TRPC channels in Purkinje neurons, which could indicate the functional role of TRPC channels in these cells.

1.1 The TRPC channel family

Transient receptor potential (TRP) channels were first described in *Drosophila melanogaster*, where photoreceptors carrying TRP gene mutations exhibited a transient voltage response to continuous light (Minke, 1977; Montell et al., 1985). Unlike most ion channels, TRP channels were rather identified by their sequence homology than by ligand function or selectivity, because their functions are disparate and often unknown (Clapham, 2003). The TRP superfamily is divided into seven subfamilies which are further divided into two groups (Venkatachalam and Montell, 2007). The group 1 consists of five subfamilies: “classical” TRPs or the TRPCs; “vanilloid” TRPs or TRPVs, which respond to heat, changes in osmolarity, odorants and mechanical stimuli; “melastatin” TRPs or TRPMs, which are involved in sensory perception and can form chanzymes; TRPN subfamily proteins which function in mechanotransduction, and TRPA subfamily proteins activated by noxious cold and required for the auditory response. The group 2 of TRP channel superfamily is composed of TRPP and TRPML subfamilies, which are only distantly related to the group 1 of TRP superfamily (Montell, 2005).

Like other members of the TRP superfamily, TRPC channel family members have a crucial role in sensory physiology. Not only do TRPC family members provide

information about the extracellular environment, but they enable cells to sense and respond to changes in their local, cellular environment (Venkatachalam and Montell, 2007). In the central nervous system, TRPC channels participate in neurite outgrowth and receptor signaling (Moran et al., 2004). TRPC1 and TRPC3 have been implicated in growth cone guidance by brain-derived neurotropfic factor (BDNF) (Li et al., 1999; Li et al., 2005; Shim et al., 2005; Wang and Poo, 2005). TRPC5 was found to operate in neurite extension (Greka et al., 2003). TRPC1 was proposed to mediate the excitatory role on mGluR1 metabotropic receptors (Kim et al., 2003). TRPC4 was connected to the inhibitory neurotransmitter GABA release from the dendrites of the thalamic interneurons (Munsch et al., 2003). Recently TRPC channels have been increasingly involved with pathological conditions and diseases, like a kidney disorder focal and segmental glomerulosclerosis (FSGS) (Reiser et al., 2005; Winn et al., 2005) and elevated blood pressure (Dietrich et al., 2005).

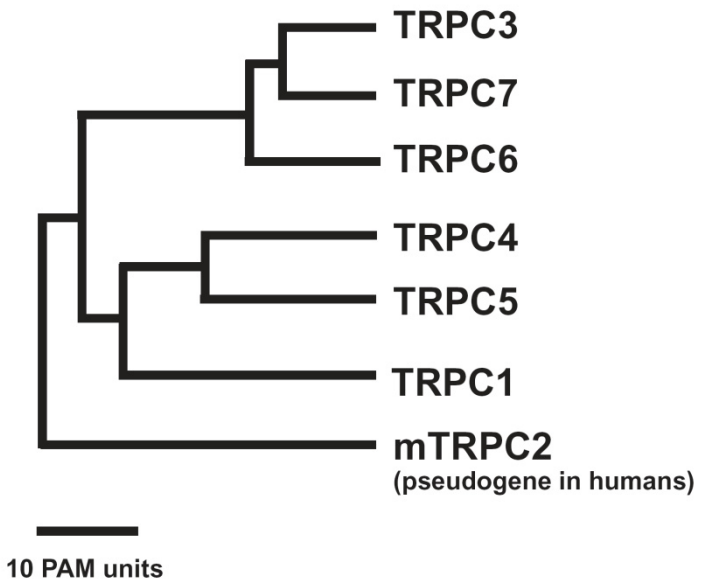

Figure 1.1 TRPC channel family phylogenetic tree. The evolutionary distance is shown by the total branch lengths in point accepted mutation (PAM) units, which is the mean number of substitutions per 100 residues (adapted from (Clapham et al., 2001; Putney, 2004)).

The TRPC family, with seven members (TRPC1 to TRPC7), is the TRP family most closely related to the original *Drosophila* channel (Vazquez et al., 2004). TRPC1, TRPC2 and TRPC3 were the first to be identified (Wes et al., 1995; Zhu et al., 1995), and since then, seven mammalian TRPC proteins have been cloned (Montell et al., 2002). The TRPC channel family can be further subdivided into four different subfamilies consisting of TRPC1, TRPC2, TRPC3, 6, and 7 and TRPC4 and 5, respectively, who share a high

degree of homology (see Figure 1.1). TRPC2 is a pseudogene in humans, and in old world monkeys and apes (Liman and Innan, 2003), but apparently forms fully regulated channels in other mammalian species. TRPC3, 6 and 7 form a closely related subfamily, sharing a high degree of amino acid identity (70-80%) and functional, regulatory and pharmacological similarities. TRPC4 and 5 also share a similar structural and functional relationship (Vazquez et al., 2004)

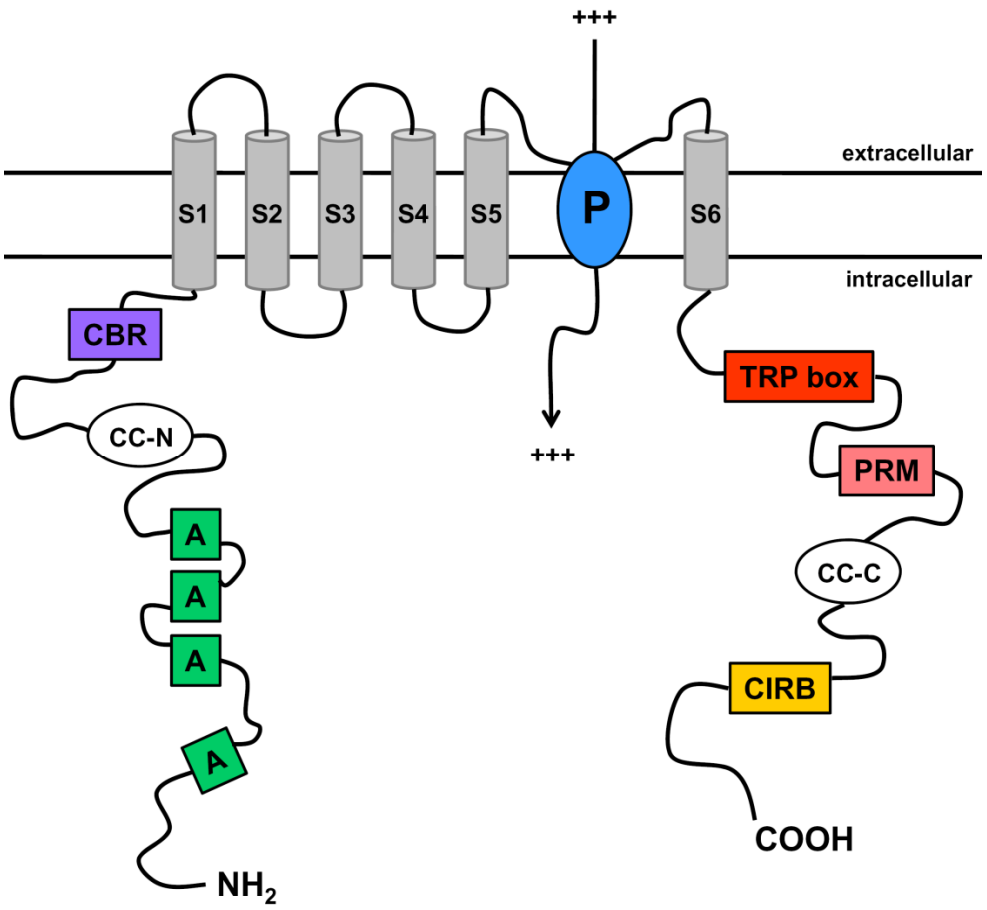

Figure 1.2 Structure of TRPC channel family proteins. Detailed structural characteristics and interaction domains are explained in the text. **abbreviations**: A – ankyrin-like domains (green); CC-N – N-terminal coiled-coil region (white); CBR – caveolin binding region (violet); S1-S6 – transmembrane domains (grey); P – putative pore (blue); TRP box - the EWKFAR sequence in TRPCs (red); PRM – proline rich motif (pink), CC-C – C-terminal coiled-coil region (white) and CIRB – calmodulin/IP_3 receptor binding region (yellow). (figure was adapted from (Vannier et al., 1998; Clapham, 2003; Putney, 2004; Venkatachalam and Montell, 2007)).

TRPC family members are believed to have a common topology (Vannier et al., 1998). The primary structure of TRPC channel proteins shows the presence of six transmembrane domains (S1-S6), with both N- and C-termini located intracellularly (see Figure 1.2). Transmembrane segments S5 and S6 are thought to form the putative pore

(Vannier et al., 1998). The N-terminus of TRPC proteins is composed of three to four ankyrin-like repeats, a predicted coiled-coil region and a putative caveolin binding region. The cytoplasmic C-terminus includes the so called TRP domain, a highly conserved proline rich motif, the CIRB (calmodulin/IP_3 receptor binding) region and a predicted coiled-coil region. TRPC4 and TRPC5 have a unique extended C-terminus, ending with PDZ binding domain (Vazquez et al., 2004). The coiled-coil (CC) is a ubiquitous protein motif with the common function to control oligomerization, and is present in TRPC proteins at each N- and C-terminus (CC-N and CC-C). This arrangement of CC motifs in TRPC protein structure suggests their possible involvement in homo- and heteromerization of different TRPC subunits to form ion channel tetramers, or to link TRPCs to other coiled domain containing proteins. The TRP box is a highly conserved sequence present in all TRP superfamily members. In TRPCs, TRP box is represented with EWKFAR sequence. Downstream of the highly conserved TRP box motif on the C-terminus of TRPCs, a proline-rich motif (LPXPFXXXPSPK) is located. This motif is conserved in all TRPCs and it has been shown that it is responsible for interaction of TRPC1 with Homer, a protein reported to interact with metabotropic receptors and IP_3 receptor (Yuan et al., 2003). PDZ binding motif is specific for TRPC4 and TRPC5, and it seems to be responsible for the interaction with an adapter protein possibly linking the channels to phospholipase Cß (PLCβ) and the cytoskeleton (Tang et al., 2000).

TRPC channels are thought to be formed by the combination of four TRPC subunits, similarly to voltage-gated K^+ channels (Villereal, 2006). Thus, TRPC channels could be formed as homo - or heterotetramers (Putney, 2004). There are no specific rules for TRPC subunit interaction in heteromeric channel formation, but certain published studies investigated in a systematic way the combinatory rules for TRPC channel subunit assembly (Goel et al., 2002; Hofmann et al., 2002), (Goel et al., 2002). These studies concluded that TRPC2 does not interact with other TRPC subunits, that TRPC1 can interact with TRPC4 or TRPC5, and that TRPC3/6/7 subfamily members only interact with each other. Nevertheless, many studies reported heteromeric TRPC channel formation that did not follow the above stated rules (Xu et al., 1997; Lintschinger et al., 2000; Strubing et al., 2003; Zagranichnaya et al., 2005; Poteser et al., 2006). When TRPC channels form heteromultimers, the properties of the novel channels were usually found to be different from the homomeric channels. This has been demonstrated for the TRPC1-TRPC3 (Lintschinger et al., 2000), TRPC1-TRPC4 (Strubing et al., 2003) and TRPC1-TRPC5 (Strubing et al., 2001, 2003; Xu et al., 2006) heteromultimeric channels. With such a variety of combinations between different TRPC proteins an incredible diversity of

channels with an array of distinct biophysical properties and biological functions can be expected.

TRPC channels like all TRP channels are nonselective cation channels, with $P_{Ca}/P_{Na} \leq 10$. They depolarize cells and raise intracellular Ca^{2+} and/or Na^{+} (Clapham et al., 2003). While there is general consensus that all TRPC channels are activated by PLC-coupled receptors, there is considerable conflict regarding their exact mode of activation (Ambudkar et al., 2006). Activation of cell surface receptors which are coupled to inositol lipid signaling, results in phosphatidylinositol 4,5-bisphosphate (PIP_2) hydrolysis by the PLC, generation of diacylglycerol (DAG) and inositol triphosphate (IP_3), release of Ca^{2+} from internal Ca^{2+} stores, and activation of plasma membrane Ca^{2+} influx channels. Agonist-generated signals can activate two major types of Ca^{2+} entry (see Figure 1.3). The first type is "store-operated" Ca^{2+} entry (SOCE), which is regulated by the depletion of Ca^{2+} from internal Ca^{2+} stores. Three main models of SOCE activation have been proposed: (i) IP_3 receptor and the plasma membrane Ca^{2+} channel direct physical interaction; (ii) a diffusible factor released during or in response to Ca^{2+} store depletion and, (iii) channel recruitment to the plasma membrane by regulated vesicle trafficking. The second type is the Ca^{2+} entry through "second messenger-operated" channels (SMOC), which are most likely activated directly by DAG or by PIP_2 hydrolysis per se (Putney et al., 2001; Venkatachalam et al., 2001; Bird et al., 2004; Putney, 2005; Ambudkar, 2006). TRPC1, TRPC4 and TRPC5 have usually been reported to be store-operated Ca^{2+} channels, while TRPC3, TRPC6 and TRPC7 are generally thought to be store-independent (see Figure 1.3).

TRPC1 has consistently been the strongest candidate for the store-operated channel activation. Several studies in different cell types, including salivary gland (Liu et al., 2000; Singh et al., 2001), DT40 cells (Mori et al., 2002), platelets, smooth muscle and endothelial cells (Beech et al., 2003), reported convincing evidence that TRPC1 is indeed a SOC channel. Nevertheless, contradictory findings have also been reported, stating that heterologously expressed TRPC1 channel activation is store-independent (Venkatachalam et al., 2001; Beech et al., 2003; Montell, 2005; Pedersen et al., 2005). TRPC4 and TRPC5 are closely related TRPC channel family members, and have shown similar ways of activation. Conflicting reports exist about the modes of activation of these two TRPC subunits. TRPC4 is suggested to be a component of SOC. While other studies show that TRPC4, like TRPC5 is constitutively active. TRPC5 modes of regulation have been reported to be both store-dependent and independent. For the TRPC3/6/7 subfamily, the vast majority of published results suggest that DAG, produced upon PLC activation, is the signal activating these channels (Hofmann et al., 1999; Okada et al.,

1999; Lintschinger et al., 2000; Trebak et al., 2003; Venkatachalam et al., 2003). It has been reported that endogenous TRPC3 contributes to heteromeric store-operated Ca^{2+} channels in HEK-293 (Zagranichnaya et al., 2005), HSY (Liu et al., 2005) and neuronal cells (Wu et al., 2004). The store-dependent regulation of TRPC3 has been suggested to be dependent on the level of channel expression. When expressed in high levels, TRPC3 seems to be able to form spontaneously activated channels (Putney, 2004). Also, it has been shown, that TRPC3 can be activated by oleylacetylglycerol (OAG) but not by thapsigargin (SERCA pump blocker). This suggests that TRPC3 is not regulated by store depletion (Venkatachalam et al., 2003; Liu et al., 2005). Less is known about TRPC7 activation, although both store-dependent and independent mechanisms of activation have been reported (Zagranichnaya et al., 2005).

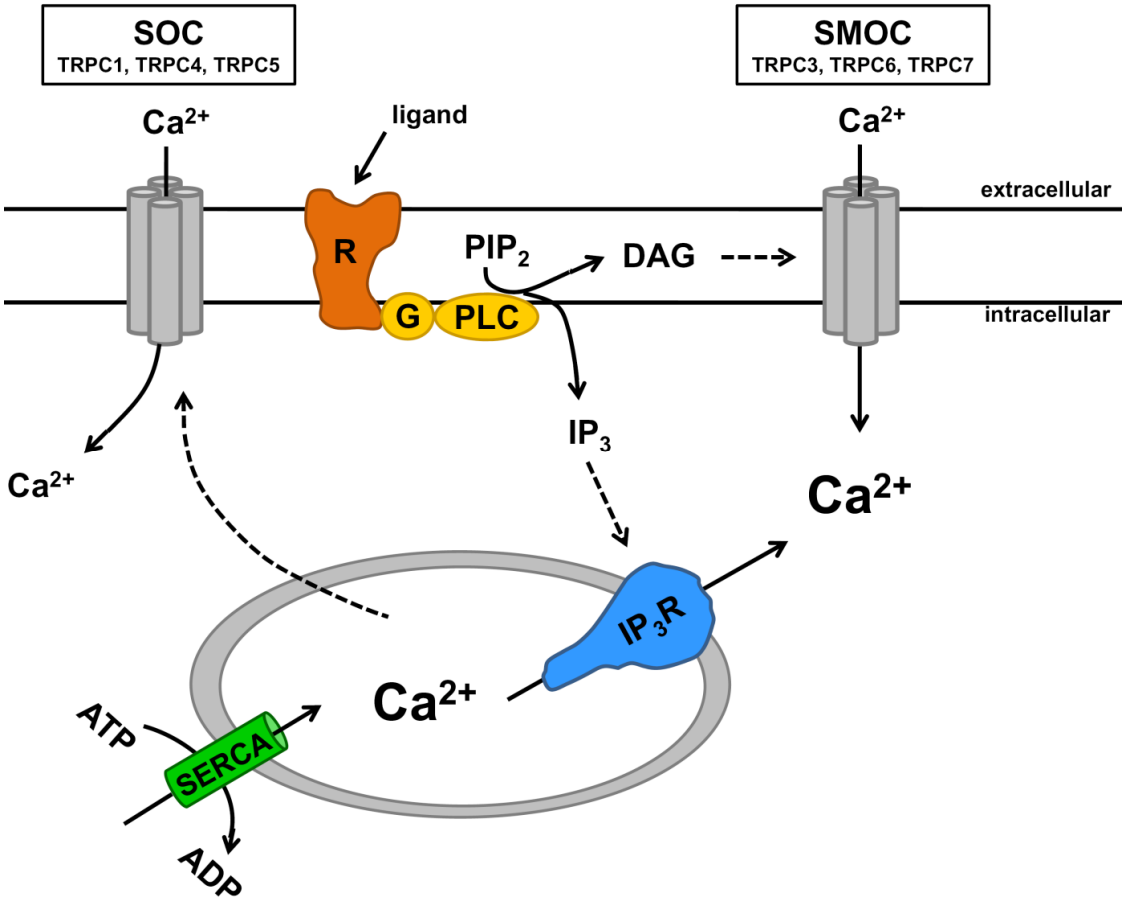

Figure 1.3 Possible models of TRPC channel functional regulation. Detailed explanation of the TRPC activation mechanisms can be found in the text. (adapted from (Putney, 2004; Ambudkar et al., 2006)).

TRPC channel family members are widely expressed. TRPC1 was found to be expressed in brain, heart, kidneys, endothelium, ovaries, testis and in smooth muscle cells (Freichel et al., 2004a; Freichel et al., 2004b; Inoue et al., 2004; Montell, 2005). TRPC2 is a pseudo gene in humans, while it is a functional gene in rodents where it is expressed in vomeronasal organ (VNO) and possibly in the testis (Vannier et al., 1999; Jungnickel et al., 2001). TRPC3 RNA has been shown to be enriched in the adult human brain (Zhu et al., 1996) but another study showed that in rats the TRPC3 protein is predominantly expressed in the brain during a relatively narrow developmental period before and after birth (Strubing et al., 2003). Based on results from RT-PCR studies TRPC3 might also be expressed in smooth muscle cells and endothelial cells from blood vessels (Freichel et al., 1999; Inoue et al., 2001; Beech et al., 2004; Inoue et al., 2004). TRPC4 was reported to be expressed in brain, endothelium, kidney, retina, testis and adrenal gland and TRPC5 was predominantly expressed in the brain (Freichel et al., 2004a; Montell, 2005). TRPC5 transcripts and proteins have been shown to be abundantly present in hippocampal neurons (Greka et al., 2003). TRPC6 expression has been reported in the lung, the brain (Montell, 2005) and in smooth muscle cells (Yu et al., 2004). Expression of the TRPC6 protein in glomerular podocytes was demonstrated by immunostaining (Pavenstadt et al., 2003).

TRPC channel family members were found to be expressed and widely distributed in the mammalian brain (Moran et al., 2004), but not many quantitative studies were performed on TRPC transcripts or proteins.

1.2 TRPC channels in cerebellar Purkinje neurons

The cerebellum has an essential role in motor coordination, implicit learning of automated movements, timing of conditioned reflexes as well as the acquirement of a number of cognitive skills (Ito, 2002). The cerebellum receives information from many brain areas through direct or indirect inputs. Purkinje neurons receive the entire cerebellar activity through thousands of synapses located on their enormously large dendritic trees. Purkinje neurons receive two types of excitatory synapses. The first comes from the granule cell axons, the so-called parallel fibers, which form at least 100 000 weaker synapses onto Purkinje neuron dendrites. And the second, from climbing fibers, originating in the inferior olive, with each forming a powerful synaptic input involving hundreds of synapses (Ito, 2002). Repeated stimulation of both inputs at low frequencies causes a further long-lasting weakening of synaptic transmission at the parallel fibers.

This phenomenon is called cerebellar long term depression, or cerebellar LTD, which is thought to be critical for the formation of motor learning (Ito, 2002).

Glutamatergic synaptic transmission at parallel fiber synapses, where LTD is expressed postsynaptically, is mediated exclusively by the AMPA-receptors and metabotropic glutamate receptors of the mGluR1 subtype. MGluR1 is crucial for cerebellar function and mice lacking this receptor suffer from ataxia and also completely lack cerebellar LTD. Purkinje neurons express high levels of the metabotropic glutamate receptor (mGluR) of the subtype mGluR1. Together with mGluR5, this subtype constitutes the group I mGluRs. MGluRs are implicated in many forms of neural plasticity including cerebellar long-term depression (Linden et al., 1991; Aiba et al., 1994; Conquet et al., 1994). MGluR-dependent Ca^{2+} release in spines and dendrites of Purkinje cells can be synaptically evoked by burst stimulation of parallel fibers (Takechi et al., 1998). Activation of mGluR1 is followed by slow synaptic transmission, which consists of the release of Ca^{2+} ions from intracellular Ca^{2+} stores through IP_3 receptors, and activation of a slow excitatory postsynaptic current (EPSC) (Batchelor et al., 1997; Tempia et al., 1998; Tempia et al., 2001). The coupling between mGluR1 and PLCβ occurs mainly through $G\alpha_q$ proteins, G protein members of the Gq family (Hartmann et al., 2004). After mGluR1 activation, $G\alpha_q$ coupled PLCβ cleaves the membrane PIP_2 to yield DAG and IP_3. This results in both Ca^{2+} mobilization through a PLCβ–IP_3 cascade and activation of a slow excitatory postsynaptic current (EPSC) carried by a mixed cation conductance (see Figure 1.4).

The ion channel underlying the slow EPSC has not been identified in Purkinje cells or in any other cell type. However, a number of observations exist that constrain the identity of the ion channel underlying this slow current. EPSC is a mixed-cation conductance that reverses at about +20mV (Knopfel et al., 2000; Canepari et al., 2001; Tempia et al., 2001), and requires the presence of external Ca^{2+} (Tempia et al., 2001; Tabata et al., 2002). This current is also not blocked by antagonists of Na^+/Ca^{2+} exchangers, purinergic receptors, hyperpolarization-activated cation channels or voltage-gated Ca^{2+} channels (Hirono et al., 1998; Canepari et al., 2001; Tempia et al., 2001). At glutamatergic synapses group I mGluRs form interactions with scaffolding molecules. The most important of these molecules are the Homer family proteins, which form multimers capable of regulating coupling of group I mGluRs to a number of targets including IP_3 receptors, ryanodine receptor and voltage-gated Ca^{2+} channels (Xiao et al., 2000). It has also been reported that Homer binds and regulates the gating of members of the TRPC family of nonspecific cation channels (Yuan et al., 2003).

Due to their physiological properties and expression patterns, TRPC channels have become the most likely candidates for the ion channels conducting the slow EPSC in the Purkinje neurons. It has, indeed, been reported that the mGluR1-evoked slow postsynaptic current (EPSC) is mediated by the TRPC1 cation channel (Kim et al., 2003).

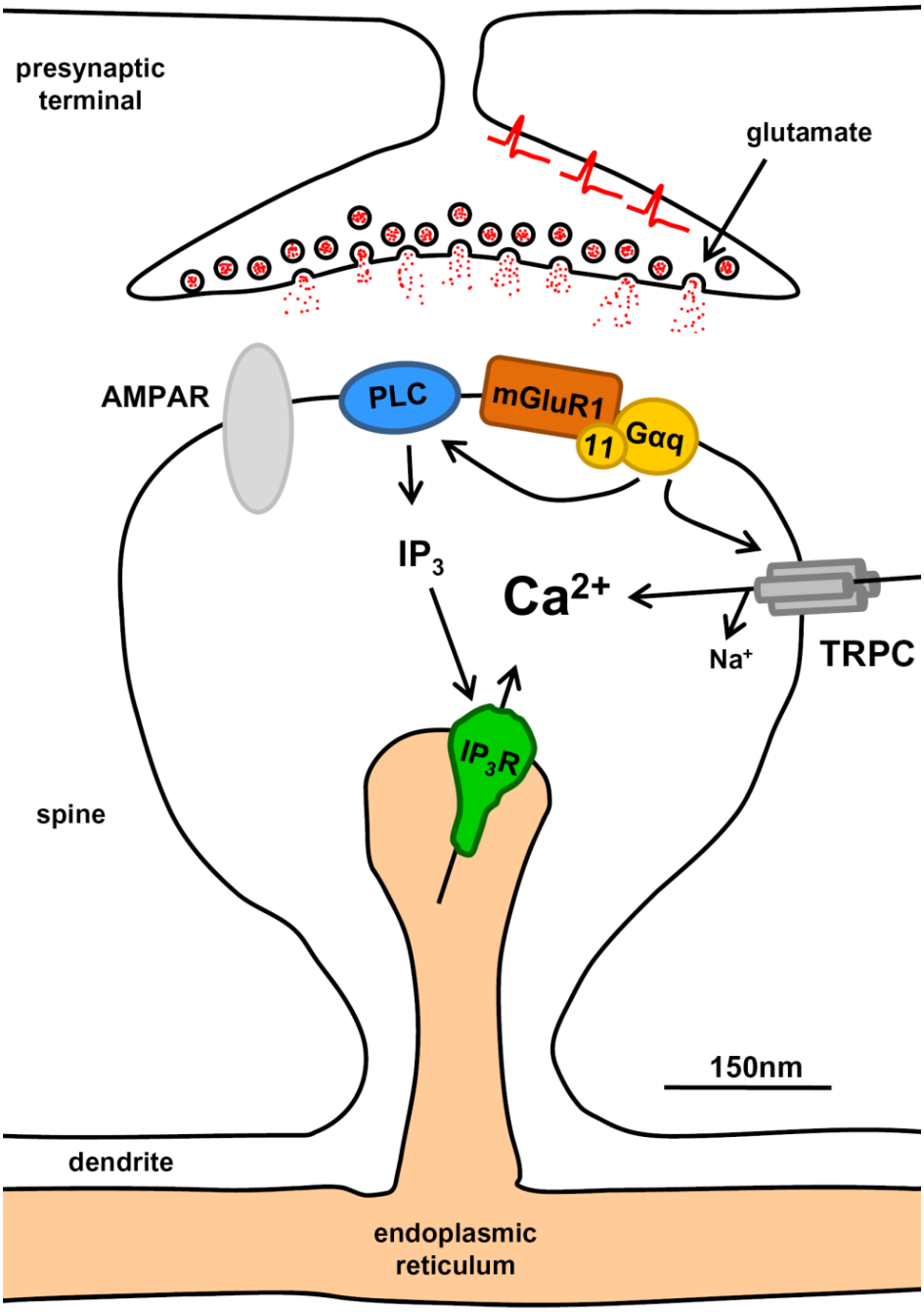

Figure 1.4 TRPC channel activation in Purkinje cell dendrites. Detailed explanation of TRPC channel activation mechanism can be found in the text (adapted from (Hartmann and Konnerth, 2005)).

TRPC1 was found to be expressed in perisynaptic regions of the cerebellar parallel fibre–Purkinje cell synapse and has been shown that it is physically associated with mGluR1. In the same study, manipulations were made on TRPC1 protein, by substituting phenylalanine residue at position 561 of the primary structure, with alanine residue (TRPC1/F561A). These manipulations on the TRPC1 have been shown to block the mGluR1-evoked slow current in Purkinje cells, with no affect on fast transmission mediated by AMPA-type glutamate receptors. Furthermore, co-expression of mGluR1 and TRPC1 in a heterologous system reconstituted a mGluR1-evoked conductance that closely resembles the slow EPSC in Purkinje cells (Kim et al., 2003). Nevertheless, another study described the EPSC mediated by TRPC1 to be different from heterologously expressed TRPC1 channels concerning single channel conductance and pharmacological properties (Canepari et al., 2004), indicating that the native channel could be a heteromultimer containing TRPC1.

Interestingly, the results obtained on the TRPC1 knockout mouse by Hartmann et al. (2008, in press), show conflicting evidence of the role of TRPC channels in Purkinje neurons than the previous study. Hartmann et al. have found the presence of the above mentioned slow EPSC in the TRPC1 knockout mice. In these mice, the TRPC1 gene was inactivated using gene targeting in murine embryonic stem cells. Exon 8 of TRPC1 gene was deleted, which resulted in loss of the coding region for amino acids 584–670 that form transmembrane segments 4 and 5 and a small part of the putative pore domain (Dietrich et al., 2007). This fact raised a question if any other TRPC subunit, present in Purkinje neurons, was involved in the mediation of the slow EPSC in the Purkinje neurons. The expression pattern of TRPC subunits in the Purkinje neurons was not known to date.

1.3 Quantitative single-cell RT-PCR

Quantitative single-cell RT-PCR is a technique widely used for quantitative investigations of cell type-specific gene expression patterns. The first successful amplification of specific RNA transcripts was performed on Purkinje cells (Lambolez et al., 1992). This technique was a breakthrough discovery after which many protocols were established for quantitative single-cell expression analysis (Geiger et al., 1995; Chow et al., 1998; Liss et al., 2001; Tsuzuki et al., 2001; Liss, 2002; Durand et al., 2006).

No study up to date presented any quantitative RT-PCR data on the expression levels of TRPC1-7 subunits in the cerebellar Purkinje cells or any other central neuron for that matter. In order to profile the expression pattern of TRPC family subunits in Purkinje

neurons, quantitative single-cell RT-PCR technique, established in our group was used (Hartmann et al., 2004; Durand et al., 2006). Our method is fluorescence based real-time quantitative RT-PCR done by using the LightCycler™ technology and chemistry (Roche, Mannheim). Experimental procedure consisted of several steps (see Figure 1.5), (Durand et al., 2006). After the harvest of single Purkinje neuron somata, reverse transcription reaction using N_6 random primers, followed. Synthesized cDNA was then purified and real-time PCR amplification was performed using the LightCycler™ (Roche). After the amplification step, quantification was performed by using gene-specific standard curves (see 3.5). This method has the sensitivity to quantify even a single DNA template molecule and is highly reproducible.

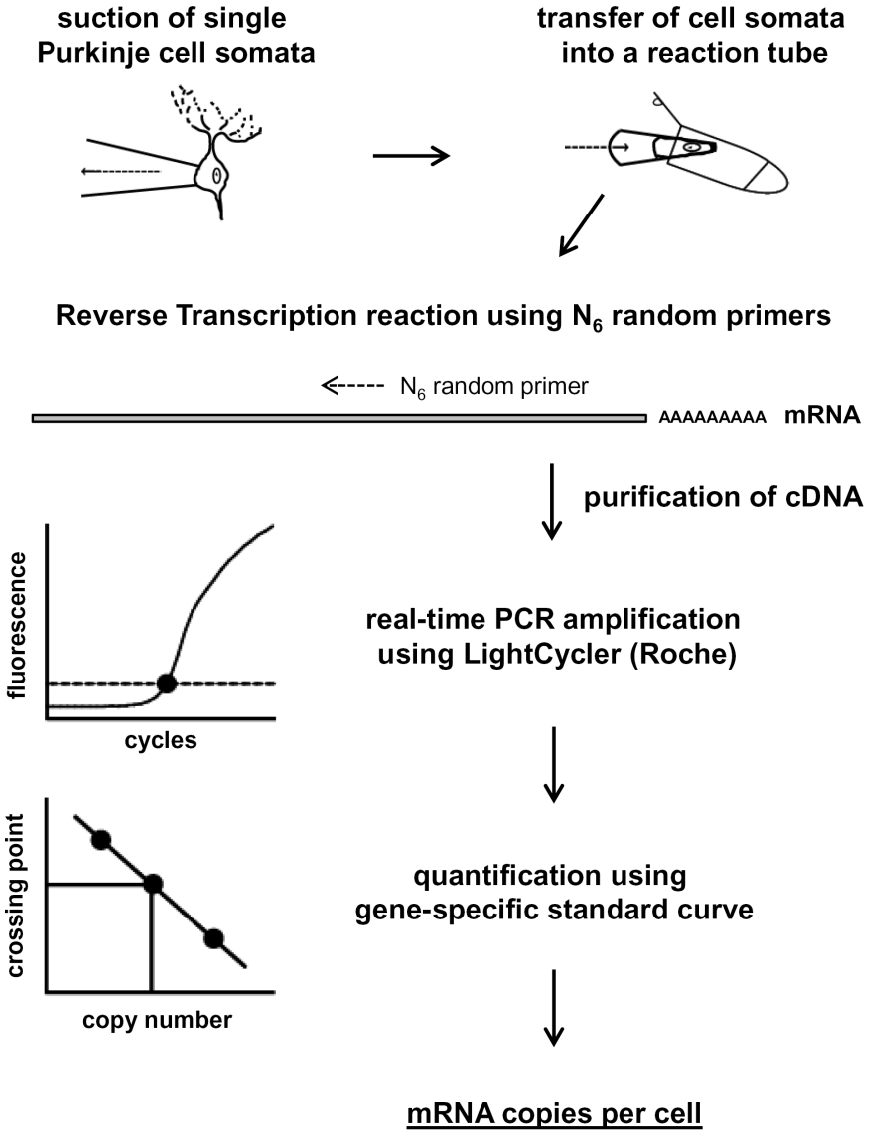

Figure 1.5 Scheme of the quantitative single Purkinje cell RT-PCR procedure
Scheme explanation can be found in the text. (adapted from (Durand et al., 2006).

1.4 Experimental goals

The main goal of this study was to describe the expression profile of TRPC channel subunits in the mouse brain, with the emphasis on cerebellar Purkinje cells.

This was the first attempt up to date to quantify the expression levels of TRPC channels in Purkinje cells by using single-cell quantitative RT-PCR. Specific experimental goals in this study were:

- to design specific primers for TRPC1-7 subunits and use them to create highly reproducible and sensitive quantitative RT-PCR assays. TRPC2 subunit was not taken into consideration in this study, since TRPC2 was reported to be expressed only in the vomeronasal organ (VNO) and possibly in the testis (Vannier et al., 1999; Jungnickel et al., 2001; Kimchi et al., 2007).

- to construct high-resolution external standard curves specific for all TRPC1-7 subunits transcripts and to test and compare their efficiency in the native material

- to quantify the expression pattern of TRPC subunits in the whole brain and cerebellum

- to quantify the expression pattern of TRPC subunits in the single Purkinje cells of the wild type and TRPC1 knockout animals.

2. Materials and Methods

2.1 Materials

2.1.1 Chemicals

The chemicals used for the experimental work were ordered from the following companies: Roche (Mannheim), Carl Roth (Karlsruhe), DeltaSelect (Dreieich), Difco (Detroit, MI), Fluka Biochemika (Buchs Switzerland), Gibco BRL (division of Invitrogen), Invitrogen (Karlsruhe), Merck (Darmstadt), Serva (Heidelberg) and Sigma-Aldrich (Schnelldorf). The complete list of chemicals and suppliers can be found in the Supplemental material (see 7.1).

2.1.2 Buffers and solutions

1M $MgCl_2$ (25ml)

dissolve 5,0825g $MgCl_2$ (203,3 g/mol) in 25ml sterile water

10X Ringer (500ml)

- 260 mM $NaHCO_3$ (84,01g/mol) = 10,9213g
- 12,5 mM NaH_2PO_4 (138g/mol) = 0,8625g
- 1250 mM NaCl (58,44g/mol) = 36,5250g
- 25 mM KCl (74,56g/mol) = 0,9319g

1M $CaCl_2$ (50ml)

dissolve 7,35g $CaCl_2 \bullet H_2O$ (147 g/mol) in 50ml sterile water

Agarose gel (standard)

- add 0,5g (1% gel) into 50ml 1xTAE buffer
- boil shortly
- add 25µl Ethidium Bromid (0,1%)

Agar plates (for approximately 20 plates)

- add 7,5g Agar into 500ml LB buffer
- autoclave immediately
- cool down to 64°C
- add antibiotic of wish and mix
- pour into sterile Petri dishes and leave to solidify
- store at +4°C

Artificial cerebrospinal fluid (ACSF)

- 125mM NaCl
- 2,5mM KCl
- 2mM $CaCl_2$
- 1mM $MgCl_2$
- 1,25mM NaH_2PO_4
- 26mM $NaHCO_3$
- 20mM glucose

Cell harvest pipette solution (per reaction)

- 1µl first strand buffer 5X
- 4µl RNase free water

dNTP-Mix (10mM)

- 50µl of each 100mM dATP / dCTP / dGTP / dTTP
- 300µl 10mM TRIS, pH: 8.0

DNA loading buffer (10ml)

- 0,05g Xylene cyanol
- 5ml 80% Glycerol
- 5ml 1xTAE

Ethidium bromide solution (0,1%)

dilute 60µl 1% ethidium bromide solution in 600µl water

LB - medium (5L)

- 25g Yeast
- 50g NaCl
- 50g Peptone form casein
- dissolve completely
- adjust pH to 7,4 with NaOH
- pour into 500ml bottles
- autoclave

N_6 random primers (50µM)

dilute 4µl N_6 random primer stock solution (5mM) in 396µl RNase free water

RNA normal ringer (1l)

- 2mM $CaCl_2$ (2ml 1M CaCl2)
- 900 ml Aqua dest
- 1mM $MgCl_2$ (1ml 1M $MgCl_2$)
- 100ml 10X Ringer

RT mix (per reaction)

- 1µl Igepal CA-630 (1%)
- 1µl N_6 random primers 50 µM
- 1µl dNTPs 10mM
- 1µl first strand buffer 5X

TAE, 50x (500ml)

- 2M Tris BASE (121g)
- 50ml 0,5M EDTA
- adjust pH to 8.0. with acetic acid at room temperature
- add Delta water until 500ml and autoclave immediately

TBE, 10x (500ml)

- use sterile bottle
- 890mM Boric acid (27,5g)
- 890mM Tris BASE (54g)
- 20ml 0,5M EDTA pH 8.0
- add Delta water until 500ml and autoclave

X-Gal solution

40mg/ml X-Gal in N´N´-Dimethylformamide

2.1.3 Enzymes and enzyme buffers

Restriction enzymes and corresponding enzyme buffers were ordered from New England Biolabs (Frankfurt am Main). M-MLV reverse transcriptase and M-MLV RT buffer, as well as RNA protecting agent, RNasin® Plus, were purchased from Promega (Mannheim). The Taq (*Thermus aquaticus*)-DNA-Polymerase, and the corresponding

PCR buffer were ordered from PeqLab (Erlangen). Information on enzymes and corresponding enzyme buffers is listed in the Supplemental material (see.7.2).

2.1.4 Antibodies

The Taq-Start™ Antibody (1,1µg/ml, 7µM), was ordered from Clontech (a Takara Bio Company, Mountain View, CA, USA).

2.1.5 Nucleotides and oligonucleotides

Nucleotides dATP, dCTP, dGTP and dTTP, all 100mM, were purchased from Amersham Pharmacia Biotech (New Jersey, USA). Random hexamer primers ($p(dN)_6$, 50 A_{260} units) were ordered from Roche Diagnostics (Mannheim). The PCR primers were ordered from MWG-Biotech AG (Ebersberg) and Metabion (Munich).

2.1.6 Vectors

The pGEM®-T Easy Vector (3018bp) was ordered from Promega (Mannheim), and the pSPT18 phagemid vector (3104bp) from Roche Diagnostics (Mannheim).

2.1.7 Dyes and markers

The Xylene cyanol FF, C.I. 43535, indicator was purchased from Serva (Heidelberg). The DNA marker, MassRuler™, DNA Ladder Mix was ordered from Fermentas (St. Leon-Rot).

2.1.8 Kits

The LightCycler® DNA Master SYBR Green I kit and the LightCycler® Capillaries (20µl) were purchased from Roche Diagnostics (Mannheim). The QIAEX® Gel Extraction Kit, QIAquick® Gel Extraction Kit, QIAquick® PCR Purification Kit, RNeasy® Protect Maxi Kit and RNeasy® Protect Midi Kit were ordered from Qiagen (Hilden). The NucleoSpin® Plasmid for plasmid isolation and NucleoBond® Plasmid Purification Maxi kit were ordered from Machery-Nagel (Düren), and pGEM®-T Easy Vector System I from Promega (Mannheim).

2.1.9 Microorganisms

The *Escherichia Coli* strains XL10-Gold ultra-competent cells were ordered for Stratagene (La Jolla, CA). One Shot® TOP10 chemically competent cells and DH5Alpha™ Competent Cells were purchased from Invitrogen (Karlsruhe).

2.1.10 Animals

The wild type mice used in this study, carried a mixed genetic background 50:50 (SV129:C57BL/6). The TRPC1 knockout and corresponding control animals were maintained on a SV129 genetic background (Dietrich et al., 2007).

2.2 Methods

2.2.1 Cloning

2.2.1.1 Ligation

a) Quick ligation of DNA fragments into pSPT18 phagemid

Before the ligation reaction was performed, the inserts and the pSPT18 phagemid were treated with restriction endonucleases EcoRI and Hind III, in order to make the so-called “sticky-ends” (see 2.2.7). After the restriction cut, preparative gels were made in order to purify modified inserts and plasmid. Ligation procedure was performed using TOPO cloning, 5 minute PCR cloning kit (Invitrogen, Karlsruhe):

- 10µl 2x Quick buffer
- 5µl insert
- 1µl pSPT18 phagemid vector
- 4µl water
- 1µl Quick ligase
- incubate 5min at 25°C

b) Ligation of DNA fragments using the pGEM Easy vector system 1

- 5µl 2x R.L. Buffer
- 1µl vector
- 3µl PCR product
- 1µl T4 ligase
- incubate 1h at 25°C

2.2.1.2 Transformation of *E.Coli* bacterial strains with plasmid DNA

The transformation of competent cells (see 2.1.9.) was performed with small amounts of the ligation product following the protocol below:

1. melt aliquots of competent cells (50µl each) on ice
2. immediately mix the aliquots with the ligation product
3. incubate on ice for 30min
4. "heat-shock" the probes on 42°C for exactly 30s and return on ice
5. add 250µl SOC medium into each probe
6. incubate 1h at 37°C, under constant shaking
7. distribute 50µl of probe on to an agarose plate with needed antibiotic and X-Gal (Blue/white staining method)
8. incubate at 37°C over night

After the overnight incubation, transformed *E.coli* created white, antibiotic resistant colonies on the agar plates.

2.2.2 Isolation and purification of DNA

2.2.2.1 Small scale DNA isolation (Mini-prep)

In order to verify the successful transformation of *E.coli*, plasmid DNA was isolated from the transformed cultures (see 2.2.1.2.) Colonies of *E.coli* were collected from the agarose plates and incubated in 5ml LB-medium (containing antibiotic, ampicillin) over night at 37°C, under constant shaking.

For the small scale DNA plasmid isolation the NucleoSpin® Plasmid kit (Machery-Nagel, Düren) was used. The procedure was done following the modified kit protocol bellow.

1. centrifuge 1-5ml of saturated E.coli LB culture at 11000xg, for 30s
2. remove supernatant completely
3. add 250µl of buffer A1 to each sample and vortex vigorously to resuspend the cell pellet
4. add 250ml of buffer A2 to each sample and mix gently by inverting the tube couple of times. Do not vortex.
5. incubate at room temperature for a maximum of 5min
6. add 300µl buffer A3 and mix gently by inverting the tube couple of times. Do not vortex.

7. centrifuge at 11000xg, for 10min, at room temperature
8. place NucleoSpin® plasmid column in a 2ml collecting tube and add the supernatant collected from the samples
9. centrifuge at 11000xg , for 1min and discard flow-through
10. add 500ml pre-warmed buffer AW (50°C) to each sample tube
11. centrifuge at 11000xg, for 1min and discard flow-through
12. wash with 600µl buffer A4 (with ethanol)
13. centrifuge at 11000xg, for 1min and discard flow-through
14. centrifuge at 11000xg for additional 2min and discard flow-through
15. place the NucleoSpin® plasmid column in a 1,5ml micro-centrifuge tube and add elute the DNA with 50µl buffer AE
16. incubate 1min at room temperature
17. centrifuge at 11000xg, for 1min
18. store the DNA at -20°C

2.2.2.2 Large scale DNA isolation (Maxi-prep)

In order to produce higher amounts of DNA, a large scale production and isolation of plasmid DNA, a so-called Maxi-preparation, was made. For this procedure a NucleoBond® Plasmid Purification Maxi kit (Machery-Nagel, Düren) was used, following the modified kit protocol.

1. bacterial culture containing 50ml LB-medium, 50µl antibiotic (ampicillin) and 240µl of Mini-prep cell suspension was grown over night at 37°C, under constant shaking
2. centrifuge the suspension at 6000xg for 10min to pellet the bacteria
3. remove the supernatant
4. add 15ml of S1 and vortex to completely dissolve the pellet
5. add 15ml of S2 and mix gently
6. after exactly 5 minutes add 15ml S3 and mix gently
7. incubate on ice for 10 minutes
8. centrifuge lysate at 10000xg for 8 minutes and then filter through a NucleoBond® Folded Filter
9. equilibrate the NucleoBond® cartridge with 6ml N2 buffer
10. load the cleared lysate from step 8 onto the NucleoBond® cartridge
11. wash the cartridge with 35ml N3 buffer
12. elute the cartridge with 15ml N5 buffer into a clean 50ml tube

13. add 11 ml isopropanol and mix gently
14. centrifuge at 10000xg for 40min at 4°C
15. remove isopropanol and wash the pellet with 15ml 70% ethanol
16. centrifuge at maximum speed for 10min
17. remove ethanol and wash the pellet again with 5ml 70% ethanol
18. centrifuge at maximum speed for 5min
19. remove ethanol completely under the sterile conditions (under the flow)
20. leave the tubes open for 45min to dry the pellet
21. dissolve the pellet in 150µl 10mM Tris pH:8.0
22. before final storage at -20°C check DNA purity and concentration

2.2.2.3 Long scale storage of clones

The clones obtained from Maxilyse preparation were stored on -80°C, mixed in ratio 1:1 with clean glycerin. In this case 600µl glycerin and 600µl of Maxilyse preparation were mixed, and stored in special “cryo-tubes” at -80°C.

2.2.2.4 Isolation and purification of DNA fragments from agarose gels

In order to purify DNA out of a gel, desired DNA fragment (approximately 50µl) must be loaded and run on a preparative, clean agarose gel (see 2.2.4.1.2). After the electrophoretic separation of DNA on the gel, the desired DNA fragment is precisely cut out of the agarose gel under UV-light (312nm). Further isolations and purification steps are a modification of a protocol from QIAquick Gel Extraction Kit (Qiagen).

1. centrifuge shortly to place all the pieces of the gel on the bottom of the tube
2. add 3X of gel weight of Buffer QG (yellow) + 10µl 3M Na-acetate
   (example: gel weights 200mg ⇒ add 600µl of Buffer QG)
3. leave at 50°C for 10min to dissolve the gel completely in the buffer
4. shortly centrifuge at maximum speed
5. add 1X of the gel weight of isopropanol, and vortex shortly
6. load the filter tubes (max volume of a filter tube 750µl)
7. centrifuge at maximum speed, for 1min
8. discard flow-through and add 750µl of Buffer PE (with added ethanol)
9. incubate for 5 min at room temperature
10. centrifuge at maximum speed, for 1 min

11. discard flow-through and centrifuge at maximum speed again for 3 min to remove all the ethanol
12. place QIAquick columns in tubes
13. add 50µl of 10mM Tris-Cl, pH:8,0 on the center of the column
14. incubate at room temperature for 2 min
15. centrifuge at maximum speed, for 2 min
16. store the DNA at -20°C

After the isolation and purification, analytical agarose gel was prepared and loaded with 5µl of the purified DNA, in order to verify the identity of the purified sample, and to make sure that the DNA was not lost during the purification procedure.

2.2.2.5 Purification of PCR products

The purification of PCR products was performed following the bellow described protocol, using the QIAquick PCR Purification Kit.

1. add 5 volumes of buffer PB to 1 volume of the PCR sample and vortex shortly
2. place a QIAquick spin column in a provided 2ml collection tube
3. apply the sample to the column and centrifuge at 8000 rpm, for 1min
4. discard flow-through. Place the column back into the same tube
5. wash the column with 750µl buffer PE and centrifuge at 8000 rpm, for 1min
6. discard flow-through. Place the column back into the same tube
7. centrifuge at max speed for 1min to remove the remaining ethanol
8. place the column in a clean 1,5ml tube
9. add 50µl of 10mM Tris-HCl, pH:8,0 and incubate for 1min on room temperature
10. centrifuge at max speed, for 1min
11. store the DNA on –20°C

After the purification of PCR products analytical agarose gel was prepared and loaded with 5µl of the purified DNA, in order to verify the identity of the purified sample, and to make sure that the DNA is not lost during the purification procedure.

2.2.3 Isolation and purification of RNA

Total RNA from the whole brain and cerebellum was isolated and purified using the RNeasy Maxi or *Midi* kit (Qiagen), respectively, due to the different amounts of tissue used in the procedure.

1. immediately after isolation homogenize tissue in 15ml/*4ml* RLT (10µl β-mercapto-ethanol should be added per 1 ml RLT buffer) in a 50ml/*15ml* tube
2. centrifuge at 4500xg, for 10min
3. carefully transfer the supernatant into a new 50ml/*15ml* tube by pipetting
4. add 15ml/*4ml* of 70% ethanol (1 volume) to the homogenized lysate and shake vigorously immediately. Ensure that any precipitates are resuspended.
5. apply the sample to an RNeasy maxi/*midi* column placed in a 50ml/*15ml* tube
6. centrifuge at 4500xg, for 10min, and discard the flow-through
7. add 15ml/*4ml* of Buffer RW1 to the RNeasy column
8. centrifuge at 4500xg, for 5min and discard the flow-through
9. add 10ml/*2,5ml* of Buffer RPE to RNeasy column
10. centrifuge at 4500xg, for 2min to wash the column and discard the flow-through
11. add another 10ml/*2,5ml* of Buffer RPE to RNeasy column
12. centrifuge at 4500xg for 10min to dry the column and discard the flow-through
13. to elute, transfer the RNeasy column to a new 50ml/*15ml tube*
14. pipette 800µl/*150µl* RNase free water directly on to the column
15. incubate for 1 min at room temperature
16. centrifuge at 4500xg, for 3min and store the eluted RNA at -70°C

2.2.4 DNA electrophoresis

2.2.4.1 DNA electrophoresis on agarose gels

DNA electrophoresis was performed in horizontal gel chambers, DNA Pocket Block-UV (Biozym Diagnostik). Depending on the number of probes and volume needed, combs of different shape and size have been used, to give the final shape to the agarose gel. Concentration of agarose in the gels depended on the size of the fragment, meaning that for smaller fragments and higher separation, higher percentage agarose gels were used.

2.2.4.1.1 Analytical gels

Analytical gels were prepared in order to visualize DNA. After the agarose gel solution preparation (see 2.1.2.) gels were loaded with mixes of probes and 10% (v/v) DNA-load buffer. The electrophoresis was performed usually at a voltage of 70mV. Separated DNA bands in the gels were visualized under UV-light (312nm) and printed on Gel Doc 2000 (Biorad).

2.2.4.1.2 Preparative gels

Preparative gels were used in order to separate, isolate and purify DNA fragments. For that reason when making preparative gels, agarose with low melting point was used. Also, in order to obtain better separation, electrophoresis was performed at lower voltages (50mV). Due to the hazardous impact of UV light on DNA, fragments were cut out of preparative gels on lower UV-light intensity (70% power).

2.2.4.2 DNA size markers

DNA size markers are designed to evaluate DNA fragment´s size and quantity during agarose gel electrophoresis. For this work, MassRuler ™ DNA Ladder Mix (Fermentas) was used. Marker was applied directly onto gels by pipetting 5-10µl into gel pocket.

2.2.5 RNA electrophoresis

To test the RNA integrity RNA electrophoresis was performed in horizontal gel chambers, DNA Pocket Block-UV (Biozym Diagnostik). Gel chambers were previously cleaned with 3% hydrogen peroxide.

1,4% agarose gel was prepared in 1 x TBE buffer using the standard protocol (see 2.1.2.), without ethidium bromide. Loading buffer consisted of:

- 7µl formaldehyde
- 3µl formamide
- 1µl ethidium bromide (1µl/µl)
- 1,5µl 10x Trisborate-EDTA
- 1µg RNA (max. 5µl)

The sample was then heated at 70°C for 10min and loaded directly onto the gel. Gel electrophoresis was performed at 40mA.

2.2.6 Quantification of DNA and RNA

The amount of DNA and RNA in solution was determined in "Gene Quant" Spectrophotometer (Pharmacia) at 260nm. Measurements were performed in 500µl or 1000µl quartz cuvettes (Pharmacia) at 260nm and 280nm. Depending on the absorption obtained on 260nm, concentration of DNA and RNA in the solution can be calculated by knowing that:

OD_{260} 1.0 = 50µg/ml double stranded DNA

OD_{260} 1.0 = 40µl/ml single stranded DNA or RNA

Ratios between the absorption measurements at 260nm and 280nm depict the purity of the DNA or RNA.

2.2.7 DNA analysis with restriction endonucleases

Restriction analysis has been performed according to the protocols of Sambrook et al. (1989). The reactions were performed in a standard 20µl volume, with buffers obtained from the supplier together with the enzymes (see 2.1.3). Depending on the enzymes or enzyme mixes used, fitting buffer was chosen as recommended by the supplier (New England Biolabs). Concentration of enzyme used was dependent of the DNA concentration and has ranged from 1-5U/µg DNA. Incubation time was 3 hours on 37°C. After the incubation was finished, analytical gel was run to confirm the cut.

2.2.8 Cell harvest

2.2.8.1 Preparation of glass capillaries for cell harvest

For the cell harvest, standard patch-clamp, Hilgenberg Borosilicate glass pipettes were used (outer diameter = 2,00mm, Wgd. = 0,30mm). The capillaries were cut to the length of 7,5cm and were flamed to smooth the edges. Before usage, capillaries were

incubated in a beaker filled with 70% ethanol for 4h, then washed with RNase free water and finally sterilized at 180°C.

Using the double-pull routine on a Narishige PC-10 puller, tip diameters were set to the size of about half of the Purkinje cell soma diameter.

2.2.8.2 Preparation of cerebellar slices

The experimental animals were decapitated after being anesthetized with CO_2. The cerebella were removed rapidly and placed in ice cold ACSF (see 2.1.2), saturated with 95% O_2 and 5% CO_2. Parasagittal slices (300µm) were cut and incubated in ACSF, for 60min, at 34°C. After the 60min incubation, slices were kept in ACSF up to 8 hours, at 25°C. For the cell harvest, the slices were placed in a recording chamber and perfused with RNA normal ringer (see 2.1.2.) at 37°C. Each slice was used for a maximum of 3 h.

2.2.8.3 Cell harvest procedure

Cerebellar Purkinje cells were identified visually using an upright microscope (Eclipse E600FN, Nikon, Melville, NY) equipped with a 60x objective (Olympus, Tokyo, Japan), N.A. 1.0., at the working distance of 2mm.

After a Purkinje cell was visualized, a pipette filled with cell harvest solution (see 2.1.2.) was moved into the bath solution under positive pressure. Application of the positive pressure is needed to avoid aspiration of extracellular solution and the tissue surrounding the cell. The pressure in the pipette was released when the pipette tip approached the cell. This procedure protected the selected cell from swelling or bursting caused by pipette solution.

Under visual control, the tip of the pipette was gently attached to the selected cell. Then, suction (negative pressure) was applied, through a mouthpiece connected to the pipette. The suction lasted until the entire cell entered the tip of the pipette. The moment the complete cell had been visually located inside the tip, the negative pressure was released to minimize the contamination with extracellular solution. The pipette was quickly removed from the bath. Content of the harvest pipette was pressure expelled into the tube containing pre-prepared reverse transcription reaction components (see 2.2.9.2.).

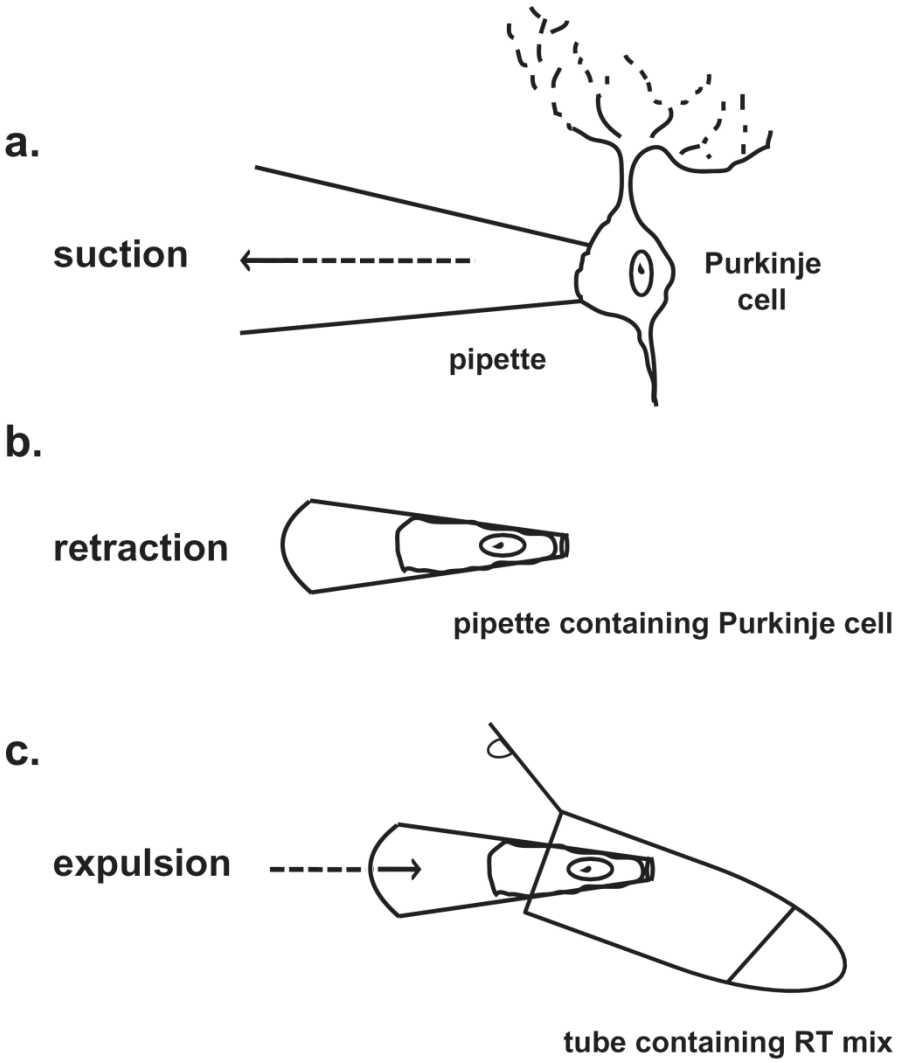

Figure 2.1 Single Purkinje cell harvest procedure: **a.** Suction of the entire Purkinje cell soma inside the harvest pipette. **b.** Retraction of the harvest pipette after the cell was successfully collected. **c.** Expulsion of the harvested cell under positive pressure into a collecting tube, containing previously prepared RT mix.

2.2.9 Reverse Transcription (RT)

2.2.9.1 Reverse Transcription of total RNA

The reverse transcription of total RNA was performed from the whole brain and cerebellar samples. The range of RNA concentration used for the RT reactions was between 100ng/µl and 1ng/µl, in order to obtain final cDNA concentrations of 10ng/µl to

0,1ng/µl, needed for the real-time PCR runs. Reactions (20µl final volume) were performed following the protocol listed below.

1. dilute RNA isolated from tissue (see 2.2.3) into a range of concentrations from 100ng/µl to 1ng/µl
2. pipette into each tube:
   - 4µl RTmix (see 2.1.2.)
   - 1µl RNasin® Plus, RNase inhibitor (40u/µl)
   - 1µl RNA (desired concentration)
   - 1µl 5X FSB (contains 10mM DTT)
   - 4µl Sigma water
3. incubate for 5min, at 70°C
4. incubate for 5min, at 0°C
5. pipette into each tube:
   - 2µl 5X FSB (contains 10mM DTT)
   - 6µl Sigma water
6. incubate for 5min, at 37°C
7. add 1µl MMLV reverse transcriptase (200u/µl) into each sample tube, or 1µl Sigma water into control tubes.
8. incubate for 3 hours, at 37°C
9. store at -80°C

2.2.9.2 Reverse Transcription of single-cell material

The reverse transcription of single-cell material was performed immediately after the Purkinje cell harvest by following the protocol listed below.

1. expel under pressure the pipette solution containing the harvested cell (see 2.2.8.3.) into a tube containing:
   - 4ml RT mix (see 2.1.2.)
   - 1µl RNasin® Plus RNase inhibitor (40u/µl)
2. spin down the solution the tube
3. incubate for 5min, at 70°C
4. spin down the solution the tube
5. incubate for 5min, at 0°C (ice)
6. add into tube:
   - 2µl 5XFSB (contains 10mM DTT)
   - 6,5µl Sigma water

7. incubate for 5min, at 37°C
8. control 1: cell present, but no RT = add 1,5 µl sigma H_2O
   control 2: no cell, but RT present = add 1,5 µl MMLV
   test cells: cell present and RT present = add 1,5 µl MMLV
9. incubate for 3 hours, at 37°C
10. store at -80°C

2.2.10 cDNA purification

After the reverse transcription, sample cDNA was purified using the QIA-EX II gel extraction kit (Qiagen), in order to clean the sample from the residual reverse transcriptase activity (Durand et al., 2006). The purification was conducted following a modified QIA-EX II gel extraction kit protocol.

1. **Binding step:**

- unfreeze the Eppi, shortly centrifuge, put at 0°C and open the lid
- add 90µl QX-I buffer; change the pipette tip after each probe
- add 2,5µl QiaEX-II-Suspension (Silica-Matrix; vortex 30s before using)
- change the pipette tip after each probe, close the lid, gently centrifuge
- vortex the silica-matrix in the QXI-Cell suspension
- incubate in the thermo-mixer at 1400rpm, for 20min, at 25°C
- centrifuge the samples for 2min at full speed
- discard the supernatant with the new pipette tip (do not touch the yellow pellet)

2. **Washing step:**

- add 90µl PE buffer, and vortex until matrix is homogenized
- centrifuge the samples at full speed, for 2min
- discard the supernatant with the new pipette tip (do not touch the white pellet)
- add 90µl PE buffer, and vortex until matrix is homogenized
- centrifuge the samples at full speed, for 2min
- discard the supernatant with the new pipette tip (do not touch the white pellet)
- close the sample tubes and leave them on ice until all probes are finished
- centrifuge the samples at full speed, for 2min

- discard the rest of the supernatant with 10µl tips very carefully (do not touch the white pellet)
- open the lids of the tubes and incubate in the thermo-mixer at 900rpm, for 10min, at 37°C to dry the pellet

3. **Elution step:**

- suspend 10µl EB-buffer (10mM Tris, pH 8,0) with the Matrix-pellet by pipetting 5 times
- incubate in the thermo-mixer at 1400rpm, for 3min, at 50°C
- centrifuge the samples for 2min at full speed
- collect the supernatant into new 0,5µl clean tubes
- repeat the procedure if higher volume is needed
- store the samples on -70°C

2.2.11 Polymerase Chain Reaction (PCR)

2.2.11.1 Primer selection

Specific primers for different TRPC subunits were selected using the Oligo 6.0 primer analysis software (MedProbe, Oslo, Norway). Primer pairs need to have high specificity since TRPC channel subunits have high homology. In addition, high primer binding sensitivity is needed to prevent primer dimer formation (interactions between primers, giving rise to an unspecific amplification product) which act as competitive inhibitors of PCR. In order to obtain the high-resolution standard curves with the highest PCR efficiency, the following primer parameters were preferred when possible:

1. selection of intron-spanning primers
2. primer length: 17-21 bp
3. 3 ´-terminal dimer formation: < (3.0) kcal/mol
4. optimal annealing temperature: 58-65°C
5. amplicon length: 100-250 bp
6. product melting temperature: 85-91°C
7. G/C-content: 45-60%
8. high internal stability at the 5 ´-end and medium internal stability at the 3 ´-priming site

9. minimal acceptable loop (hairpin formation) at the 3 ´-end: 0.0 kcal/mol
10. maximal length of acceptable dimers (5 ´-end/internal region): 4 bp.

2.2.11.2 Nested PCR

In order to reduce the contaminations due to the amplification of unexpected primer binding sites, so-called “nested PCR” technique was used. The nested PCR involves two sets of primers, used in two successive PCR runs. During the primary PCR run, the first set of primers yields a longer product, a “primary target”. The second set of primers amplifies the “secondary target” within the primary run product, during the successive, secondary PCR. The nested PCR is based on the fact that is highly unlikely that any of the unwanted PCR products from the primary PCR run contains the binding sites for both of the second set of primers. In this way it was ensured that the product of the secondary PCR has little or no contamination of unwanted products or mis-amplification of homologous cDNA.

a) Primary PCR run

The primers used in this stage of nested PCR yielded large products (1000bp – 3000bp). Primary PCR primer sets were ordered from MWG-Biotech AG (Ebersberg) are described in Table 2.1. The PCR reaction mix consisted of:

- 37,5µl H_2O
- 5µl 10x PCR-buffer
- 4µl 25mM $MgCl_2$
- 1µl forward primer (10pmol)
- 1µl reverse primer (10pmol)
- 1µl dNTPs
- 0,5µl Taq Polymerase

The primary PCR runs were conducted under the conditions described in Table 2.2. Each reaction run consisted of 40 cycles.

Table 2.1 Primary PCR run primer sequences

gene	accession number	forward primer / reverse primer	product length (bp)	intron spanning
TRPC1	U73625	611-for 5´ -TGATGGCGCTGAAGGATGT- 3´ 2850-rev 5´ -AAGTCCGAAAGCCAAGCAAA- 3´	2259	yes
TRPC3	AF190645	999-for 5´ -CATCGCTATCAAGTGTCTGG- 3´ 2275-rev 5´ -TGCTGATATCGTGTTGGCTG- 3´	1296	yes
TRPC4	U50922	302-for 5´ -CTGTGGAGAAGGGGGACTAT- 3´ 2707-rev 5´ -CGTCTATGAAATAACCCGAA- 3´	2425	yes
TRPC5	AF060107	562-for 5´ -GAGGCCGAGATCTACTACAA- 3´ 3249-rev 5´ -AAGCCTCTCCCCAAGTTTCA- 3´	2707	yes
TRPC6	U49069	456-for 5´ -TTCCGGGGTAATGAAAACAG- 3´ 2254-rev 5´ -TGCGCCAATGTAGTAGGAGT- 3´	1818	yes
TRPC7	AF139923	525-for 5´ -AGGAGCTGCGGGATGATGA- 3´ 2308-rev 5´ -CAGGTCGTTTTCACAGCGT- 3´	1802	yes

Table 2.2 Primary PCR run cycle protocols

gene	TRPC1	TRPC3	TRPC4	TRPC5	TRPC6	TRPC7
initial denaturation	94°C, 2 min	94°C, 2 min	94°C, 2 min	94°C, 2 min	94°C, 2 min	94°C, 2 min
denaturation annealing elongation	94°C, 15 s 59°C, 30 s 72°C, 2 min 30 s	94°C, 15 s 58°C, 30 s 72°C, 2 min	94°C, 15 s 58°C, 30 s 72°C, 3 min	94°C, 15 s 58°C, 30 s 72°C, 3min	94°C, 15 s 56°C, 30 s 72°C, 2min 30 s	94°C, 15 s 60°C, 30 s 72°C, 2 min
final elongation	72°C, 10 min	72°C, 10 min	72°C, 10 min	72°C, 10 min	72°C, 10 min	72°C, 10 min
cycle end	4°C, forever	4°C, forever	4°C, forever	4°C, forever	4°C, forever	4°C, forever

a) Secondary PCR run

The secondary PCR run primer sets with specific characteristics (see 2.2.11.1.) are described in Table 3.1. In order to make the cloning of the final products easier, Eco RI restriction sites (5´-GCGAATTC-3´) were added to the 5´end of the forward primers. Hind III (5´-ATGCAAGCTT-3´) restriction sites were added to the 5´end of the reverse primers. The PCR reaction consisted of:

- 37,5µl H_2O
- 5µl 10x PCR-buffer
- 4µl 25mM $MgCl_2$
- 1µl forward primer (10pmol)
- 1µl reverse primer (10pmol)
- 1µl dNTPs
- 0,5µl Taq Polymerase

The secondary PCR runs were conducted under the conditions described in Table 2.3. Each reaction run consisted of 40 cycles.

Table 2.3 Secondary PCR run cycle protocols

gene	TRPC1	TRPC3	TRPC4	TRPC5	TRPC6	TRPC7
initial denaturation	94°C, 2 min	94°C, 2 min	94°C, 2 min	94°C, 2 min	94°C, 2 min	94°C, 2 min
denaturation annealing elongation	94°C, 15 s 61°C, 30 s 72°C, 25 s	94°C, 15 s 60°C, 30 s 72°C, 25 s	94°C, 15 s 57°C, 30 s 72°C, 25 s	94°C, 15 s 56°C, 30 s 72°C, 25 s	94°C, 15 s 56°C, 30 s 72°C, 25 s	94°C, 15 s 58°C, 30 s 72°C, 25 s
final elongation	72°C, 10 min	72°C, 10 min	72°C, 10 min	72°C, 10 min	72°C, 10 min	72°C, 10 min
cycle end	4°C, forever	4°C, forever	4°C, forever	4°C, forever	4°C, forever	4°C, forever

2.2.12 Real-time quantitative PCR

The absolute quantification was performed to determine the copy number of specific TRPC channel subunits in different brain areas and in single Purkinje neurons.

2.2.12.1 Basis of real-time quantitative PCR

A PCR cycle consists of three phases. The amplification reaction starts with a background phase. In this phase, the signal from the PCR product is lower than the background signal. The second phase starts when the sufficient amount of PCR product is accumulated to be detected above the background signal. In this phase, amplification is exponential (Rasmussen, 2001). Within the exponential phase, a point in the amplification

curve can be defined that represents the same amount of PCR product in every curve. This point is called crossing point and is the cycle number (x-axis) of identical copy numbers (y-axis) in all reactions. A PCR cycle finishes in a plateau phase when the efficiency of the reaction falls.

The exponential phase is crucial for the quantification of the unknown initial amount of amplicons. This phase of a PCR cycle is explained in the following equation:

$$T_n = T_o(E)^n$$

, where T_n is the amount of amplicon at cycle n; T_o is the initial amount of amplicon; E is the efficiency of the PCR and n is the cycle number. Efficiency of the PCR can be maximally 2, meaning that each DNA molecule was doubled after each cycle, and minimally 1, meaning that no amplification occurred. The equation above is characteristic only for the exponential phase of the reaction, which limits the quantification only to the exponential phase of the reaction.

The efficiency for a gene-specific PCR assay is obtained from the slope of the gene-specific standard curve (see 2.2.12.4.) and is described with the following equation:

$$\text{Eff.} = 10^{(-1 / \text{slope})}$$

When the expression of different genes is compared, the efficiencies of the different gene-specific PCR assays must be comparable. The efficiency difference between PCR assays of only 0,1 yields a 3,6 fold underestimate of the copy amounts. Therefore, the comparable PCR efficiencies are essential for the successful absolute value calculation.

2.2.12.2 The LightCycler™

The rapid cycler of choice in our experiments was the LightCycler™, purchased from Roche Diagnostics (Mannheim). The LightCycler™ is a combination of a rapid cycler and a micro-volume fluorimeter utilizing high quality optics. The accumulation of the

double stranded DNA was followed with SYBR Green I dye. SYBR Green I is a fluorescent dye that, just like ethidium bromide, binds to the minor groove of the DNA helix. Upon binding to DNA, fluorescence of SYBR Green I is greatly enhanced and it is proportional to the DNA concentration. The signal was then measured once per cycle during the PCR run and immediately displayed on the computer screen.

The PCR runs were conducted in special 20µl glass capillaries, with high surface to volume ratio, which enables the fast and equally distributed change of temperature inside the samples. The capillaries were placed into a specially designed carousel, with capacity of 32 samples. In our experiments, not more than 14 samples were used due to discrepancies in the signal when more samples were used (Durand et al., 2006).

The product verification was done by melting curve analysis, gel electrophoresis and finally sequencing. The melting curve of specific products was obtained after the amplification was finished. When using SYBR Green I dye chemistry, it is possible to elevate the temperature in the capillaries above the melting temperature of the PCR product and measure fluorescence. The dye is released upon denaturation of the PCR product, providing accurate melting temperatures specific for every amplified product. Computer software automatically plots the first negative derivate (-dF/dT) of the curve with temperature, and a characteristic melting peek is presented. The longer the length and the higher the concentration of GC pairs in the PCR product, the higher is the melting temperature of the amplification product.

2.2.12.3 Quantification on the LightCycler™

In this study, the LightCycler™ system and SYBR Green I chemistry was used. The signal of the amplified PCR product was proportional to the SYBR Green I signal and was displayed on the computer screen during the amplification.

The crossing points of the samples were obtained by using the “fit point” method of the LightCycler 3.5 software. The “fit point” method allows the user to discard all the background information and determine the crossing point value, by setting a “noise band”. The noise band is set when the reaction is finished and the logarithm of the fluorescence is plotted to the cycle number. This line is placed in the logarithmic phase of the reaction. Once set, the same noise band was used in all quantification experiments.

The absolute copy values of the unknown samples were calculated using the

high-resolution gene specific standard curves (see 2.2.12.5.). Based on the standard curves parameters, following formula was used to calculate the unknown copy number of specific gene-transcripts:

$$\text{copy \#} = 10^{(\text{cross.point} - Y) / \text{slope}}$$

By definition, Y intercept (point were the standard curve cuts the Y axis) is the expected crossing point of the sample containing one copy and the slope of the curve is the number of crossing points between two samples containing copy number difference of one order of magnitude.

2.2.12.4 Construction of high-resolution external standard curves

In order to determine the absolute amount of transcripts in an unknown sample, high-resolution external standards were developed. The standard curves were created specifically for each of the TRPC subunits.

The TRPC subunit gene specific standards were prepared from plasmids containing cDNA inserts for mouse TRPC1, TRPC3, TRPC4, TRPC5, TRPC6 and TRPC7. The TRPC subunit inserts were cut out of these plasmids, purified and later used in subunit-specific, real-time PCR. The resulting PCR products were purified, analyzed, and quantified at 260 nm in "Gene Quant" spectrophotometer (Pharmacia) The Nucweight algorithm of the Husar sequence analysis software (DKFZ, Heidelberg) was used to calculate the molecular weight of the cDNA fragments. After the quantification and determination of molecular weight of all TRPC subunit fragments, it was possible to calculate the copy number of different TRPC subunit fragments per µl, using the following formula, where M_W stands for molecular weight:

$$M_W \text{ (single stranded copy)} = \frac{M_W \text{ (sequence)}}{2 \times \text{Avogadro number}}$$

Quantified cDNA was then diluted in 16 steps, from 10^{10} to 4 copies per 2µl in volumes ranging from 100µl to 200µl and put into reaction tubes pre-coated with 10 mM Tris-HCl, pH 8.0, and 1 mg/ml purified BSA (New England Biolabs, Frankfurt). In this case, one copy is referred to one copy of single-stranded cDNA, and therefore two copies are equivalent to one double-strand cDNA copy. The cDNA standards were stored at -20°C and used to create external standard curves.

2.2.12.5 Rapid-cycle, real-time PCR

The cDNAs encoding TRPC1, TRPC3, TRPC4, TRPC5, TRPC6 and TRPC7 were amplified using specific, HPLC-purified primers (Metabion, Munich) shown in Table 3.1. All reactions were performed in a volume of 20µl. Reactions included 2µl 10xDNA Master SYBR-Green mix (Roche) previously incubated for 5min with 0,16µl/reaction of Taq Start antibody (Clontech, a Takara Bio Company, Mountain View, CA, USA) to ensure 'hot start conditions'. All the PCR assays were optimized for magnesium concentration, primer concentration, annealing temperature, and the product specificity temperature, at which the specific products melt (see Table 3.2). PCR products verification was performed by melting curve analysis, DNA gel electrophoresis and, in selected cases, DNA sequencing.

3. Results

3.1 Nested PCR

In the first stages of the experimental work, expression of the TRPC1-7 subunits in the mouse brain was confirmed. In order to verify the accuracy of the primers created to specifically detect different TRPC subunits, the nested PCR was performed.

The nested PCR consists of two consecutive PCR runs. The primary run used primers (see Table 2.1) that yielded long PCR products. The verification of these products was done by agarose gel electrophoresis. Figure 3.1 represents the agarose electrophoresis gels loaded with the products of the primary nested PCR runs. The fragments have range of lengths between 1296bp for TRPC3 and 2707 for TRPC5. As expected, the primary run TRPC subunit specific primers detected their target in the total brain cDNA.

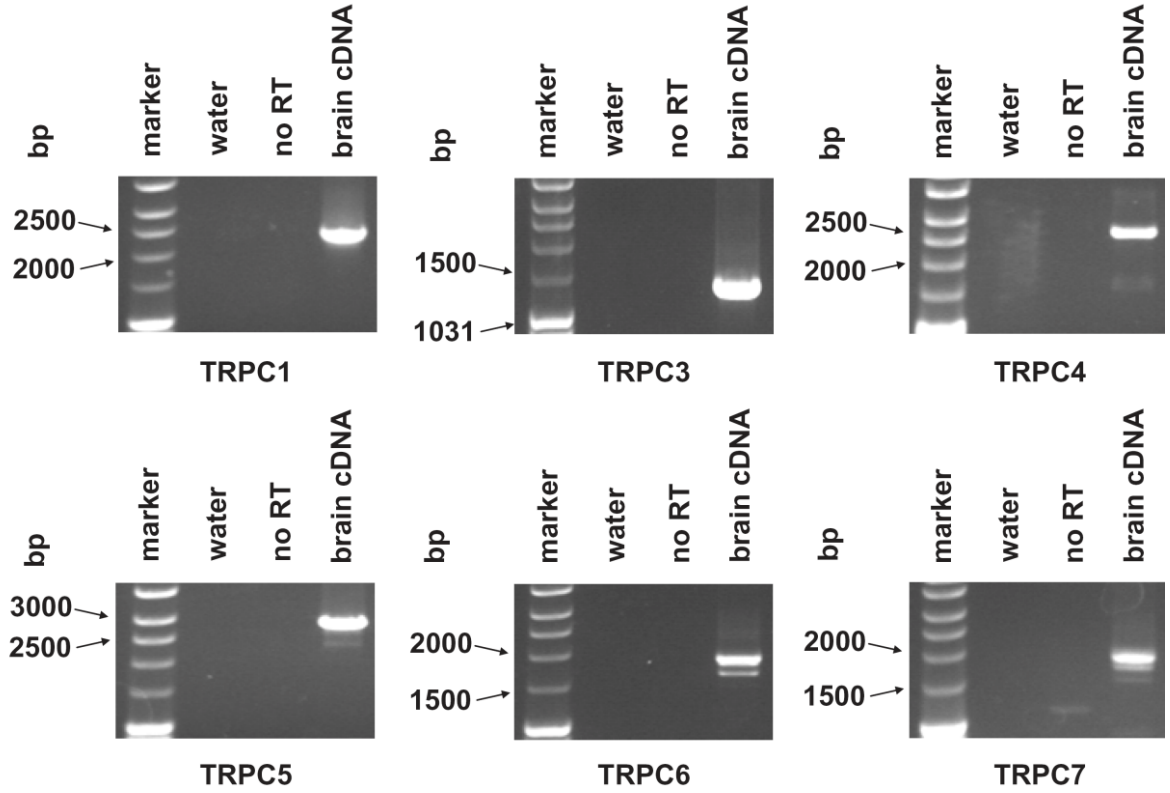

Figure 3.1 Agarose gel electrophoresis of primary run nested PCR products. Water and a reaction without the reverse transcriptase are shown as the negative controls. TRPC subunits amplicons are presented with the bands of different sizes; 2259 bp for TRPC1, 1296 bp for TRPC3, 2425 bp for TRPC4, 2707 bp for TRPC5, 1818 bp for TRPC6 and 1802 bp for TRPC7.

In order to verify the specificity of the products obtained from the primary nested PCR runs, the secondary runs were performed using the primary run products as templates. In that way any possibility of false specificity, contamination and cross-reaction between primers was dismissed (see 2.2.11.2). The primers of the secondary run were created to satisfy the parameters for good real-time PCR (see 2.2.11.1). In this way, it was possible to use secondary run primers for quantitative real-time PCR analysis (see 3.2). Identity of the secondary run PCR products was first verified on agarose gels (Figure 3.2). The secondary run PCR primers were designed to yield products of about 200bp. Due to the assertion of the EcoRI and HindIII restriction sites to the forward and reverse primers, respectively, secondary run PCR products were 18bp longer then presented in the Table 3.1.

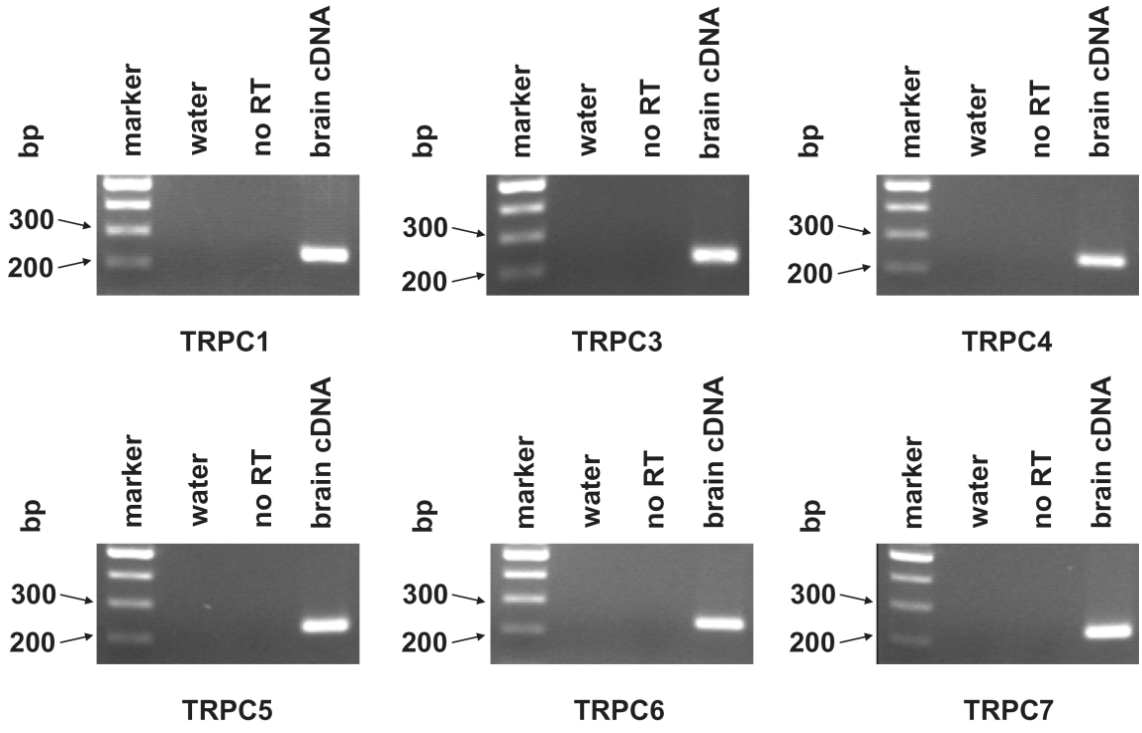

Figure 3.2 Agarose gel electrophoresis of secondary run nested PCR products. Water and a reaction without the reverse transcriptase are shown as the negative controls. TRPC subunits amplicons are presented with the bands of different sizes; 227 bp for TRPC1, 225 bp for TRPC3, 235 bp for TRPC4, 228 bp for TRPC5, 227 bp for TRPC6 and 223 bp for TRPC7.

The negative controls in primary and secondary nested PCR runs were water (PCR reaction control) and the reactions without reverse transcriptase (no RT), as control for genomic contamination. Both negative controls yielded no products in all primary and secondary nested PCR runs, meaning that the PCR runs were performed in clean conditions and that no genomic contamination was present.

The nested PCR experiments confirmed the specificity of the second run PCR primers and the presence of TRPC1-7 subunits in the mouse whole brain cDNA.

3.2 Gene-specific primers selected for the real-time PCR

The primers were created using the Oligo 6.0 Primer Analysis Software. The primers with high specificity, high selectivity, acceptable size and thermodynamic characteristics were selected (see 2.2.11.1). Since the target of the primers is cDNA, intron-spanning primers were favored, when possible, in order to prevent genomic contamination artifacts.

After the confirmation of primer specificity by nested PCR (the secondary nested PCR runs), primer sets were used in further optimization of the gene-specific real-time PCR. The primers were created, for TRPC1, TRPC3, TRPC4, TRPC5, TRPC6, and TRPC7 and their sequences and gene accession numbers are listed in Table 3.1 below. The gene-specific primers sequences for GAPDH were taken from the literature (Durand et al., 2006), and adapted to fit with mouse cDNA.

Table 3.1 Optimized primers for LightCycler reactions

gene	accession number	forward primer / reverse primer	product length (bp)	intron spanning
TRPC1	U73625	2553-for 5´ -GCCCCCACCTTTCAACATTA- 3´ 2742-rev 5´ -GTCGCATGGACGTCAGGTAG- 3´	209	yes
TRPC3	AF190645	1451-for 5´ -AGGCGCAGCAGTATGTGGA- 3´ 1639-rev 5´ -GGCCAAAGCTCTCGTTTGC- 3´	207	yes
TRPC4	U50922	1654-for 5´ -CTCCGCCTGATCTCTCTGT- 3´ 1850-rev 5´ -AAACGCGTTGTTCTGTTTCT- 3´	217	no
TRPC5	AF060107	2606-for 5´ -ATGAGGGGCTAACAGAAGA- 3´ 2797-rev 5´ -TGCAGCCTACATTGAAAGA- 3´	210	yes
TRPC6	U49069	565-for 5´ -CAAGCCTGTCTATTGAGGAA- 3´ 755-rev 5´ -CCCAACTCGAGACAAGTTT- 3´	209	no
TRPC7	AF139923	1668-for 5´ -CCTACGCCAGGGATAAGTG- 3´ 1854-rev 5´ -AAGGCCACAAATACCATGA- 3´	205	yes
GAPDH	BC095932	216-for 5´ -GCAAATTCAACGGCACA- 3´ 338-rev 5´ -CACCAGTAGACTCCACGAC- 3´	141	no

3.3 Optimization of real-time PCR cycles

All real-time PCR cycles were optimized for magnesium and primer concentration, annealing and melting temperatures (Table 3.2). Finally, the concentrations that yielded the curves with the best efficiency were used in further PCR assays. The annealing and melting temperature depend on the primers and the PCR product, respectively. In order to obtain the conditions for the higher specificity of the primers, annealing temperatures were usually set to 1-2°C higher than the recommended values obtained from the Oligo 6.0 Primer Analysis Software. The melting temperatures were always set 1-2°C below the products melting temperature in order to ensure that none of the SYBR Green I signal is lost during the cycling. For all TRPC subunits, the PCR assays consisted of 50 cycles and for the GAPDH, the PCR assay consisted of 40 cycles.

Table 3.2 Optimized parameters of real-time PCR using the LightCycler

gene	TRPC1	TRPC3	TRPC4	TRPC5	TRPC6	TRPC7	GAPDH
[$MgCl_2$] (mM)	3	3	3	3	4	3	3
[primer] (µM)	1,5	1	1,5	1,5	2	1,5	1,5
denaturation	95°C, 0s	95°C, 0s	95°C, 0s	95°C, 0s	95°C, 0s	94°C, 0s	94°C, 0s
annealing	61°C, 5s	60°C, 5s	59°C, 5s	56°C, 5s	58°C, 5s	58°C, 5s	58°C, 5s
elongation	72°C, 9s	72°C, 9s	72°C, 9s	72°C, 9s	72°C, 9s	72°C, 9s	72°C, 9s
melting	82°C, 5s	84°C, 5s	83°C, 5s	82°C, 5s	82°C, 5s	83°C, 5s	83°C, 5s
final elongation	72°C, 10min	72°C, 10min	72°C, 10min	72°C, 10min	72°C, 10min	72°C, 10min	72°C, 10min

3.4 Verification of the PCR products by sequencing

After the correct sizes of the secondary nested PCR products were confirmed by agarose gel electrophoresis (see Figure 3.2), additional product identity was verified by sequencing. All secondary nested PCR products were cloned into pSPT18 phagemid

(Roche Diagnostics, Mannheim), and positive clones were sequenced (MWG-Biotech AG, Ebersberg). Sequencing confirmed the product identity.

Similar procedure was performed for the products obtained from real-time PCR. The products of all quantitative real-time PCR runs were verified by agarose gel electrophoresis. Additionally, the products specific for different TRPC subunits, obtained after the real-time PCR of the whole brain, cerebellar and single Purkinje cells samples were successfully cloned into pGEM Easy vector system 1 (Promega, Mannheim). The positive clones were sequenced (SeqLab, Göttingen). Also in this case, sequencing confirmed the identity of the PCR products.

3.5 High-resolution external standard curves

In order to quantify the copy number of TRPC1-7 subunits in the different brain areas and single Purkinje cells, gene-specific high-resolution standard curves were produced for each of the TRPC subunits. Depending on the parameters of the individual standard curves and the crossing point values obtained from the samples, the absolute copy number of different TRPC subunits was calculated (see 2.2.12.3).

The standard dilutions of TRPC1-7 subunits in the range from 10^4 to 4 copies per 2µl standard volume were amplified in real-time PCR runs. For each of the TRPC subunits, the real-time PCR runs of standard dilutions were repeated ten times. The mean values of SYBR Green I fluorescence for each cycle were plotted against the cycle numbers in Figure 3.3 – 3.8 (panel **a**.). The exponential phase of the runs, where quantification is possible, is presented in panel **b** of Figures 3.3 – 3.8. The method of choice for the quantification was the fit point method (see 2.2.12.3). The dashed line on the panel **b** of the Figures 3.3 – 3.8 represents the noise band set at 0.25 for all of the TRPC subunits specific runs. The same noise band value was used in all further quantification experiments.

When the noise band was set, it was possible to obtain the crossing point values for TRPC subunit specific standards. The crossing point values of the standards were collected from all ten repeated runs and the mean values were calculated for each standard. To create master standard curves, the mean values of crossing points for different standard dilutions were plotted against the logarithm of the copy numbers corresponding to these dilutions. The panel **c** in the Figures 3.3 – 3.8 represent the specific master standard curves for each of the TRPC subunits.

The real-time PCR products of the standard dilution runs were verified by melting curve analysis and agarose gel electrophoresis (panel **d** in Figures 3.3 – 3.8). The negative controls in these reactions were water (PCR reaction control), and the elution buffer used during the preparation of the standard dilutions (dilution buffer control). Both controls were indeed negative, meaning that the reactions were performed under clean conditions.

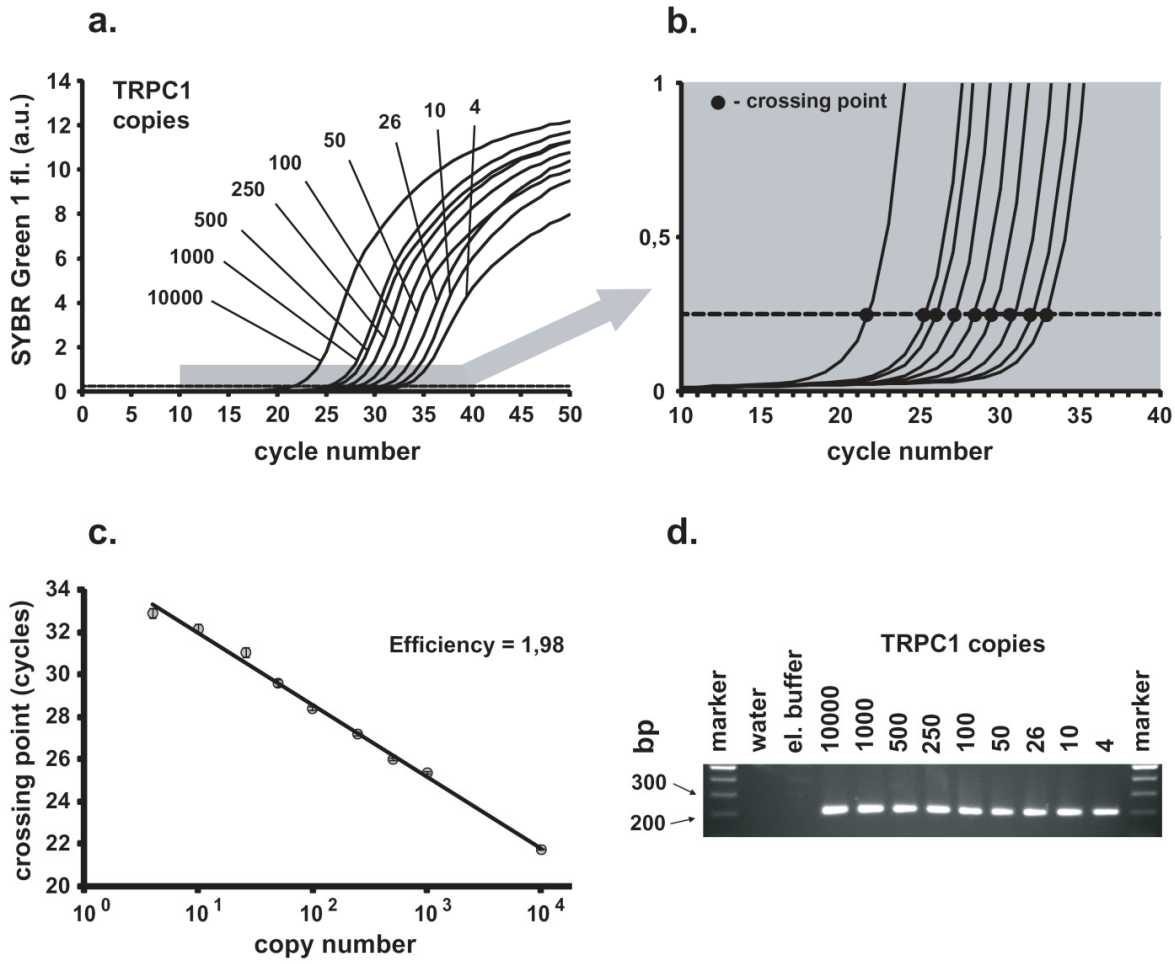

Figure 3.3 PCR calibration with TRPC1 amplicons.

a Real-time monitoring of the fluorescence emission of SYBR Green I during the PCR amplification of defined amounts of TRPC1 amplicons (serial dilutions containing 4-10,000 copies in this example). The small *grey rectangle* is enlarged in **b**. **b** Fluorescence monitoring of the PCR amplification of the TRPC1 amplicon dilutions shown in **a** during the exponential phase of the PCR. At a gene-specific fluorescence value (*dashed line*), the crossing point is calculated by the fit point method. **c** Standard curve of the TRPC1 amplicon serial dilutions. Individual data points represent mean ±SEM of ten samples of equal amounts of TRPC1 amplicon copies. **d** Agarose gel electrophoresis of PCR products obtained in **a** after 50 cycles of PCR amplification. The TRPC1 amplicon size is 209bp.

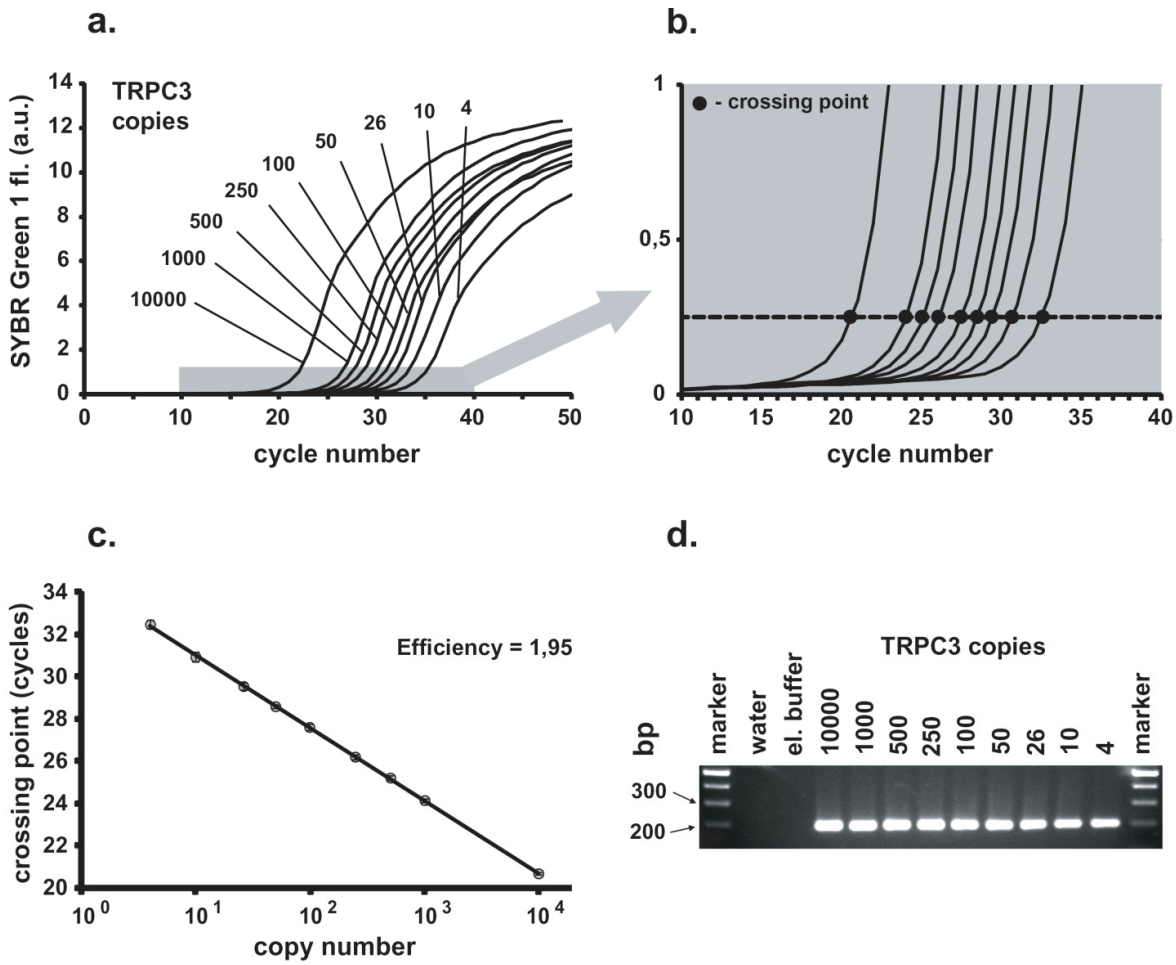

Figure 3.4 PCR calibration with TRPC3 amplicons.

a Real-time monitoring of the fluorescence emission of SYBR Green I during the PCR amplification of defined amounts of TRPC3 amplicons (serial dilutions containing 4-10,000 copies in this example). The small *grey rectangle* is enlarged in **b**. **b** Fluorescence monitoring of the PCR amplification of the TRPC3 amplicon dilutions shown in **a** during the exponential phase of the PCR. At a gene-specific fluorescence value (*dashed line*), the crossing point is calculated by the fit point method. **c** Standard curve of the TRPC3 amplicon serial dilutions. Individual data points represent mean ±SEM of ten samples of equal amounts of TRPC3 amplicon copies. **d** Agarose gel electrophoresis of PCR products obtained in **a** after 50 cycles of PCR amplification. The TRPC3 amplicon size is 207bp.

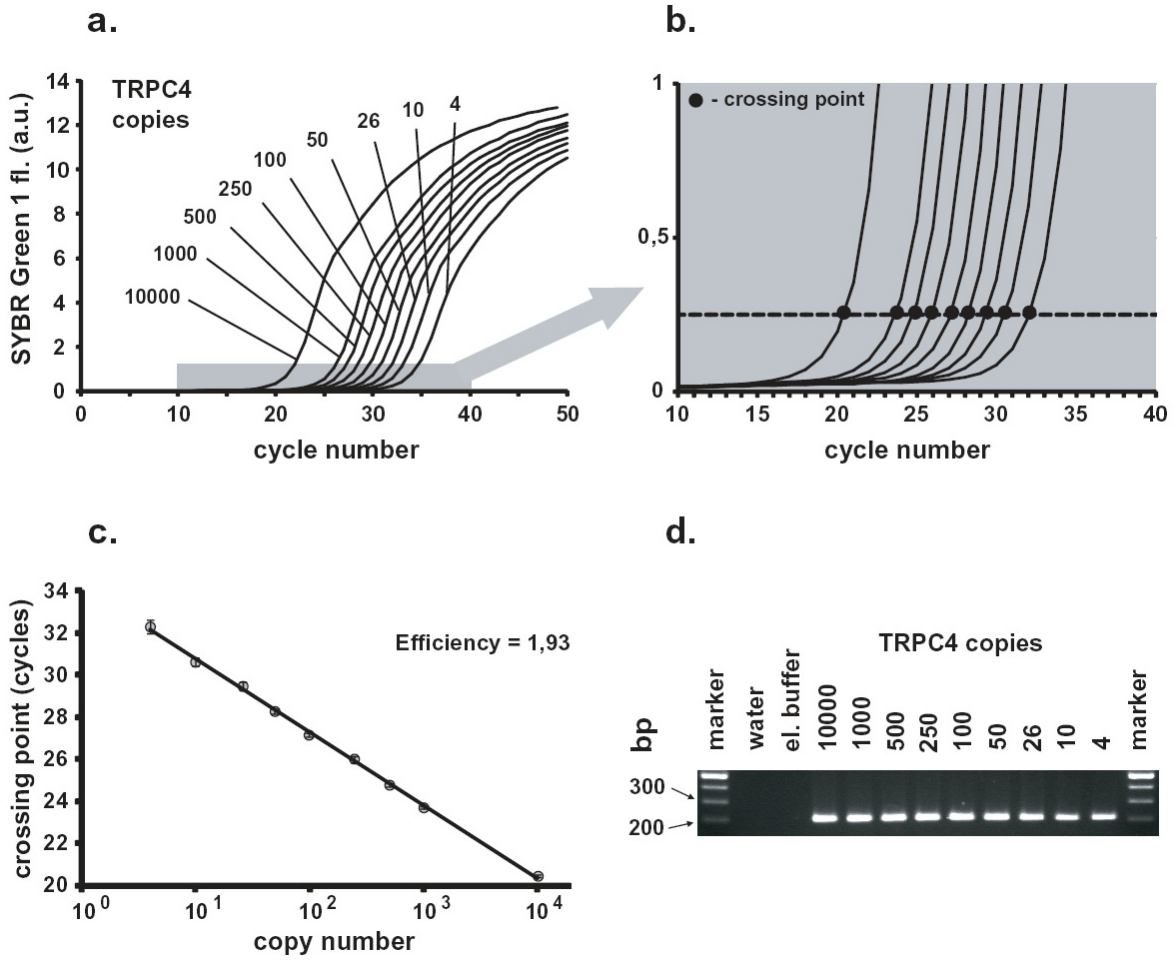

Figure 3.5 PCR calibration with TRPC4 amplicons.

a Real-time monitoring of the fluorescence emission of SYBR Green I during the PCR amplification of defined amounts of TRPC4 amplicons (serial dilutions containing 4-10,000 copies in this example). The small *grey rectangle* is enlarged in **b**. **b** Fluorescence monitoring of the PCR amplification of the TRPC4 amplicon dilutions shown in **a** during the exponential phase of the PCR. At a gene-specific fluorescence value (*dashed line*), the crossing point is calculated by the fit point method. **c** Standard curve of the TRPC4 amplicon serial dilutions. Individual data points represent mean ±SEM of ten samples of equal amounts of TRPC4 amplicon copies. **d** Agarose gel electrophoresis of PCR products obtained in **a** after 50 cycles of PCR amplification. The TRPC4 amplicon size is 217bp.

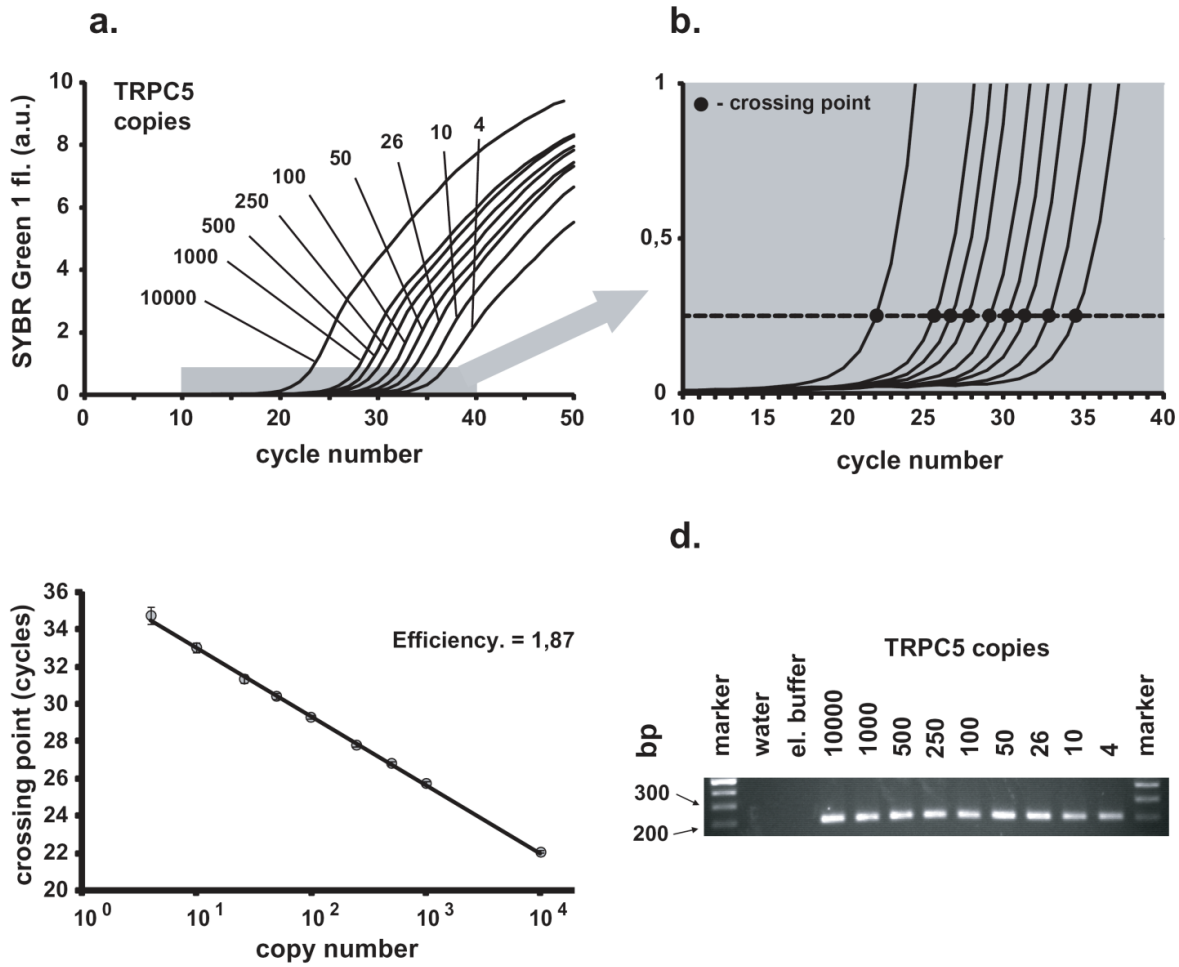

Figure 3.6 PCR calibration with TRPC5 amplicons.

a Real-time monitoring of the fluorescence emission of SYBR Green I during the PCR amplification of defined amounts of TRPC5 amplicons (serial dilutions containing 4-10,000 copies in this example). The small *grey rectangle* is enlarged in **b**. **b** Fluorescence monitoring of the PCR amplification of the TRPC5 amplicon dilutions shown in **a** during the exponential phase of the PCR. At a gene-specific fluorescence value (*dashed line*), the crossing point is calculated by the fit point method. **c** Standard curve of the TRPC5 amplicon serial dilutions. Individual data points represent mean ±SEM of ten samples of equal amounts of TRPC5 amplicon copies. **d** Agarose gel electrophoresis of PCR products obtained in **a** after 50 cycles of PCR amplification. The TRPC5 amplicon size is 210bp.

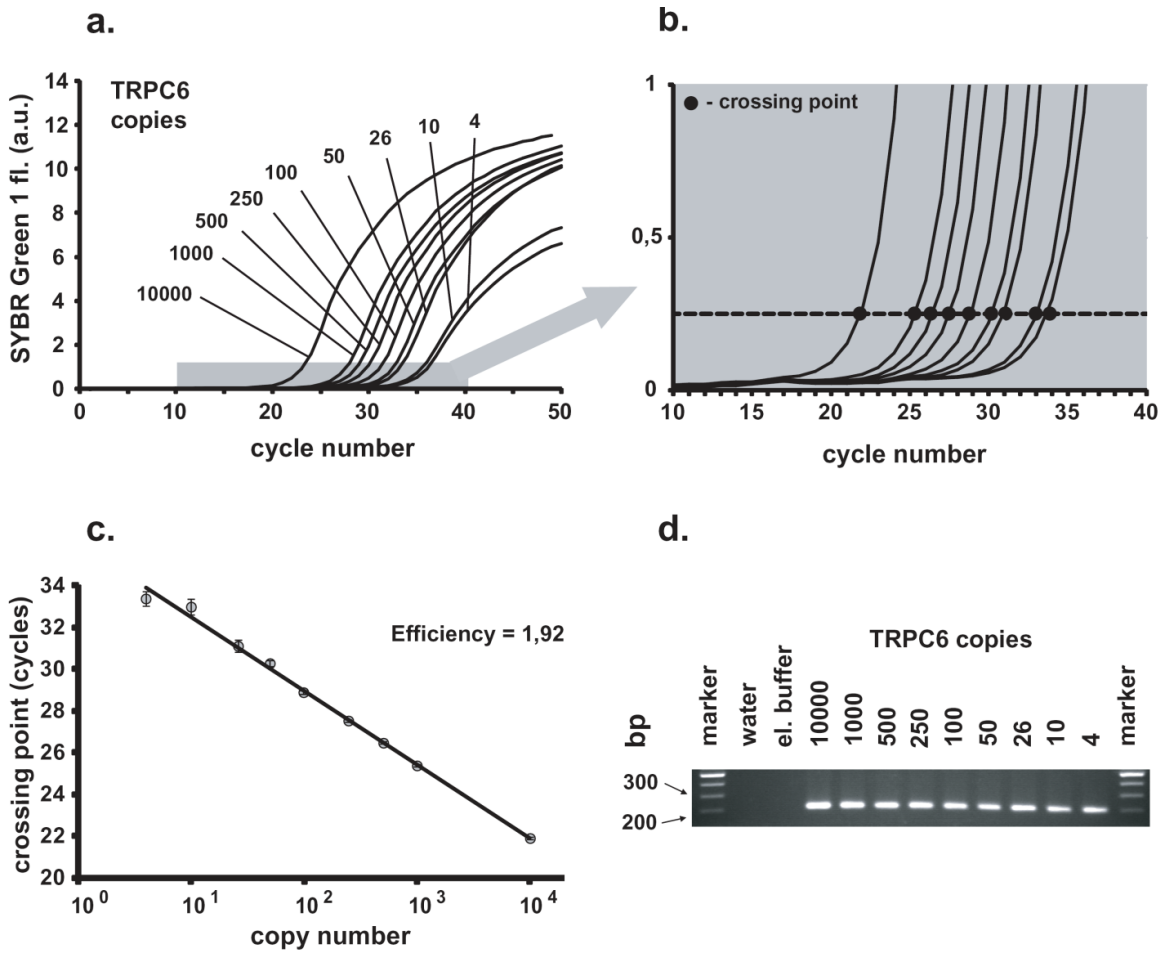

Figure 3.7 PCR calibration with TRPC6 amplicons.

a Real-time monitoring of the fluorescence emission of SYBR Green I during the PCR amplification of defined amounts of TRPC6 amplicons (serial dilutions containing 4-10,000 copies in this example). The small *grey rectangle* is enlarged in **b**. **b** Fluorescence monitoring of the PCR amplification of the TRPC6 amplicon dilutions shown in **a** during the exponential phase of the PCR. At a gene-specific fluorescence value (*dashed line*), the crossing point is calculated by the fit point method. **c** Standard curve of the TRPC6 amplicon serial dilutions. Individual data points represent mean ±SEM of ten samples of equal amounts of TRPC6 amplicon copies. **d** Agarose gel electrophoresis of PCR products obtained in **a** after 50 cycles of PCR amplification. The TRPC6 amplicon size is 209bp.

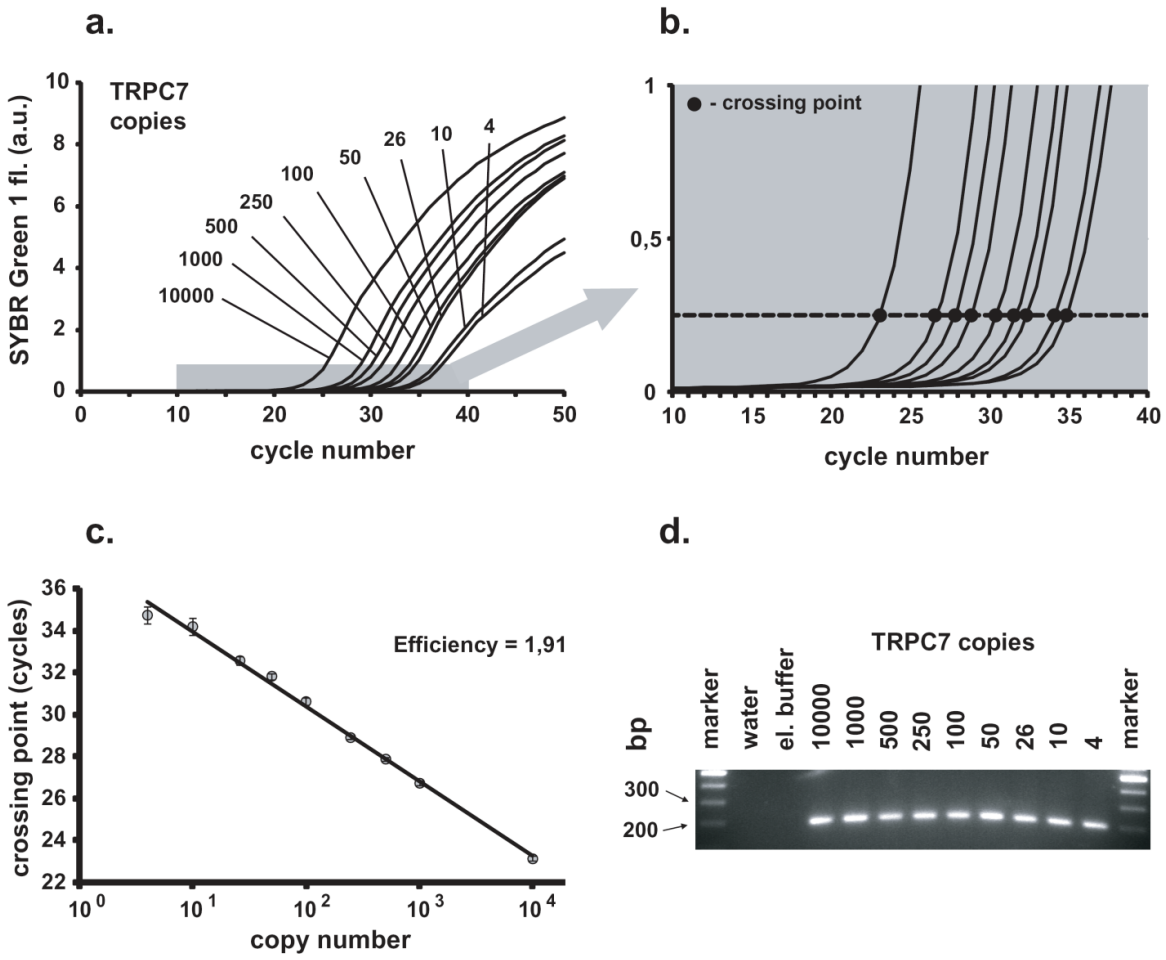

Figure 3.8 PCR calibration with TRPC7 amplicons.

a Real-time monitoring of the fluorescence emission of SYBR Green I during the PCR amplification of defined amounts of TRPC7 amplicons (serial dilutions containing 4-10,000 copies in this example). The small *grey rectangle* is enlarged in **b**. **b** Fluorescence monitoring of the PCR amplification of the TRPC7 amplicon dilutions shown in **a** during the exponential phase of the PCR. At a gene-specific fluorescence value (*dashed line*), the crossing point is calculated by the fit point method. **c** Standard curve of the TRPC7 amplicon serial dilutions. Individual data points represent mean ±SEM of ten samples of equal amounts of TRPC7 amplicon copies. **d** Agarose gel electrophoresis of PCR products obtained in **a** after 50 cycles of PCR amplification. The TRPC7 amplicon size is 205bp.

The slopes of the curves and the Y interceptions (see 2.2.12.3) for the calculation of TRPC1-7 subunit copy numbers from the unknown samples were obtained from the TRPC subunit specific master standard curves. The slopes of the master standard curves were also used to calculate the efficiencies of the TRPC subunit specific PCR assay (see 2.2.12.1). The values of the slopes, Y-interceptions

and the calculated efficiencies of TRPC1-7 gene specific master standard curves are listed in the Table 3.3.

Table 3.3 Parameters of the TRPC1-7 gene-specific high-resolution master external standard curves

gene	mean slope	Y-interception	efficiency	regression
TRPC1	- 3,382	35,32	1,98	0,994
TRPC3	- 3,45	34,48	1,95	0,999
TRPC4	- 3,489	34,27	1,93	0,999
TRPC5	- 3,683	36,71	1,87	0,999
TRPC6	- 3,533	36,06	1,92	0,994
TRPC7	- 3,56	36,85	1,91	0,994

3.6 Verification of external standard curves efficiencies

Since the master high resolution external curves for TRPC1-7 subunits were created using the plasmid DNA, the verification of the standard curves efficiencies needed to be performed on the native material. Therefore, the RNA standard curves were created.

The total RNA was isolated from the mouse whole brain and cerebellum (see 2.2.3). The isolated RNA was quantified in “Gene Quant” Spectrophotometer (Pharmacia) at 260nm (see 2.2.6). After the quantification, RNA was diluted in five steps, from 10ng to 100pg per 2µl standard volume. Only in the case of TRPC7, due to the low expression levels in the brain, RNA was diluted in three steps, from 50ng to 5ng. The reverse transcription reaction was done on these dilutions (see 2.2.9.1). Next, the cDNA was purified as described above. Analogous to the creation of the high resolution external standard curves, different cDNA dilutions were amplified in real-time PCR runs. For each of the TRPC subunits, real-time PCR runs of cDNA dilutions were repeated five times. The mean values of SYBR Green I fluorescence for each cycle were plotted against the cycle numbers as presented in the panel **a** of Figures 3.9 – 3.14. The exponential phase of the runs, where quantification is possible, is presented in the panel **b** of

Figures 3.9 – 3.14. The dashed line on the panel **b** of the Figures 3.9 – 3.14 represents the noise band set at 0.25 for all of the TRPC subunits specific runs (see 3.5). The crossing point values of the cDNA dilutions were collected from the repeated runs and the mean values were calculated for each standard. The mean values of crossing points for different RNA dilutions were plotted against the logarithm of the RNA concentration corresponding to these dilutions to create specific RNA standard curves (panel **c** in Figures 3.9 – 3.14). The RT reactions yielded highly reproducible results.

The real-time PCR products of the RNA dilution runs were verified by melting curve analysis and agarose gel electrophoresis (panel **d** in Figures 3.9. – 3.14). The negative controls in these reactions were water as the PCR run control, the RNase free elution water used in preparation of the RNA dilutions, as a control for the contamination of the standard dilutions. The reactions without reverse transcriptase (no RT) served as control for genomic contamination.

Analogous to high-resolution gene-specific standard curves, the RNA standard curves parameters were obtained and are described in Table 3.4. The efficiencies of the TRPC specific real-time PCR assays obtained for high resolution standard curves are comparable with the efficiencies values of RNA standard curves. This shows that TRPC specific real-time PCR assays are applicable to the native cDNA samples and are useful for the quantification in single Purkinje cells.

Table 3.4 Parameters of the TRPC1-7 gene-specific RNA standard curves

gene	mean slope	Y-interception	efficiency	regression
TRPC1	- 3,552	36,32	1,91	0,999
TRPC3	- 3,539	34,95	1,92	0,997
TRPC4	- 3,568	38,48	1,91	0,988
TRPC5	- 3,703	39,88	1,86	0,989
TRPC6	- 3,576	40,63	1,90	0,980
TRPC7	- 3,493	41,82	1,93	0,969

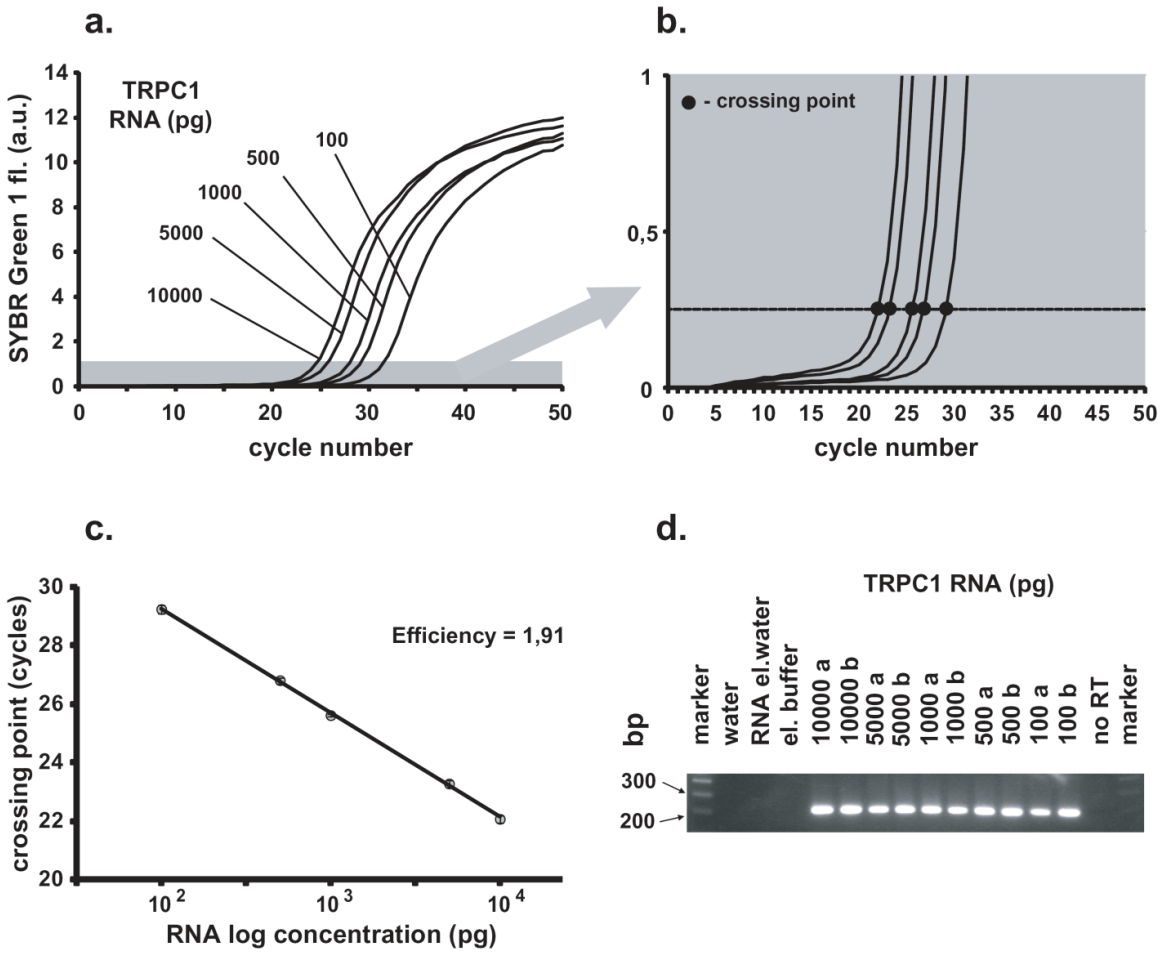

Figure 3.9 PCR calibration with brain total RNA TRPC1 amplicons.

a Real-time monitoring of the fluorescence emission of SYBR Green I during the TRPC1 specific RT-PCR amplification of defined amounts of total brain RNA (serial dilutions containing 100-10,000pg total brain RNA). The small *grey rectangle* is enlarged in **b**. **b** Fluorescence monitoring of the PCR amplification of the TRPC1 specific RT-PCR amplification shown in **a** during the exponential phase of the PCR. At a gene-specific fluorescence value (*dashed line*), the crossing point is calculated by the fit point method. **c** Correlation between the amount of total brain RNA and the corresponding TRPC1 cycle crossing points. Individual data points represent mean ±SEM of five samples of equal amounts of total brain RNA. **d** Agarose gel electrophoresis of PCR products obtained in **a** after 50 cycles of PCR amplification. The TRPC1 amplicon size is 209bp.

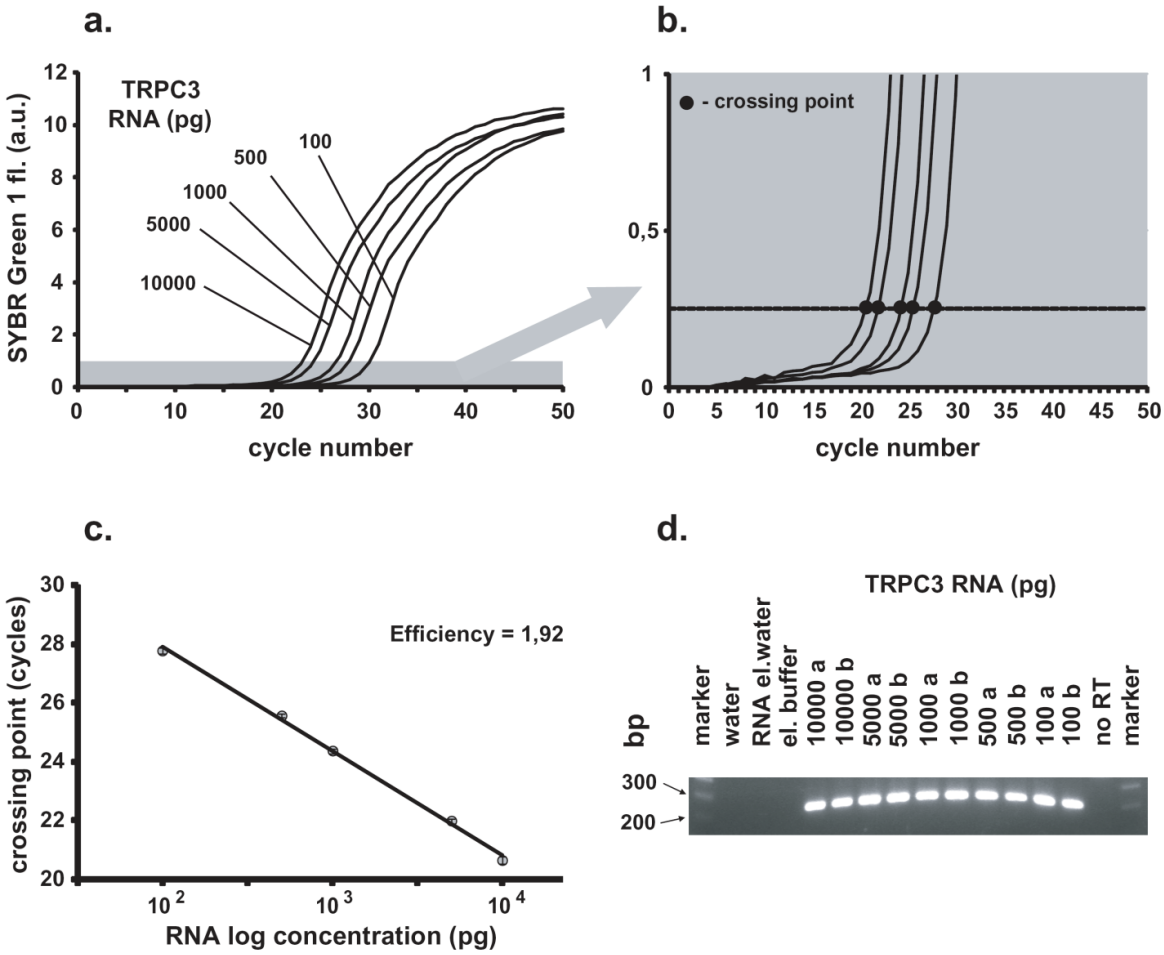

Figure 3.10 PCR calibration with brain total RNA TRPC3 amplicons.

a Real-time monitoring of the fluorescence emission of SYBR Green I during the TRPC3 specific RT-PCR amplification of defined amounts of total brain RNA (serial dilutions containing 100-10,000pg total brain RNA). The small *grey rectangle* is enlarged in **b**. **b** Fluorescence monitoring of the PCR amplification of the TRPC3 specific RT-PCR amplification shown in **a** during the exponential phase of the PCR. At a gene-specific fluorescence value (*dashed line*), the crossing point is calculated by the fit point method. **c** Correlation between the amount of total brain RNA and the corresponding TRPC3 cycle crossing points. Individual data points represent mean ±SEM of five samples of equal amounts of total brain RNA. **d** Agarose gel electrophoresis of PCR products obtained in **a** after 50 cycles of PCR amplification. The TRPC3 amplicon size is 207bp.

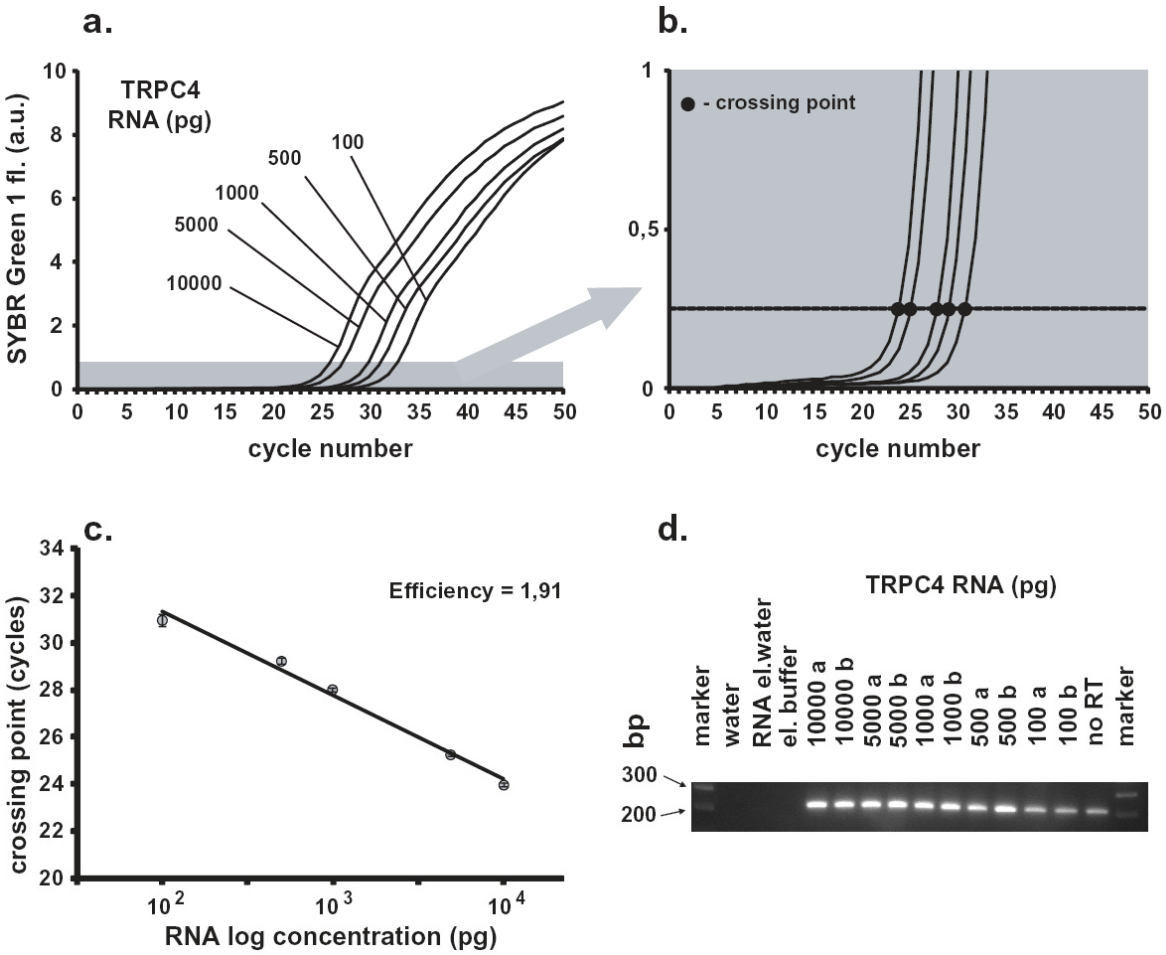

Figure 3.11 PCR calibration with brain total RNA TRPC4 amplicons.

a Real-time monitoring of the fluorescence emission of SYBR Green I during the TRPC4 specific RT-PCR amplification of defined amounts of total brain RNA (serial dilutions containing 100-10,000pg total brain RNA). The small *grey rectangle* is enlarged in **b**. **b** Fluorescence monitoring of the PCR amplification of the TRPC4 specific RT-PCR amplification shown in **a** during the exponential phase of the PCR. At a gene-specific fluorescence value (*dashed line*), the crossing point is calculated by the fit point method. **c** Correlation between the amount of total brain RNA and the corresponding TRPC4 cycle crossing points. Individual data points represent mean ±SEM of five samples of equal amounts of total brain RNA. **d** Agarose gel electrophoresis of PCR products obtained in **a** after 50 cycles of PCR amplification. The TRPC4 amplicon size is 217bp.

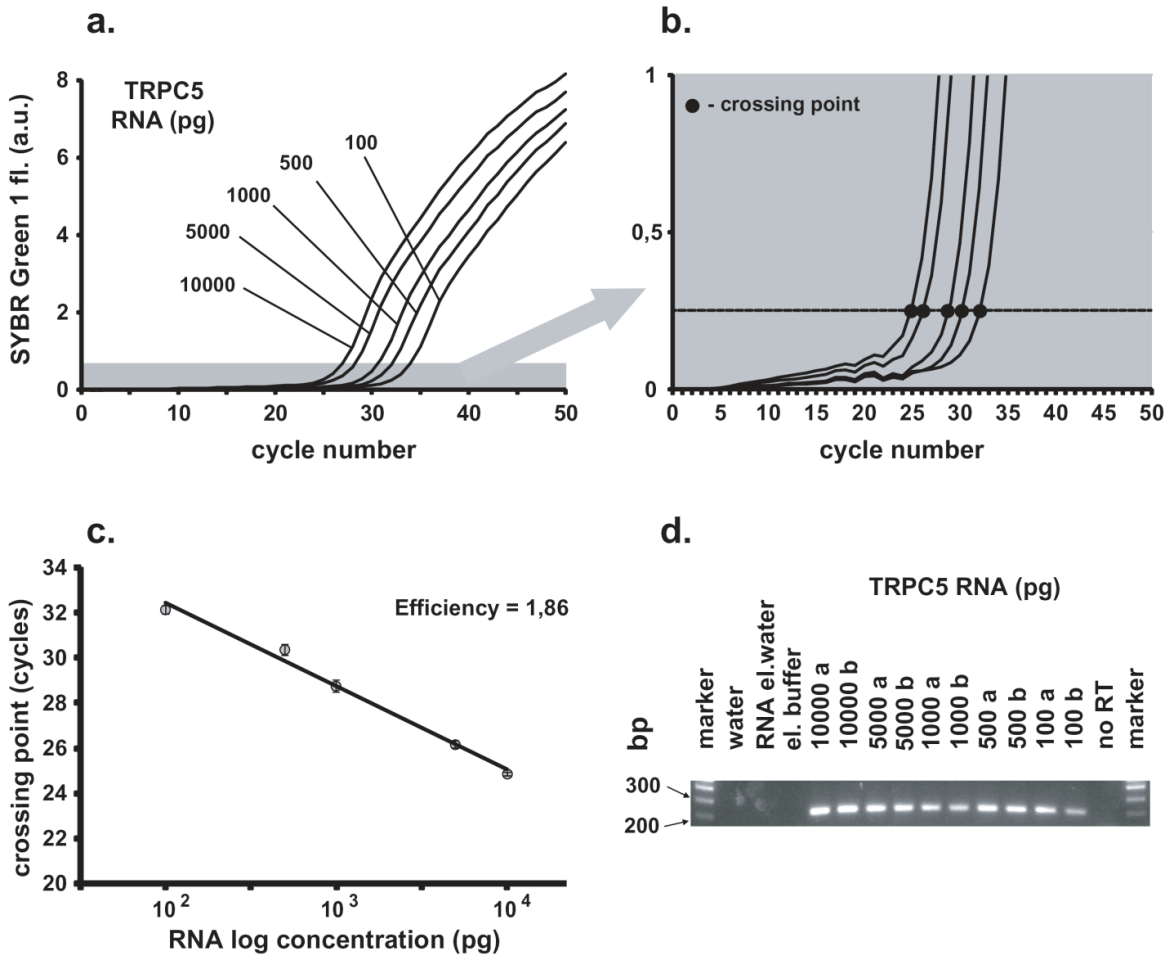

Figure 3.12 PCR calibration with brain total RNA TRPC5 amplicons.

a Real-time monitoring of the fluorescence emission of SYBR Green I during the TRPC5 specific RT-PCR amplification of defined amounts of total brain RNA (serial dilutions containing 100-10,000pg total brain RNA). The small *grey rectangle* is enlarged in **b**. **b** Fluorescence monitoring of the PCR amplification of the TRPC5 specific RT-PCR amplification shown in **a** during the exponential phase of the PCR. At a gene-specific fluorescence value (*dashed line*), the crossing point is calculated by the fit point method. **c** Correlation between the amount of total brain RNA and the corresponding TRPC5 cycle crossing points. Individual data points represent mean ±SEM of five samples of equal amounts of total brain RNA. **d** Agarose gel electrophoresis of PCR products obtained in **a** after 50 cycles of PCR amplification. The TRPC5 amplicon size is 210bp.

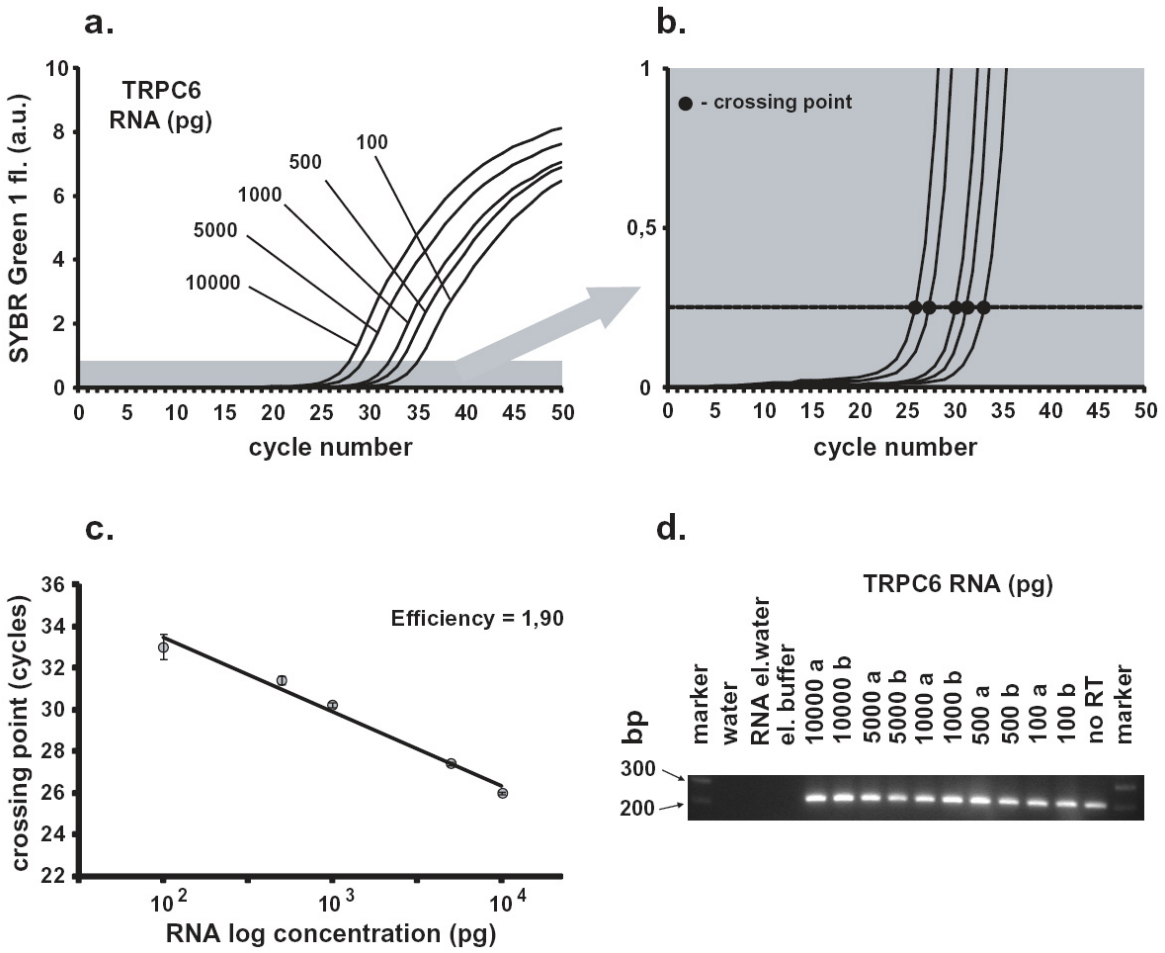

Figure 3.13 PCR calibration with brain total RNA TRPC6 amplicons.

a Real-time monitoring of the fluorescence emission of SYBR Green I during the TRPC6 specific RT-PCR amplification of defined amounts of total brain RNA (serial dilutions containing 100-10,000pg total brain RNA). The small *grey rectangle* is enlarged in **b**. **b** Fluorescence monitoring of the PCR amplification of the TRPC6 specific RT-PCR amplification shown in **a** during the exponential phase of the PCR. At a gene-specific fluorescence value (*dashed line*), the crossing point is calculated by the fit point method. **c** Correlation between the amount of total brain RNA and the corresponding TRPC6 cycle crossing points. Individual data points represent mean ±SEM of five samples of equal amounts of total brain RNA. **d** Agarose gel electrophoresis of PCR products obtained in **a** after 50 cycles of PCR amplification. The TRPC6 amplicon size is 209bp.

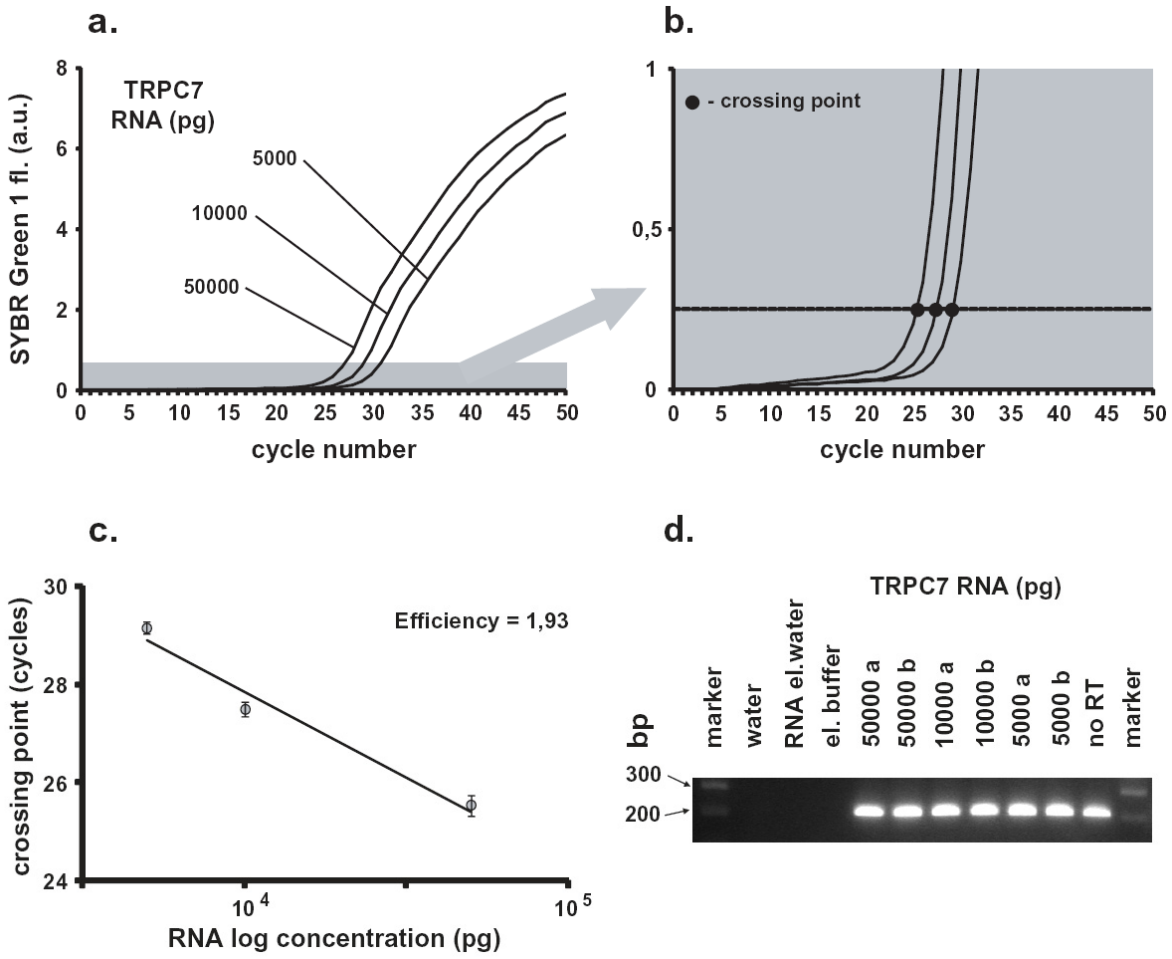

Figure 3.14 PCR calibration with brain total RNA TRPC7 amplicons.

a Real-time monitoring of the fluorescence emission of SYBR Green I during the TRPC7 specific RT-PCR amplification of defined amounts of total brain RNA (serial dilutions containing 100-10,000pg total brain RNA). The small *grey rectangle* is enlarged in **b**. **b** Fluorescence monitoring of the PCR amplification of the TRPC7 specific RT-PCR amplification shown in **a** during the exponential phase of the PCR. At a gene-specific fluorescence value (*dashed line*), the crossing point is calculated by the fit point method. **c** Correlation between the amount of total brain RNA and the corresponding TRPC7 cycle crossing points. Individual data points represent mean ±SEM of five samples of equal amount of total brain RNA. **d** Agarose gel electrophoresis of PCR products obtained in **a** after 50 cycles of PCR amplification. The TRPC7 amplicon size is 205bp.

3.7 Calculation of TRPC subunit copy numbers

After the verification of the high-resolution TRPC specific standard curves, the copy number of individual TRPC subunits in unknown samples, such as single cells or tissue total RNA, was determined. The copy numbers were calculated by using the slope and the Y-intercept value of the gene-specific standard curves (see 2.2.12.3). The

formulas used for the quantification of TRPC subunit copy number for unknown samples are listed below.

$$\text{TRPC1 copy number} = 10^{(35{,}32\text{-cross.point})/3{,}382}$$

$$\text{TRPC3 copy number} = 10^{(34{,}48\text{-cross.point})/3{,}450}$$

$$\text{TRPC4 copy number} = 10^{(34{,}27\text{-cross.point})/3{,}489}$$

$$\text{TRPC5 copy number} = 10^{(36{,}71\text{-cross.point})/3{,}683}$$

$$\text{TRPC6 copy number} = 10^{(36{,}06\text{-cross.point})/3{,}533}$$

$$\text{TRPC7 copy number} = 10^{(36{,}85\text{-cross.point})/3{,}560}$$

3.8 Quantification of TRPC subunit expression in the brain

The quantification of the TRPC subunit expression was performed using cDNA material from the whole brain as well as the cerebellum of mice. After the total RNA isolation and purification from these tissues, the quantification was performed in “Gene Quant” Spectrophotometer (Pharmacia) at 260nm (see 2.2.3 and 2.2.6). The RT reactions were performed on 1ng whole brain and cerebellar total RNA (see 2.2.9.1). The RT reactions and subsequent TRPC subunit quantification was performed on all isolated RNA. In order to obtain the absolute copy number of different TRPC subunits per 1ng total RNA, crossing point values of all TRPC gene-specific runs were determined and calculated into copy numbers by using gene-specific standard curves. The mean values of the TRPC1-7 specific copy numbers of all runs are presented in Figure 3.15.

The panel **a** in the Figure 3.15 shows that TRPC1 is the most abundant TRPC subunit in the whole brain, with the mean copy number of 342,7±28,9 copies/ng total RNA, followed by TRPC3 with 141±11,8 copies/ng total RNA. TRPC4 and TRPC5 have expression levels of 100±7 copies/ng total RNA and 95,6±7,5 copies/ng total RNA,

respectively. TRPC6 is present with 76,7±8 copies/ng total RNA and the subunit with the lowest expression in the whole brain was TRPC7 (32,5±3,5 copies/ng total RNA).

In the cerebellum (panel **b**, Figure 3.15), TRPC1 and TRPC3 have similar expression levels of 744±72,3 copies/ng total RNA and 882,7±53,7 copies/ng total RNA, respectively. This expression is approximately one order of magnitude higher than the expression level of TRPC5 and TRPC7 subunits, present in the cerebellum with 85,7±5,8 copies/ng total RNA and 81,9±14,9 copies/ng total RNA, respectively. The TRPC subunits TRPC4 and TRPC6 have been found to have the lowest expression levels in the cerebellum with 33,5±4,3 copies/ng total RNA and 32,1±7,9 copies/ng total RNA.

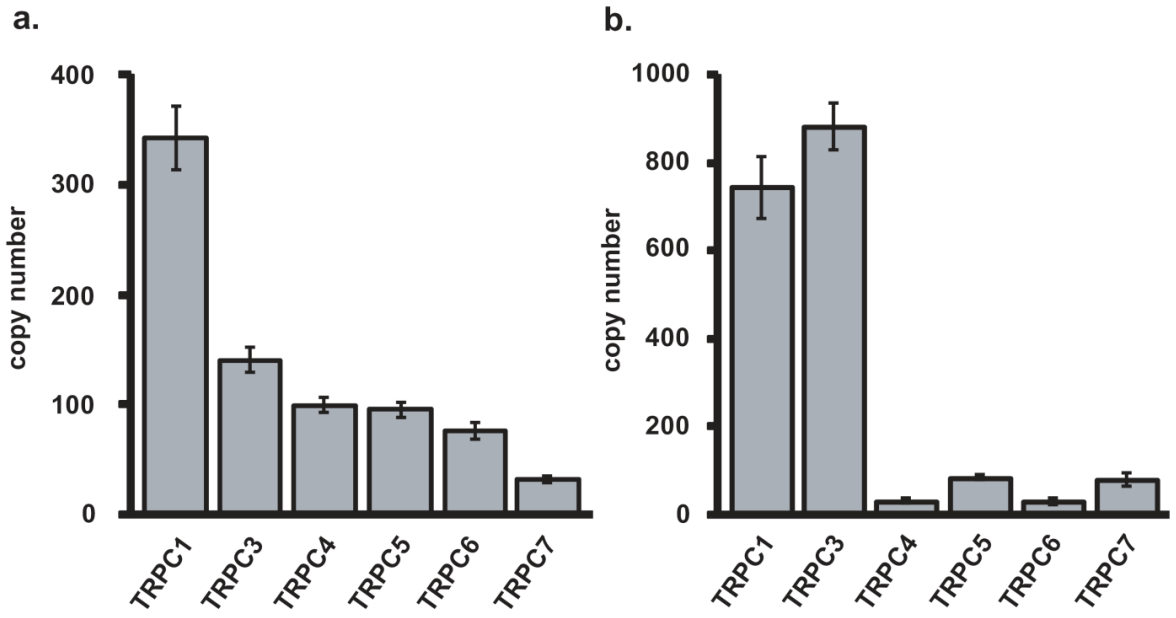

Figure 3.15 Expression levels of TRPC subunits in the whole brain and cerebellum. Mean copy number ±SEM of TRPC subunits per 1ng total RNA in the whole brain (**a**) and cerebellum (**b**) of the wild type animals. (detailed information in the text)

3.9 Quantitative single-cell RT-PCR

The Figure 3.16 shows a scheme of the individual steps of the quantitative single Purkinje cell RT-PCR. During the cell harvest procedure, cells were first visualized. Selected cells were harvested using wide-tipped glass pipettes (see 2.2.8.3). Directly after the harvest, the material was pressure injected into a PCR tube containing previously prepared RT mix solution (see Figure 2.1). The RT solution also contained the detergent Igepal (chemical substitute of Nonidet P40) to rupture the cell membrane (see 2.1.2).

Then, the standard RT reaction using random hexamers was performed for three hours (see 2.2.9.2). It has been reported that some components of the RT reaction, and especially the reverse transcriptase itself, reduce the PCR efficiency, presumably by inhibiting *Taq*-polymerase (Chandler et al., 1998; Pfaffl, 2001; Liss, 2002). Due to this problem, a mandatory step after the RT reactions was the purification of cDNA (see 2.2.10).

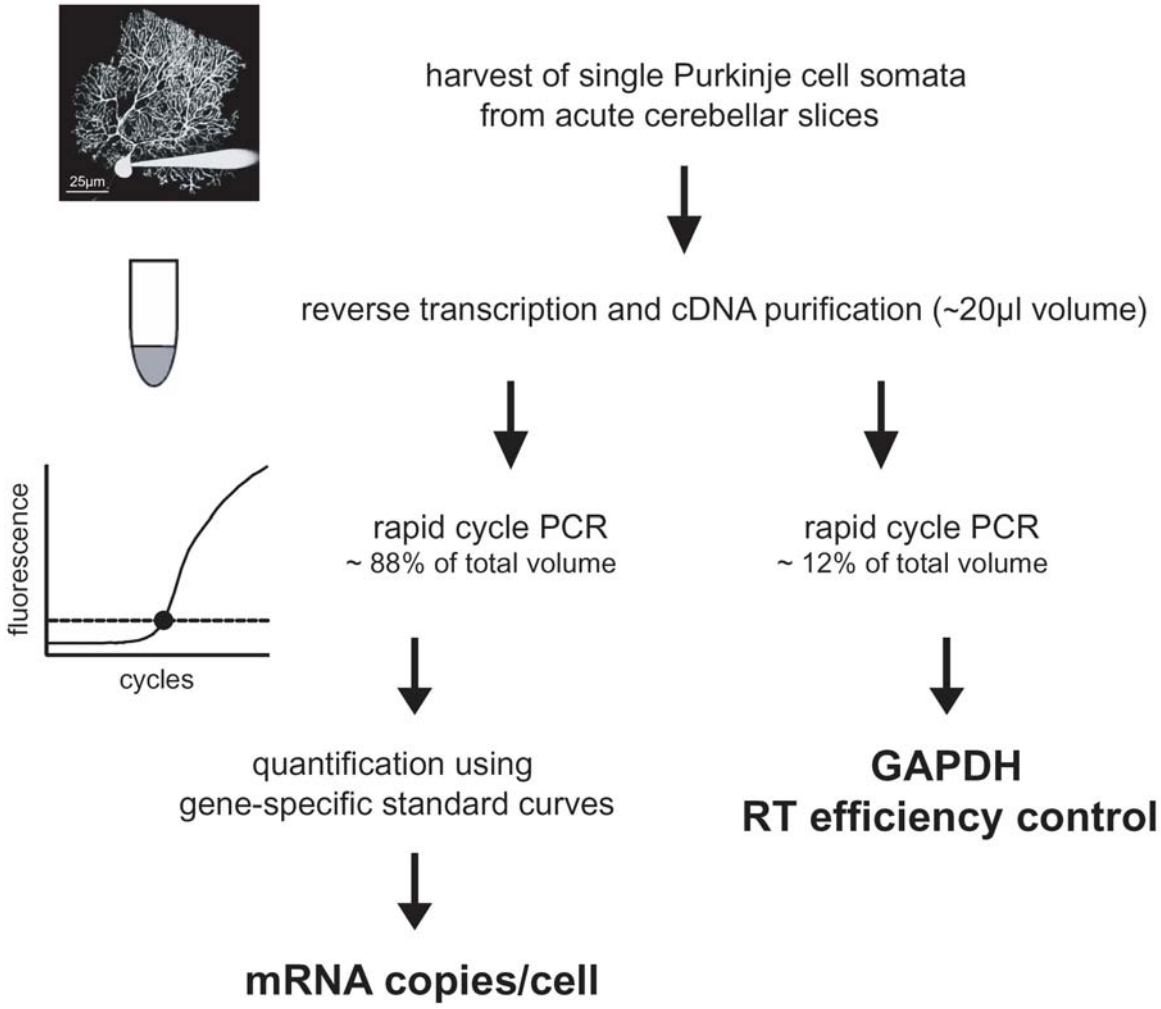

Figure 3.16 Illustration of the experimental approach for the harvest of a single Purkinje cell and the gene-specific quantification strategy. Single Purkinje cell somata are harvested from acute cerebellar slices. After reverse transcription and single-cell cDNA purification, rapid cycle PCR is performed in a LightCycler (Roche). TRPC copy numbers are determined by using the gene-specific standard curves. GAPDH (glyceraldehyde-3-phosphate dehydrogenase) was used to control the RT reaction.

After the cDNA purification, the RT reaction volume was divided in two parts and the real-time monitoring of PCR kinetics was performed using the LightCycler (Roche). The first part, corresponding to the 88% of the RT reaction was used for TRPC subunit expression quantification. The mRNA levels in single cells obtained in this way were

quantified using previously established gene-specific, high-resolution external standard curves (see 2.2.12.3). The second part of the RT, corresponding to the 12% of the RT reaction was used as a control for the efficiency of the RT reaction itself. The “housekeeping” gene, glyceraldehyde-3-phosphate dehydrogenase (GAPDH), was the gene of choice to control the performance of the RT reaction (see 3.9.1.2).

3.9.1 Control experiments

The complexity of the single-cell quantitative RT-PCR procedure (see Figure 3.16) necessitated the design of additional control experiments, in order to verify the results obtained after the quantification.

3.9.1.1 Cell harvest controls

Since high negative pressure was applied on the cells during the cell harvest, a control was necessary to verify that the harvest strategy carried minimal risk of contamination with the neuropil surrounding the cell. Therefore, the harvest procedure was simulated in the extracellular region of the slice preparation, close to the Purkinje cell. In this way neuropil surrounding the cell was collected. The test times for the negative pressure applications were 1s, 3s, and 5s. After the harvest, samples containing neuropil have gone through the same experimental procedures as harvested cells have. Meaning, the RT reactions, the cDNA purification and finally the real-time quantitative PCR specific for TRPC1-7 subunits and GAPDH were performed on these samples.

The Figure 3.17 depicts the amplification curves obtained from neuropil control samples during the real-time PCR runs specific for TRPC1-7 subunits and GAPDH. No correlation was observed between 1s (black traces), 3s (green traces) and 5s (red traces) of the negative pressure applications. No significant presence of TRPC1, TRPC3, TRPC4, TRPC5 and TRPC7 was detected in the harvested neuropil. However, TRPC6 was detected in the harvested neuropil, with mean copy number of 4,9 (panels **a**-**f**, Figure 3.17). The majority of the samples showed amplification curves for GAPDH, but the crossing points of these curves were above the acceptable range meaning that they can be discarded (see 3.9.1.2).

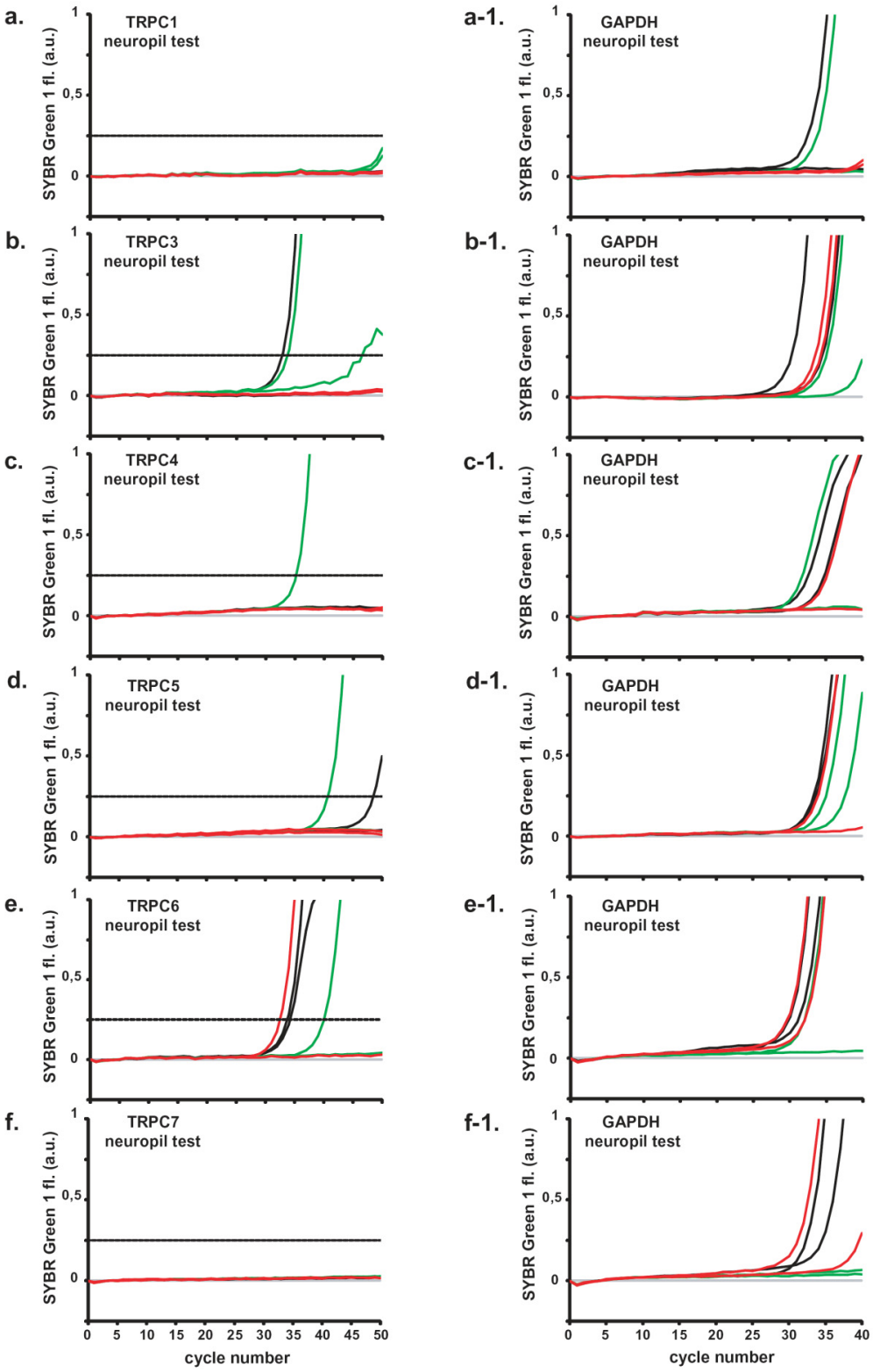

Figure 3.17 Screening of the neuropil surrounding the test cells for DNA/RNA contamination. a-f Real-time fluorescence monitoring of the PCR amplification of the different TRPC subunits from the neuropil surrounding the test cells. **a1-f1** GAPDH control runs.

legend: ■ – 1s neuropil suction; ■ – 3s neuropil suction; ■ – 5s neuropil suction.

3.9.1.2 RT efficiency controls

In order to insure that all the investigated samples had comparable RT efficiencies, glyceraldehyde-3-phosphate dehydrogenase (GAPDH) was chosen. The 20% of the single cell material (2µl per purified cell material) was used in these control reactions (see Figure 3.16). Since it was not necessary to quantify copy numbers of GAPDH in the samples, crossing points were automatically calculated by the LightCycler Software 3.5 (Roche, Mannheim), using the standard derivate maximum method (Rasmussen, 2001). The Figure 3.18 shows a plot of the crossing point values over the corresponding cell numbers. Previous reports showed, and our data confirmed the statement that intrinsic GAPDH transcripts cannot be used as a denominator due to the considerable variation in the expression level between individual cells (Bustin, 2002; Liss, 2002; Piper and Holt, 2004; Durand et al., 2006). Since we needed to compare a high number of cells for the expression of TRPC subunits, it was necessary to define a comparable RT reaction efficiency for all the cells. Therefore, the GAPDH crossing points of all samples and control reactions were analyzed. Based on these data, GAPDH expression levels in single cells, in the range of crossing point 26,5 until 32 (±1,5σ), were considered to be suitable for further analysis and TRPC subunit quantification.

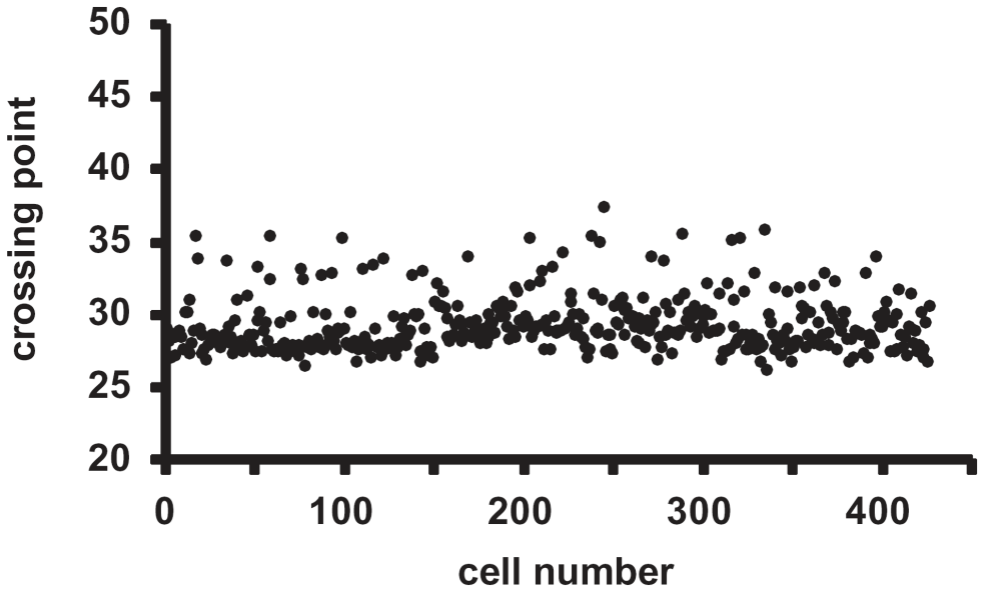

Figure 3.18 Glyceraldehyde-3-phosphate dehydrogenase (GAPDH) expression in single Purkinje cells and control reactions. Crossing points of GAPDH amplification curves specific for single Purkinje cells were ploted against the corresponding cell number.

.

3.9.2 TRPC subunit expression pattern in single Purkinje neurons of the wild type mice

The panels **a-f** of the Figure 3.19 depict the amplification curves of PCR cycles for TRPC1, TRPC3, TRPC4, TRPC5, TRPC6 and TRPC7 in single Purkinje cells of adult wild type mice, as yielded by the LightCycler (Roche, Mannheim). For each Purkinje cell, GAPDH control was performed (panels **a1-f1** in Figure 3.19) and only the cells with an acceptable range of the GAPDH crossing point values have been analyzed (see 3.9.1.2). Since a part of the harvested cell had to be used for the GAPDH control reactions, quantification was done with the 80% of the single Purkinje cell sample volume.

All TRPC subunits were found to be present in the cerebellar Purkinje cells. The TRPC2 subunit was not analyzed due to the fact that it is primarily expressed in the mammalian VNO and testis (Vannier et al., 1999; Jungnickel et al., 2001; Kimchi et al., 2007). Out of the 28 investigated cells, 24 were positive for TRPC1. The TRPC3 subunit was found in the 31 out of 34, and TRPC4 in the 22 out of 32 investigated cells. Half of the 30 investigated cells were positive for TRPC7. However, TRPC5 and TRPC6 were not found in the majority of the cells. TRPC5 was detected in the 7 out of 29, and TRPC6 in the 9 out of 24 investigated cells.

The products obtained from the real-time PCR runs on the single Purkinje cell material were verified by melting curve analysis (LightCycler 3.5 software) and agarose gel electrophoresis (Figure 3.20). In addition, representative samples were analyzed by DNA sequencing. As presented in the Figure 3.20, negative and positive controls were used in the real-time PCR runs. In all real-time PCR runs, water served as negative control. The elution buffer used in the purification of the cells served as cDNA purification control. Furthermore, the reactions without the reverse transcriptase (no RT) controlled for genomic contamination. Finally, the harvest procedure control was tested (see 3.9.1). Four TRPC specific standards were always amplified in parallel with the cells. These positive controls tested the run-specific real-time PCR efficiency.

The agarose gel electrophoresis was done for all real-time PCR runs, as an additional confirmation of the reaction products identity. The agarose gels prepared after TRPC subunit specific real-time PCR runs, using the single cell material of wild type animals, are presented in the Figure 3.20.

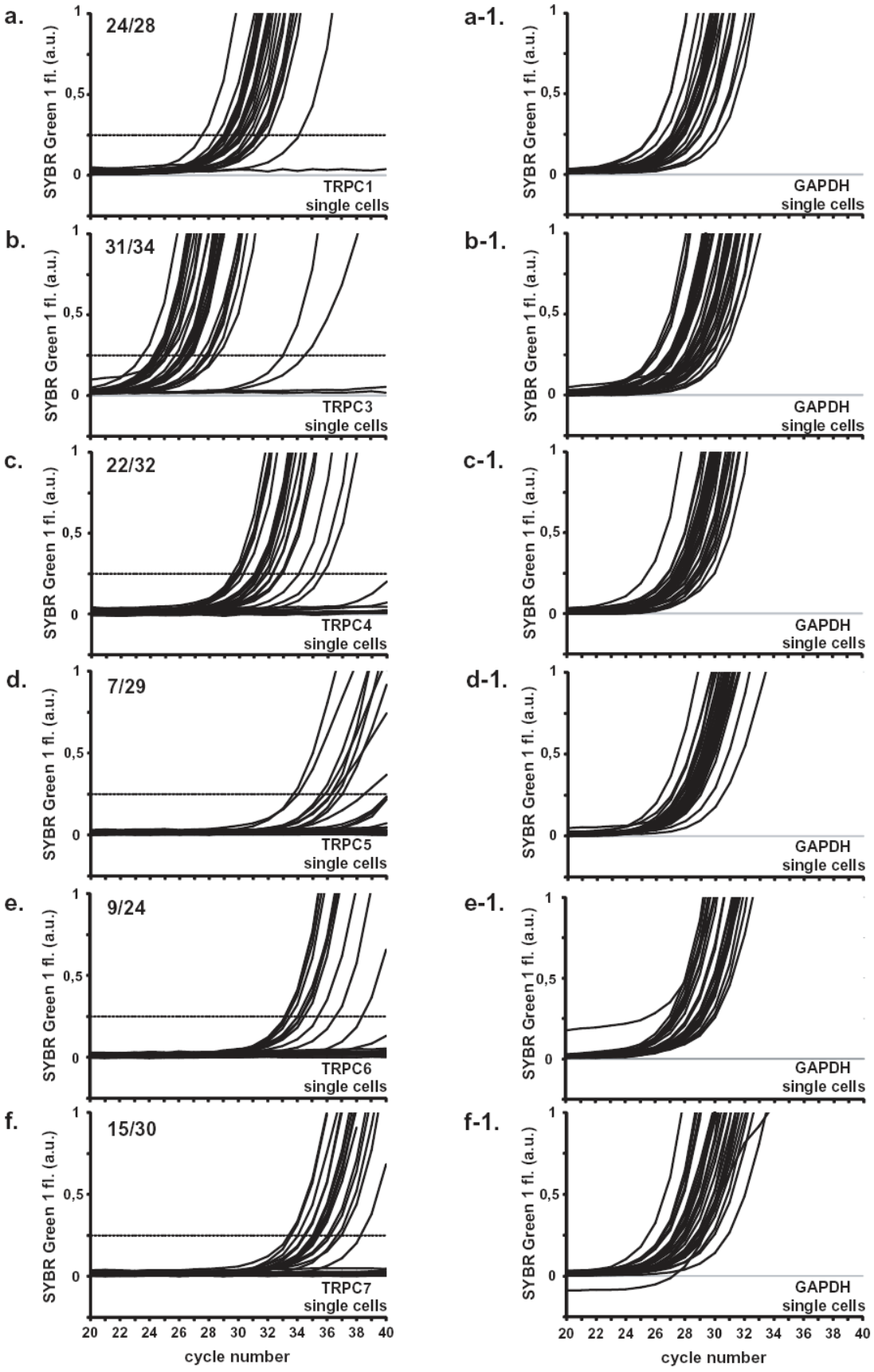
a.
24/28
TRPC1
single cells
a-1.
GAPDH
single cells
b.
31/34
TRPC3
single cells
b-1.
GAPDH
single cells
c.
22/32
TRPC4
single cells
c-1.
GAPDH
single cells
d.
7/29
TRPC5
single cells
d-1.
GAPDH
single cells
e.
9/24
TRPC6
single cells
e-1.
GAPDH
single cells
f.
15/30
TRPC7
single cells
f-1.
GAPDH
single cells
SYBR Green 1 fl. (a.u.)
0
0,5
1
20 22 24 26 28 30 32 34 36 38 40
cycle number

Figure 3.19 Real-time PCR amplification of cDNA from single Purkinje neurons in wild type animals. a-f. Amplification curves of PCR cycles for TRPC subunits amplification in single Purkinje neuron and control GAPDH amplification in the corresponding cells, **a1-f1,** as yielded by the LightCycler (Roche). At a gene-specific fluorescence value (*dashed line*), the crossing point is determined.

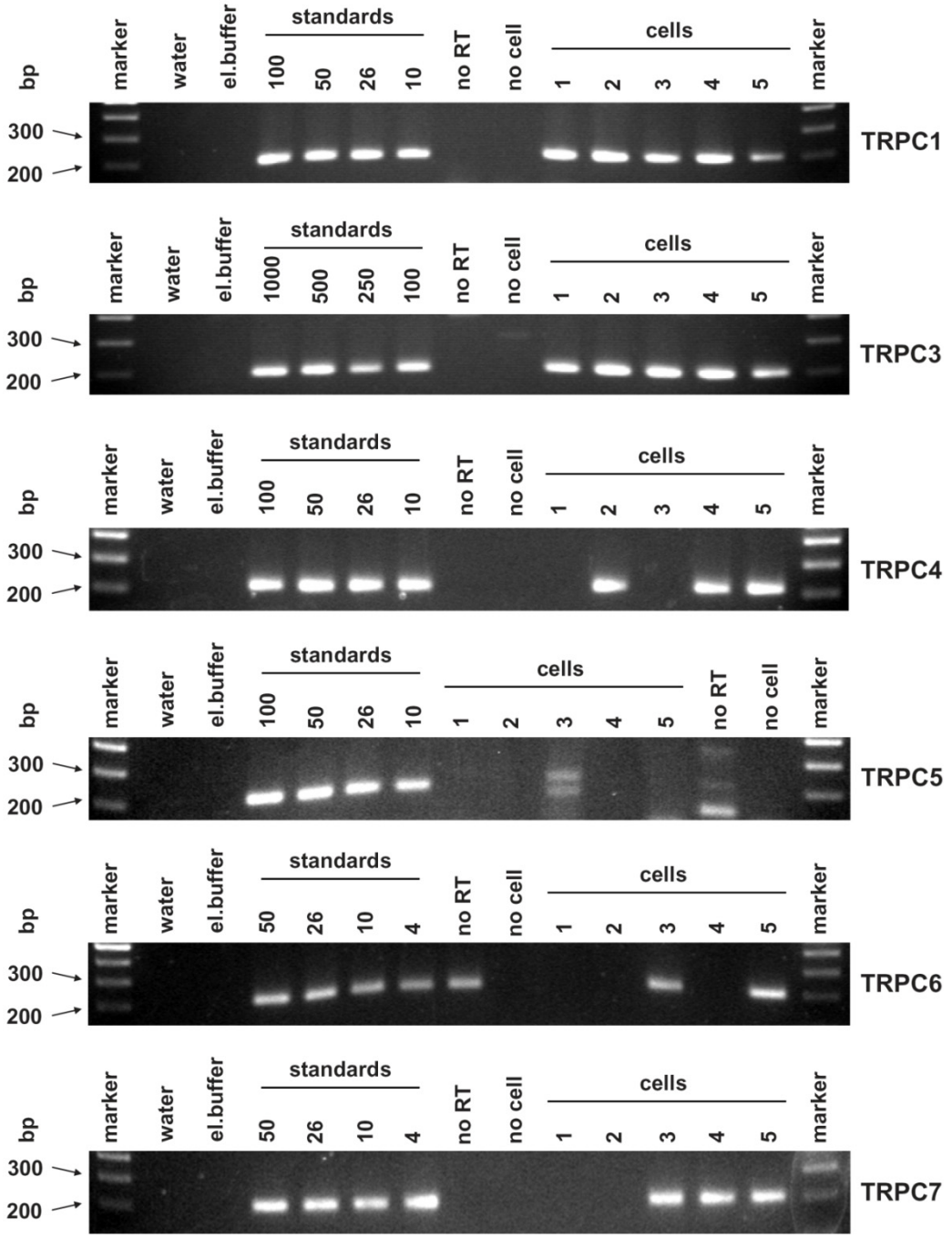

Figure 3.20 Agarose gel electrophoresis of real-time PCR products obtained from the single Purkinje cell material of the wild type animals. Water, elution buffer, the reaction without the reverse transcriptase, and the reaction without the harvested cell were used as negative controls. TRPC subunit specific standard dilutions served as positive controls. The corresponding copy number values of these standards are indicated. TRPC subunits amplicons are presented with the

bands of different sizes; 209bp for TRPC1, 207bp for TRPC3, 217bp for TRPC4, 210bp for TRPC5, 209bp for TRPC6 and 205bp for TRPC7.

The quantification of the TRPC1-7 subunits from the Purkinje cell material was performed by using fit point quantification method with a noise band always set to the value of 0,25 for the analysis of all TRPC subunits (see 2.2.12.3). The noise band is represented as a dashed line in the panels **a-f** of the Figure 3.19. When the crossing points were obtained, copy numbers of different TRPC subunits were calculated based on the parameters from the standard curves (see 3.7).

After the RT-PCR quantification, the mean copy numbers of the specific TRPC subunits in Purkinje cells were calculated. The histogram in the Figure 3.21 shows the TRPC subunit expression pattern in single Purkinje neurons. The TRPC3 subunit was the far most abundant TRPC subunit in cerebellar Purkinje cells of wild type animals, with an average copy number of 347,2±55,3 copies/cell. The TRPC1 subunit was present in one order of magnitude less than TRPC3, with 45,2±7,9 copies/cell. The TRPC4 subunit was detected with only 10,5±1,5 copies/cell. Other TRPC subunits showed very low expression levels in single Purkinje cells, below 5 copies/cell. TRPC5 was present with 2,8±0,96 copies/cell, TRPC6 with 4,3±0,6 copies/cell and finally TRPC7 with 3,66±0,64 copies/cell.

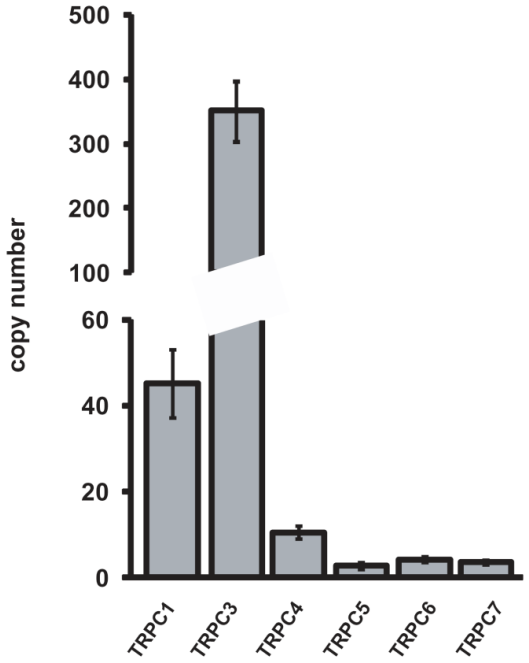

Figure 3.21 Expression levels of TRPC subunits in single Purkinje neurons of wild type animals. Histogram represents mean copy numbers ± SEM of TRPC subunits in single Purkinje neurons of wild type animals. Reactions positive for each corresponding TRPC subunits were took into account (TRPC1 24 of 28 experiments, 24/28; TRPC3 31/34; TRPC4 22/32; TRPC5 7/29; TRPC6 9/24; TRPC7 15/30).

3.9.3 TRPC subunit expression pattern in single Purkinje neurons of the TRPC1 knockout mice

The panels **a-f** of the Figure 3.22 depict the amplification curves of PCR cycles for TRPC3, TRPC4, TRPC5, TRPC6 and TRPC7 in single Purkinje cells of adult TRPC1 knockout mice as yielded by the LightCycler™ (Roche, Mannheim).

As for the analysis of the wild type Purkinje cells, GAPDH control was performed (panels **a1-f1** in Figure 3.22). Only the cells with the GAPDH crossing points in the range of 26,5 until 32 have been used in further quantification (see 3.9.1.2).

The TRPC3 subunit was found in the 32 out of 34 and the TRPC4 in the 17 out of 20 investigated cells. The TRPC6 and TRPC7 subunits were found to be expressed in the 9 out of 19 and 24 investigated cells, respectively. As already observed in the wild-type animals, the TRPC5 subunit was detected in very small number of cells (2 out of 24 cells).

After the verification by melting curve analysis (LightCycler 3.5 software), products were visualized by agarose gel electrophoresis (Figure 3.23). As shown in the Figure 3.23, the controls were tested as described above (see 3.9.2). The agarose gels prepared after TRPC subunit specific, the real-time PCR runs using the single cell material of TRPC1 knockout animals are presented in the Figure 3.23.

The quantification procedure for the TRPC1-7 subunits cDNA was repeated for the single Purkinje cells of the TRPC1 knockout animals (compare with 3.9.2). After the RT-PCR quantification procedure, the mean copy numbers of the specific TRPC subunits in Purkinje cells were calculated. The histogram in the panel **b** of the Figure 3.24 shows the TRPC subunit expression pattern in the single Purkinje neurons of the TRPC1 animals. Again, the TRPC3 subunit was found to be the far most abundant TRPC subunit with an average copy number of 183,5±19,6 copies/cell. The TRPC4 subunit was detected with only 11,6±2,1 copies/cell. As found in the wild type analysis, other TRPC subunits showed very low expression levels. TRPC6 was present with 8±3,5 copies/cell, TRPC7 with 3,4±0,8 copies/cell, and TRPC5 with only 1,6±0,35 copies/cell.

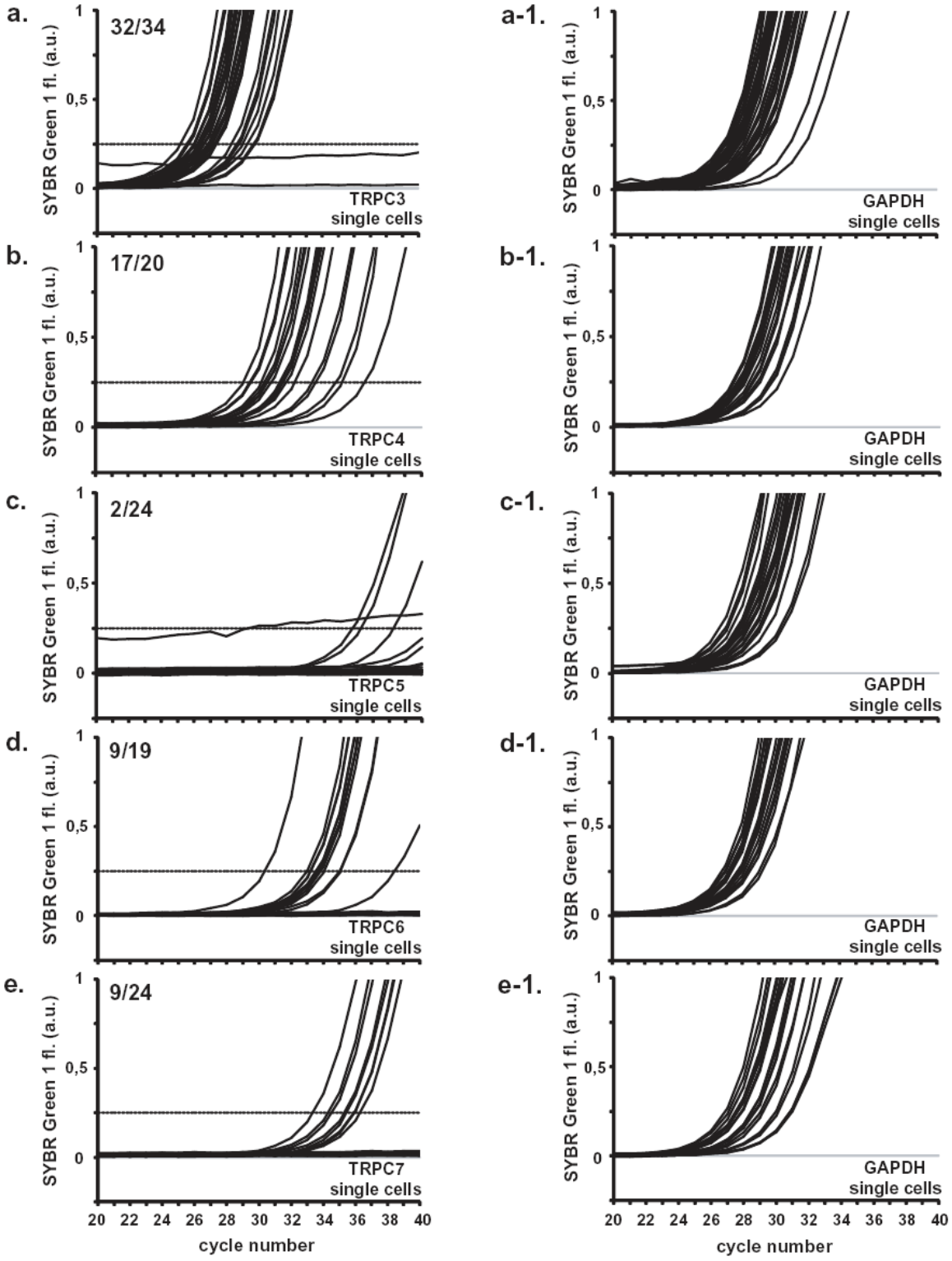

Figure 3.22 Real-time PCR amplification of cDNA from single Purkinje neurons in TRPC1 knockout animals. a-f. Amplification curves of PCR cycles for TRPC subunits amplification in single Purkinje neuron and control GAPDH amplification in the corresponding cells, **a1-f1,** as yielded by the LightCycler (Roche). At a gene-specific fluorescence value (*dashed line*), the crossing point was determined.

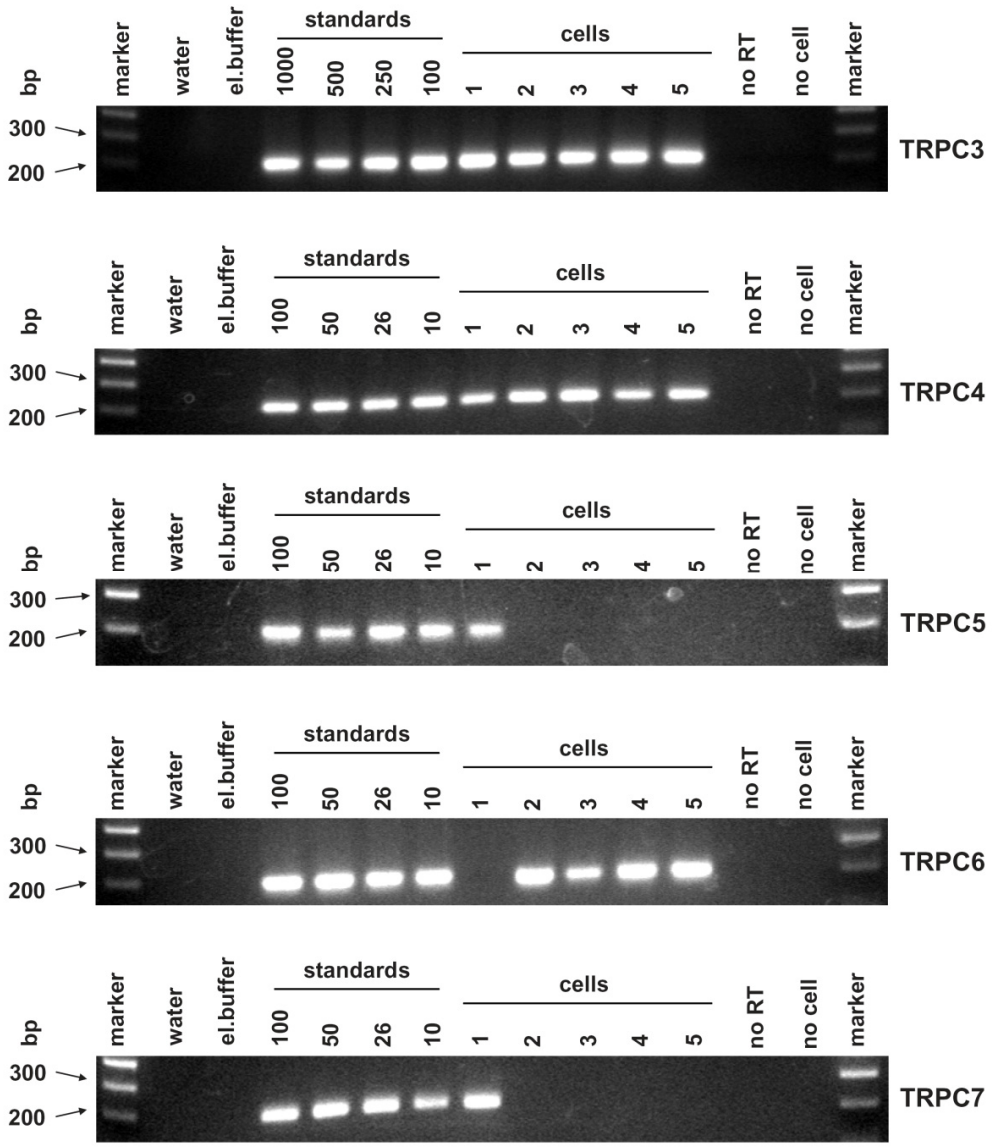

Figure 3.23 Agarose gel electrophoresis of real-time PCR products obtained from the single Purkinje cell material of the TRPC1 knockout animals. Water, elution buffer, the reaction without the reverse transcriptase, and the reaction without the harvested cell were used as negative controls. Positive controls were the TRPC subunit specific standard dilutions. TRPC subunits amplicons are presented with the bands of different sizes; 209bp for TRPC1, 207bp for TRPC3, 217bp for TRPC4, 210bp for TRPC5, 209bp for TRPC6 and 205bp for TRPC7.

Since the TRPC1 animals had different genetic background then the wild type animals previously screened for the TRPC subunit expression, the additional quantification experiments were performed on the control animals of the same genetic background as the TRPC1 knockout animals. No significant differences were noticed between the expression patterns of the TRPC subunits in single Purkinje cells of the two wild type strains. The TRPC3 subunit was, again, most prominently expressed TRPC

subunit with the 273,3±66,7 mean copy number per positive cell. The TRPC1 followed with 11,3±4,7 mean copy number per positive cell. The TRPC4 was present with 8,24±1,9 mean copy per positive cell. The TRPC6 subunit was detected in only one cell (3,1 copy/cell), while TRPC5 and TRPC7 were not detected at all. The histogram in the panel **a** of the Figure 3.24 shows the TRPC subunit expression pattern in single Purkinje neurons of the TRPC1 control animals.

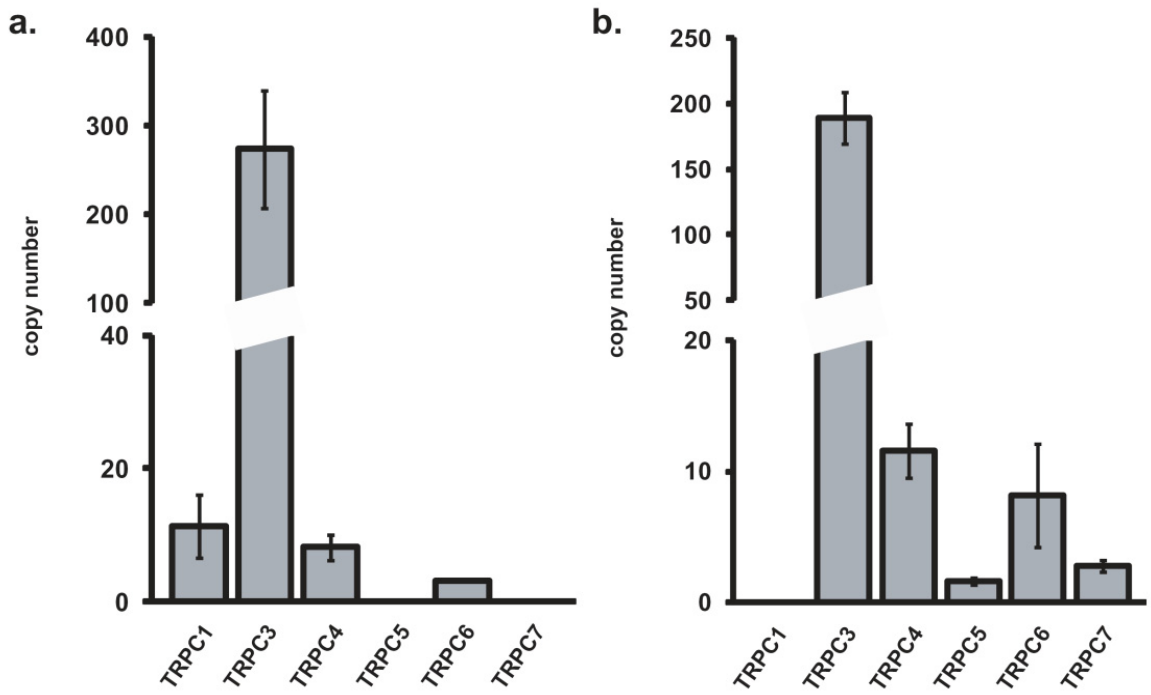

Figure 3.24 Expression levels of TRPC subunits in single Purkinje neurons of the TRPC1 knock-out and control animals. Histogram represents mean copy number ±SEM of TRPC subunits in single Purkinje neurons of **(a)** control animals which were positive for the investigated TRPC subunits (TRPC1 4/8; TRPC3 9/10; TRPC4 5/5; TRPC5 0/5; TRPC6 1/10; TRPC7 0/10) and **(b)** TRPC1 knock-out animals (TRPC3 32/34; TRPC4 17/20; TRPC5 2/24; TRPC6 9/19; TRPC7 9/24)**.**

4. Discussion

This study describes the first quantitative analysis of a complete set of TRPC subunits in one particular neuronal cell type. The TRPC3 subunit was found to be the most abundant TRPC subunit in the Purkinje neurons, followed by the TRPC1 and TRPC4 subunits. The TRPC5, TRPC6 and TRPC7 subunits were found to be present in very low amounts or not at all. The quantification of absolute RNA copy numbers of different TRPC channel subunits was performed by using a fast and highly sensitive method, the quantitative single-cell RT-PCR. In this way, it was possible to quantify and compare the expression patterns of very similar proteins, in this case TRPC channel family members. The quantitative single-cell RT-PCR is a unique technique that allows a quantitative comparison of the expression levels of different genes on the single cell level.

4.1 Qualitative detection of TRPC channels in the brain

TRPC family members have been reported to be widely expressed. Among other tissues, expression of TRPC channels has also been reported in the CNS (Moran et al., 2004). In the first part of this study, the nested RT-PCR was performed on the mouse brain cDNA in order to specifically detect the TRPC subunits. For this, two pairs of specific primers were created for all TRPC subunits, except for the TRPC2 subunit. The TRPC2 subunit was not investigated in this study due to its predominant expression in vomeronasal organ (VNO) and the testis (Vannier et al., 1999; Jungnickel et al., 2001; Kimchi et al., 2007). After the primary nested RT-PCR amplification all TRPC subunits were found to be present in the brain. Additional, secondary nested RT-PCR amplification with the products of the primary reaction as targets, yielded specific amplifications of the TRPC subunits visualized on agarose gels. The identity of the amplicons was additionally confirmed by sequencing. In this way, previously reported expression of TRPC subunits in the brain was confirmed and the primers of the secondary nested PCR run, later used in the quantitative real-time RT-PCR analysis, were shown to be highly specific.

4.2 Quantification procedure, accuracy and limits

The quantitative single-cell RT-PCR procedure consists of many steps, which include the harvest procedure, the reverse transcription of cellular RNA, the consecutive

cDNA purification and the quantification by using high-resolution gene-specific external standard curves (see Figure 1.5). All these steps influence the accuracy of the absolute target transcript quantification and are discussed in the following sections.

4.2.1 Purkinje neurons harvest, RT reactions and cDNA purification

During the past decade, many methods for harvest of RNA material from single cells have been reported. Those include the pioneer methods of consecutive cell cytoplasm harvest after the patch-clamp recordings (Eberwine et al., 1992; Lambolez et al., 1992; Monyer and Lambolez, 1995; Sucher and Deitcher, 1995), laser-based microdissection techniques (Fink et al., 1998) and atomic force microscopes (Osada et al., 2003). The patch-clamp based single cell harvest method has become a powerful tool for the correlation of the functional properties of the cells with their specific gene expression profile. In this study, a novel method based on the aspiration of complete neuronal somata of living neurons was used (Durand et al., 2006). The method consisted of complete neuronal somata aspiration into the wide-opened glass pipette after which the RT reaction was performed. In this case, the complete somatic content was used for the real-time PCR analysis. The neighboring cells were left intact and additional controls on the neuropil samples (tissue that surrounds the cell) indicated minimal risk of the RNA contamination (see Figure 3.17). The neuropil controls were negative for the TRPC1, TRPC4, TRPC5 and TRPC7 subunits. Two of six control runs were positive for TRPC3 with the mean copy number of only 2,23 copies. Four out of six control runs were positive for the TRPC6 subunit, with the mean copy number of 4,9. This number is similar to the mean copy number of TRPC6 in Purkinje neurons (4,3±0,6 copies/cell in the wild type animals and 8±3,5 copies/cell in the TRPC1 knockout mice). Therefore, it is possible that the TRPC6 copy number found in Purkinje cell harvest samples is due to contamination from the neuropil. In contrast, in case of the TRPC3 subunit, the contamination from the neuropil does not influence the mean copy number in Purkinje cells noticeably.

The RT reaction protocol on the single cell material and the cDNA purification protocol, previously established in our group (Durand et al., 2006), were used in this study. The RT reaction protocol used random hexamer primers, which were shown to be consistently more reliable and effective than the poly T-primers. The M-MLV reverse transcriptase was the enzyme of choice since other reverse transcriptases, like Superscript II were not more efficient (Durand et al., 2006). Various studies reported that the direct use of single-cell RT reactions in real-time PCR amplification reactions reduced

the amplification efficiency, presumably by *Taq*-polymerase inhibition (Chandler et al., 1998; Halford, 1999; Pfaffl, 2001; Liss, 2002; Durand et al., 2006). Importantly, this effect of the reverse transcriptase was reported to be particularly significant at lower concentrations of template DNA ($<10^5$ molecules), and was not prevented by heat inactivation of the reaction mix after cDNA synthesis (Chandler et al., 1998). Also, the decrease of the reverse transcriptase amount in order to reduce its inhibitory effect was shown to result in loss or underestimate of low abundance RNAs from single cells, due to the reduction of cDNA synthesis efficiency (Chandler et al., 1998). For all these reasons, efficient purification protocol of cDNA form single cell material by using DNA-binding matrix was used in this study (Durand et al., 2006). In this way, it was possible to purify the single-cell samples without significant cDNA loss.

The reliable efficiency of the experimental procedure was insured by monitoring the abundance of housekeeping gene GAPDH in cerebellar Purkinje cells. All single Purkinje cells tested were positive for GAPDH (20% of harvested single cell material was used). Since it was not necessary to quantify copy numbers of GAPDH in the samples, crossing points were automatically calculated by the LightCycler Software 3.5 (Roche, Mannheim), using the standard derivate maximum method (Rasmussen, 2001). Previous reports showed, and our data confirmed the statement that intrinsic GAPDH transcripts cannot be used as a denominator due to the considerable variation in the expression level between individual cells (Liss et al., 2001; Bustin, 2002; Piper and Holt, 2004; Durand et al., 2006). Therefore, in this study, the absolute copy number of each TRPC transcript per cell was directly calculated using high-resolution gene-specific standard curves. Nevertheless, the GAPDH crossing points of all samples and control reactions were analyzed. Based on these data, the GAPDH expression levels in single cells, in the range of crossing point from 26,5 until 32 (±1,5σ), were considered to be suitable for further analysis and TRPC subunit quantification. In this way, the problem of the false negative results was solved and it was ensured that the cells indeed had comparable RT reaction efficiencies.

4.2.2 High-resolution TRPC specific external standard curves

Since the goal of this study was to compare an absolute copy number of different TRPC subunits in the brain and single Purkinje neurons, comparable PCR efficiencies of the TRPC subunit specific assays were an imperative. No simple way exists to confirm that the efficiency of a PCR assay is constant up to the crossing point. Nevertheless, it is possible to demonstrate that the efficiency of any given sample is constant over a range of

initial template concentrations. This can be achieved by analyzing a dilution series of the sample by plotting the crossing point values over the logarithm of the initial template concentration. The efficiency is considered to be constant over the concentration range studied, if this plot is linear (Rasmussen, 2001). The results obtained from the repetitive real-time PCR amplification of high-resolution TRPC-specific standard curves show linear plots with the efficiency rates close to 2, indicating highly reproducible results and efficient PCR amplifications (see Figures 3.3-3.8).

It has been reported that the number of points in the standard curve can affect reproducibility (Rasmussen 2001). The variance in the standard curve will change with the square root of the number of points in the standard curve. The higher number of points in the standard curve, the less the variance. Additionally, the absolute copy number can also influence reproducibility in the way that samples containing high copy numbers are always more reproducible then samples containing low copy numbers. The main reason for this is the fact that as the number of cycles increases, the effect of any variability in amplification efficiency increases. Therefore, the accurate quantification needs the standard curves that describe the quality of a gene-specific PCR cycle at copy numbers that fit with the expression level in the sample material of interest.

In this study, the range of copy numbers for the high-resolution external standard curves ranged from 10 000 to 4 copies per reaction, and the curves were amplified ten consecutive times to obtain one master standard curve. The variances obtained for the efficiency values of different TRPC specific PCR assays repetitions were low, meaning that high reproducibility was achieved. The primers used for the different TRPC subunits amplification were selected in a way that they give reproducible quantification of minimum four copies (or two double-stranded copies). Reproducibility of 90% positive runs for ten copies and more than 50% positive runs for 4 copies was achieved (Durand et al., 2006). The real-time PCR quantifications in the range of one to four copies, when the random variation due to sampling error (called Poisson error) becomes significant, represent the theoretical limit of quantification (Rasmussen, 2001). Since the TRPC5, TRPC6 and TRPC7 were found to be present in very low amounts in the Purkinje neurons (under 10 copies/cell), copy numbers were estimated by the regression line of the standard curves.

In this study, the quantification of both, standards and unknown samples, was examined, and therefore the efficiency of the PCR assays of both needed to be comparable (see Table 4.1). This means that the external standards and the unknown samples needed to have similar amplification kinetics and slopes of the standard dilution curves (Freeman et al., 1999; Halford, 1999). It has also been reported to be difficult to

extrapolate the absolute number of corresponding RNA transcripts from the number of cDNA molecules determined. This effect is due to the fact that reverse transcriptase efficiency depends on the RNA secondary structure, the specific RNA-protein interactions, RNA integrity and the absolute amount of the individual target RNA (Zhang and Byrne, 1999; Bustin, 2002; Fleige and Pfaffl, 2006). Since the creation of serial dilutions from single cell material was impossible due to the low amounts of RNA obtained in this way, the whole brain and cerebellar total RNA was used to create RNA standards for all TRPC subunits investigated. The results obtained from RNA standards also showed linear plots with efficiency rates close to 2 (see Figures 3.9-3.14). The efficiency of TRPC subunit specific PCR assays obtained in these two procedures, showed comparable efficiency values. In this way it has been confirmed that the high-resolution external standard curves met the requirements for quantification and that they were indeed applicable in the single-cell quantitative analysis.

Table 4.1 Effects of efficiency differences between standards and unknowns
Values were obtained after 25 cycle runs. (adapted from Rasmussen, 2001).

efficiency (standards)	efficiency (unknowns)	efficiency (difference)	fold underestimate
1.90	1.90	0.00	1.00
1.90	1.89	0.01	1.10
1.90	1.80	0.10	3.60
1.90	1.65	0.25	49

4.3 Quantitative detection of TRPC channels in the brain

4.3.1 Expression of TRPC channels in whole brain and cerebellum

One of the first studies that examined the expression levels of the TRPC subunits in total RNA samples of different brain areas and cell lines identified the TRPC1-6 subunits in the cerebellum (Garcia and Schilling, 1997). The TRPC1, TRPC3, TRPC4 and TRPC6 were also identified in mouse brain by using *in situ* hybridization histochemistry

(Otsuka et al., 1998). TaqMan real-time quantitative RT-PCR assays, reported TRPC1-7 in the human tissue, especially in the CNS (Riccio et al., 2002). TRPC1, TRPC3 and TRPC5 were found to be highly expressed in the human cerebellum. By using the same technique, presence of all TRPC channel family members was reported in the brain of three different mice strains, C57BL/10, BALB/c and NOD (Kunert-Keil et al., 2006). The TRPC3 and TRPC4 were found to have the highest expression levels in the cerebellum, followed by the TRPC1 and TRPC5. The TRPC6 and TRPC7 were shown to have very low expression rates in the cerebellar tissue. Recently it has been reported that TRPC3 has a major role in postnatal development of cerebellum in rats (Huang et al., 2007). This group identified the presence of all 7 TRPC subunits in the rat cerebellum by semi-quantitative RT-PCR and immunohistochemistry. The protein expression of TRPC3 was found to be increased in the adults, while the protein expression of TRPC4 and TRPC6 decreased during the postnatal development. Two groups reported TRPC4 and TRPC5 not to be present in the rat cerebellum (Mizuno et al., 1999; Li et al., 2005). On the contrary, our quantitative RT-PCR data confirmed the claim that TRPC4 and TRPC5 are indeed present in the adult cerebellum (Huang et al., 2007). These discrepancies could be due to the age of the animals used.

Recently, the Allen brain atlas (Lein et al., 2007) described a genome-wide, three-dimensional map of gene expression in the adult mouse brain (http://www.brainatlas.org). By using *in situ* hybridization, TRPC1 was found to be widely expressed in the brain, with the highest expression level in the hippocampus. TRPC3 was found to be almost exclusively found in the cerebellum. TRPC6 had very low hybridization signal across the brain, except in the dentate gyrus, where the signal was very high indicating high expression levels of this subunit in this particular brain area. TRPC4, TRPC5 and TRPC7 were found to have low expression levels in the brain.

In the study presented here, quantitative real-time RT-PCR was performed on the 1ng total RNA of the adult mouse whole brain and cerebellum. Data obtained showed that TRPC subunit expression pattern in the cerebellum was profoundly different compared with the expression pattern in the whole brain. While TRPC1 was the dominant subunit in the whole brain, the expression of TRPC3 was as high as the expression of the TRPC1 subunit in the cerebellum. In this way, the predominant TRPC3 subunit expression in the cerebellum reported by previous studies was confirmed (Garcia and Schilling, 1997; Otsuka et al., 1998; Riccio et al., 2002; Kunert-Keil et al., 2006). Also, in comparison to the high expression levels of TRPC1 and TRPC3 in the cerebellar total RNA, TRPC4, TRPC5, TRPC6 and TRPC7 subunits showed very low expression levels which were an

order of magnitude lower than the TRPC1 andTRPC3 expression levels. The high expression of TRPC channel family members, TRPC1 and TRPC3, in the cerebellum indicated a possible dominant expression of these subunits in the different cerebellar cell types.

4.3.2 Expression of TRPC channels in single Purkinje neurons

The first quantitative analysis of TRPC channels in the Purkinje cells was done by *in situ* hybridization experiments (Otsuka et al., 1998). The TRPC3 subunit hybridization signal was reported to be intense in the Purkinje neurons, while the TRPC1 signal was weaker, indicating lower expression levels of TRPC1. The TRPC4 and TRPC6 had no distinct signals in the cerebellar Purkinje cells. Another study demonstrated the predominant expression of TRPC3 in the cerebellar Purkinje cell bodies and dendrites by using immunohistochemistry (Huang et al., 2007). The TRPC4 subunit expression was restricted to granule cells and the TRPC6 expression was found in the interneurons, Purkinje cells and postmitotic granule cells.

Nevertheless, no study up to date presented any quantitative RT-PCR data on the expression levels of TRPC1-7 subunits in the cerebellar Purkinje cells. In this study, quantitative analysis of TRPC channel family members was performed on single Purkinje neurons. Additionally, the TRPC1 knockout animals were tested for possible up- or downregulation of other TRPC subunits. The quantification was performed by using the TRPC gene specific high-resolution external standard curves. Data obtained from the adult wild type mice show that the TRPC3 subunit was the most abundant TRPC subunit in cerebellar Purkinje neurons. The TRPC1 subunit, was next in line with expression levels one order of magnitude lower than the TRPC3. The TRPC4 subunit followed with much lower expression values. More than half of the investigated cells were negative for the TRPC5, TRPC6 and TRPC7, while the positive ones showed expression under 10 copies/cell. Since the primers used for the quantification of TRPC6 were not intron-spanning, some contamination was noticed in the negative controls for this subunit. Additional neuropil controls also reported the presence of the TRPC6 subunit, meaning that TRPC6 in Purkinje cells, could have been indeed detected due to contamination from the genomic material or the neuropil.

It has been reported that the mouse genetic background can also influence the expression levels of TRPC genes in different tissues (Kunert-Keil et al., 2006). This group compared the expression patterns of the TRPC subunits in three different mice strains (C57BL/10, BALB/c and NOD strains). The most data obtained with the C57BL/10 mouse

strain were confirmed with BALB/c and NOD mice. However, cardiac expression levels of TRPC mRNAs showed considerable variability among different mouse strains. In C57BL/10 mice TRPC3 was dominantly expressed in heart muscle whereas TRPC6 was the major isoform in NOD and BALB/c hearts. The TRPC3 expression was also found to be elevated in cerebrum and skeletal muscle of C57BL/10 in comparison to BALB/c and NOD mice, while the TRPC6 expression was lower in the same tissues (Kunert-Keil et al., 2006). This strongly indicated that genetic background considerably influences expression levels of TRPC genes. Since the wild type mice used in the quantitative RT-PCR experiments here, carried mixed genetic background 50:50 (SV129:C57BL/6) and the TRPC1 knockout mice were maintained on a SV129 genetic background, additional control experiments were conducted to investigate the possible effect of the genetic background on the TRPC subunit expression in Purkinje cells. The small differences have been noticed on the absolute copy numbers of different TRPC subunits. All subunits showed lower absolute copy numbers in the animals of pure SV129 genetic background compared to the animals of the mixed genetic background 50:50 (SV129:C57BL/6). Nevertheless, the pattern of the TRPC subunit expression in the two mice strains remained the same, leading to the conclusion that in this case, the genetic background of the investigated mice was not relevant.

In the TRPC1 knockout mice, no compensatory up- or downregulation of other TRPC channel subunits in smooth muscle cells of thoracic aortas and cerebral arteries was detected (Dietrich et al., 2007). In order to investigate the possible up or downregulation in the cerebellar Purkinje neurons, the quantitative single-cell RT-PCR experiments were repeated on the TRPC1 knockout mice. All investigated TRPC subunits showed the small decrease in the absolute copy numbers, while the pattern of TRPC subunit expression remained the same as in the wild type mice. This reduction in the absolute copy numbers of the TRPC subunits can be explained by the different genetic background of the strains used. Therefore, the additional control experiments were performed on the wild type animals of the same genetic background as the TRPC1 knockout animals. No significant change in the absolute copy number of different TRPC subunits was observed. This result indicated no compensatory up- or downregulation of other TRPC channel subunits in the Purkinje neurons of TRPC1 knockout mice.

The quantitative gene expression profiling in the Purkinje cells done in this study was also recently confirmed by *in situ* hybridization experiments presented in the Allen brain atlas. The Figure 4.1 depicts the *in situ* hybridization signals of the TRPC1, TRPC3 and TRPC4 subunits, done in the brain slices of adult mice. The TRPC3 subunit has been reported to have the strongest hybridization signal in the Purkinje cell layer of the

cerebellum, indicating the highest expression levels. The TRPC1 and TRPC4 hybridization signals showed medium and very low levels of expression in the Purkinje cell layer, respectively. The TRPC5, TRPC6 and TRPC7 subunits showed no hybridization signal in the cerebellum.

So far, expression levels of TRPC channel subunits have been described only on the RNA level. However, biological processes are driven by proteins and a question arises if mRNA is a reliable indicator of protein levels in the cell (Hack, 2004). The relationship between mRNA and protein levels is very complex. Since the methods for the global analysis of protein expression have just begun to develop, the mRNA remains an indicator of active protein. The mechanisms which translate mRNA to protein are highly regulated, and it remains unclear how the transcriptome reflects the functional state of the cell, as defined by its protein output (Hack, 2004). Conflicting results have been reported concerning the usage of mRNA abundance as a useful predictor of protein abundance (Futcher et al., 1999; Gygi et al., 1999). Analysis of the transcriptome and proteome comparison of primary haematopoietic stem cells, revealed post-translational regulation of the proteome in stem cell populations (Unwin and Whetton, 2006). Nevertheless, it has also been demonstrated that the mRNA abundance of potassium Kv4.3L and KChip3.1 channels linearly correlated with the A-type potassium channel density in dopaminergic neurons of the substantia nigra (Liss et al., 2001). Unfortunately, in the study described here, this was not investigated due to the limitations of the experimental setup. However, in $TRPC3^{+/-}$ mice, the amplitude of the slow EPSC tended to be smaller than in the wild type mice (Hartmann, personal correspondence). This suggests that the activation of TRPC3 quantitatively correlates with its expression. However, the number of observations was not sufficient to demonstrate statistical significance.

Additionally, a recent study demonstrated the predominant distribution of TRPC3 channel protein in the cerebellar Purkinje cell bodies and dendrites by using immunohistochemistry (Huang et al., 2007). The results obtained for the relative TRPC protein expression levels detected by immunohistochemistry are consistent with the results obtained by quantitative real-time RT-PCR in the study presented here.

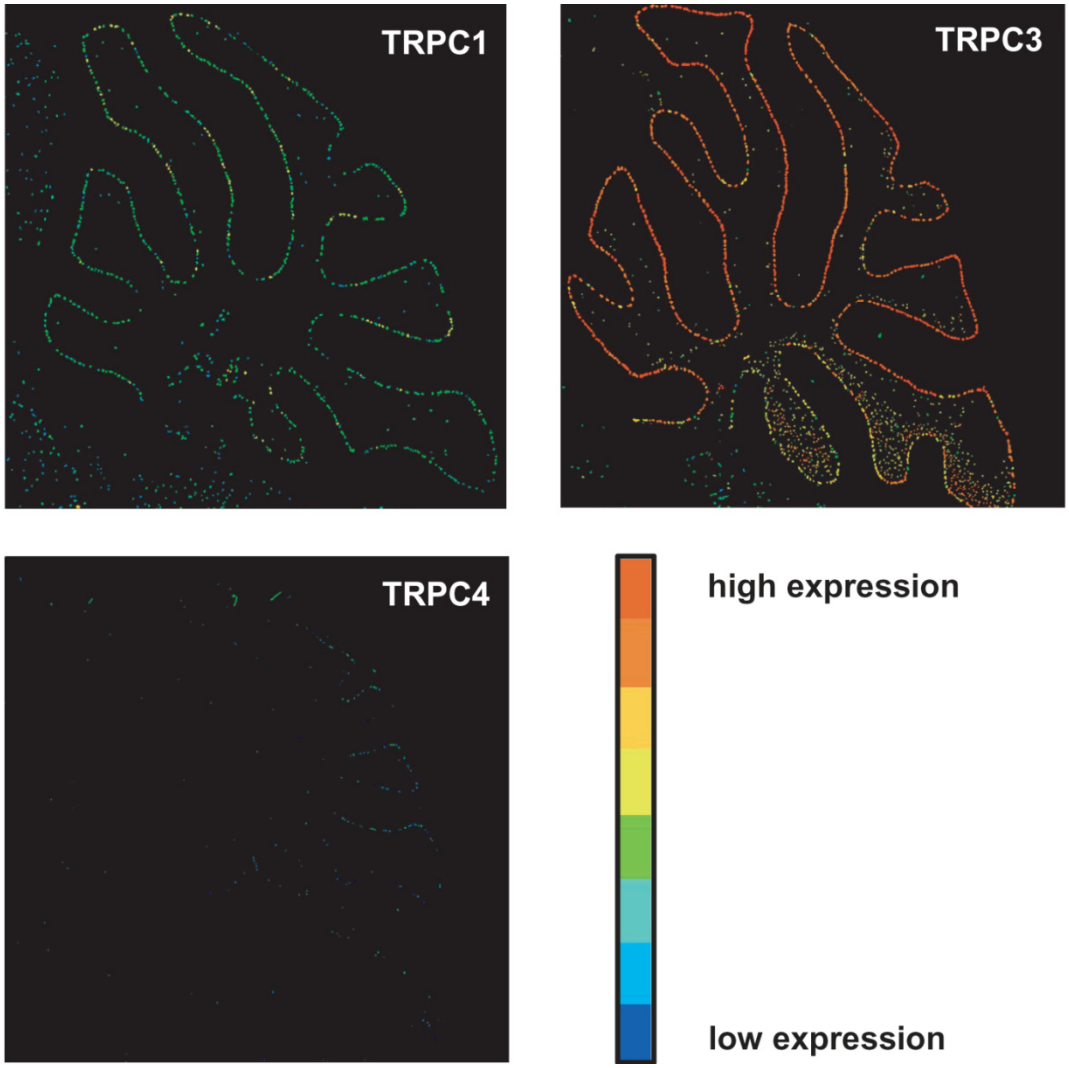

Figure 4.1 Expression pattern of TRPC subunits in the cerebellum.
Detailed explanation is found in the text. The color scale indicates the level of gene expression, with red marking the high expression and blue marking the low expression. (adapted from Allen brain atlas, available on the world wide web : http://www.brainatlas.org).

4.4 Functions of TRPC channels in Purkinje neurons

As a result of the work done in this study, the cerebellar Purkinje neurons have become the first cell type with a known quantitative expression pattern of TRPC channel subunits. The most abundant TRPC subunit in the Purkinje cells was found to be the TRPC3, indicating a possible important role of this subunit in the cerebellum. In the brain, many functional roles for the TRPC3 subunit have been reported. The TRPC3 subunit was proposed to be linked to TrkB, to mediate a slow and sustained BDNF-evoke current

and it has also been implicated in neuronal survival and growth cone guidance (Li et al., 1999; Li et al., 2005; Amaral and Pozzo-Miller, 2007b, a; Jia et al., 2007).

TRPC channels and specifically the TRPC1 channel subunit have been reported to mediate the mGluR1-evoked slow excitatory postsynaptic current (EPSC) in the Purkinje neurons (Kim et al., 2003). The mGluR1-mediated signaling is crucial for cerebellar function and mice lacking this receptor suffer from ataxia and also completely lack cerebellar LTD. Intriguingly, Hartmann et al. (2008, in press) have found the presence of the above mentioned slow EPSC in the TRPC1 knockout mice. Since it has also been reported that the slow EPSC mediated by the TRPC1 in Purkinje cells, in its biophysical characteristics differs from signals evoked by heterlogously expressed TRPC1 channels (Canepari et al., 2004), a role for another TRPC subunit in the mediation of the slow EPSC in Purkinje neurons became a possibility. The slow EPSC could be evoked also in the absence of the TRPC4 and TRPC6 subunits (Hartmann et al., 2008, in press). Data obtained from the quantitative RT-PCR show no or very small expression levels of TRPC5 and TRPC7 subunits in cerebellar Purkinje cells indicating that these subunits most probably have no crucial role in cerebellar Ca^{2+} signaling. As the subunit with highest expression level in the Purkinje neurons, the TRPC3 subunit emerged as a major candidate for the mGluR1-activated ion channel. A mGluR-activated current with voltage-dependent and pharmacological properties reminiscent of TRPC3 and TRPC7 has been reported in striatal cholinergic neurons (Berg et al., 2007). In the same study, it has been shown that the mGluR1 and mGluR5 activate TRPC3 and TRPC7 channels in a heterologous expression system. And indeed, the EPSC that was still present in the animals lacking the TRPC1, TRPC4 and TRPC6 subunits, was abolished in the TRPC3 knockout mice (Hartmann et al., 2008, in press).

Additionally, mice lacking TRPC1, TRPC4 or TRPC6 subunits were reported to show no distinct phenotype (Freichel et al., 2001; Dietrich et al., 2005; Dietrich et al., 2007). In contrast, when motor performance was analyzed on the regular and irregular ladders and the elevated beam (Hartmann et al., 2004), the TRPC3 knockout mice have been found to exhibit distinct disturbances in motor coordination indicating impaired cerebellar function (Hartmann et al., 2008, in press).

Due to very high abundance of the TRPC3 subunits found in the Purkinje cells, it can be speculated that these subunits form homotetramers as it has been previously reported (Putney, 2004). It has also been reported that the TRPC3 subunits could be activated through receptor-coupled PLC when they are highly expressed (Vazquez et al., 2003; Putney, 2004). Additionally, the TRPC3, TRPC6 and TRPC7 have been reported to be activated by DAG and its analog OAG (Hofmann et al., 1999; Lintschinger et al., 2000;

Trebak et al., 2003; Venkatachalam et al., 2003; Liu et al., 2005; Vazquez et al., 2006). Therefore, a novel hypothesis of TRPC subunit role in the cerebellar Purkinje cell can be proposed. The findings in this and other studies indicate that TRPC3 and not TRPC1, mediates the mGluR1 dependent slow EPSC in the single Purkinje neurons by it´s possible activation through DAG (see Figure 4.2).

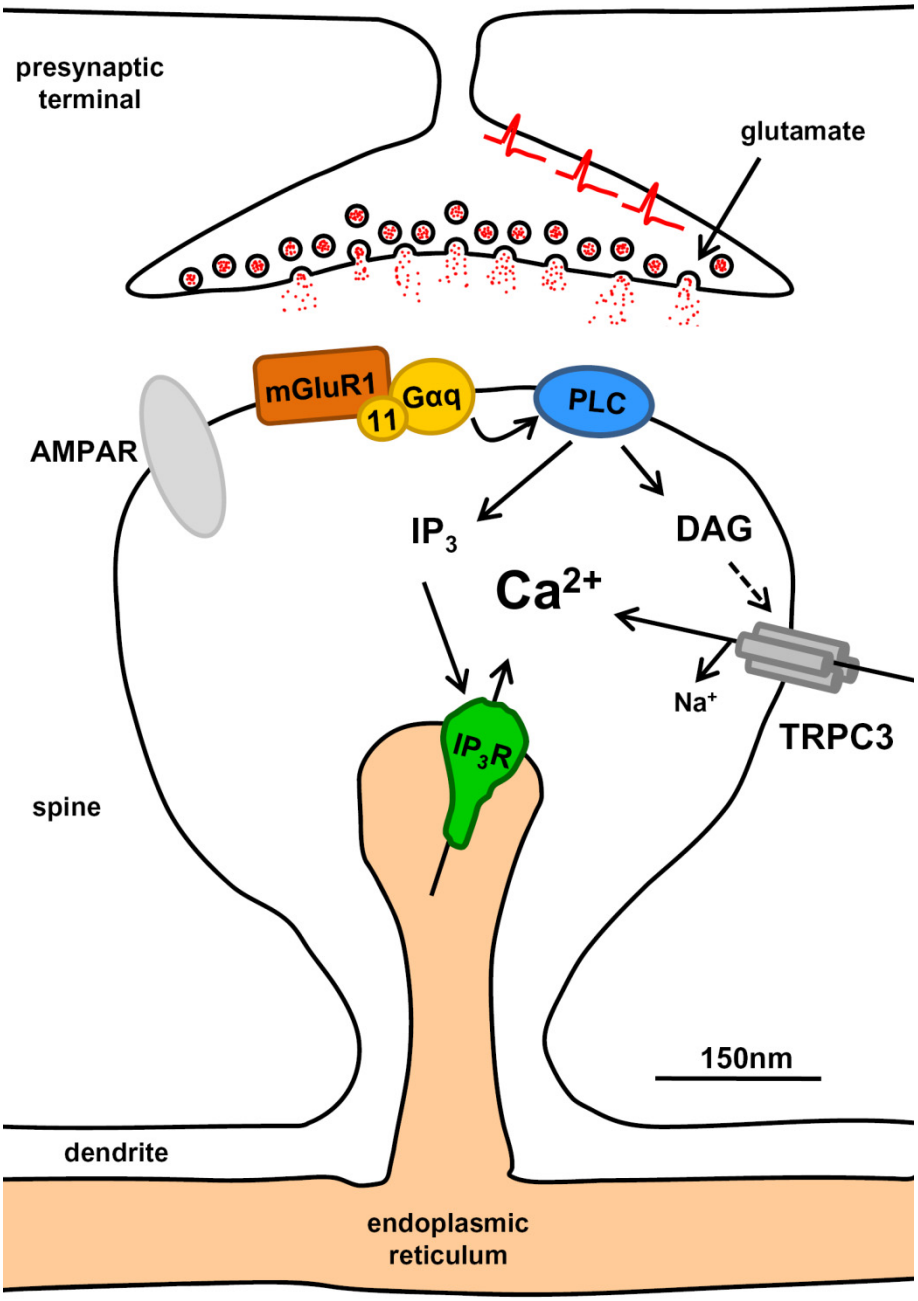

Figure 4.2 Proposed TRPC3 channel activation in Purkinje cell dendrites. Detailed explanation can be found in the text. (adapted from (Hartmann and Konnerth, 2005)).

5. Summary

In this study, the first quantitative analysis of a complete set of TRPC subunits in Purkinje neurons, by using the fast and highly sensitive method of the quantitative single-cell RT-PCR, is described.

All TRPC subunits were found to be expressed in the mouse brain by nested RT-PCR. TRPC2 was not investigated due to its predominant expression only in the vomeronasal organ (VNO) and the testis (Vannier et al., 1999; Jungnickel et al., 2001; Kimchi et al., 2007). The highly specific primer sets were created for each of the TRPC subunits. By using the TRPC gene-specific primers, high-resolution gene-specific standard curves were created for each of the TRPC subunits. This represented the base for the further quantitative analysis of the expression patterns of the TRPC subunits in the mouse brain and single Purkinje neurons. While the TRPC1 was the dominant subunit in the whole brain, the expression of TRPC3 was as high as the expression of the TRPC1 subunit in the cerebellum. In the single Purkinje neurons, the TRPC3 subunit was found to be predominately expressed followed by the TRPC1 and TRPC4 subunits. The TRPC5, TRPC6 and TRPC7 subunits were found to be present in a very low amount or not at all. No up-or downregulation of the TRPC subunits was noticed in the TRPC1 knockout mice.

Based on these results it was possible to assign a physiological function to a TRPC channel in a central neuron. The TRPC channels and specifically the TRPC1 channel subunit have been reported to mediate the mGluR1-evoked slow excitatory postsynaptic current (EPSC) in the Purkinje neurons (Kim et al., 2003). Nevertheless, namely in the TRPC3 knockout mice, the Purkinje cells lack the mGluR1 mediated slow EPSC and the motor coordination is disturbed (Hartmann et al., 2008, in press).

This proves that the quantification of expression levels of genes can be used as a powerful tool in order to design specific physiological experiments.

Publication resulting from this study

J. Hartmann, **E. Dragicevic**, H. Adelsberger, H. Henning, M. Sumser, J. Abramowitz, R. Blum, A. Dietrich, M. Freichel, V. Flockerzi, L. Birnbaumer and A. Konnerth. TRPC3 channels are required for synaptic transmission and motor coordination (in press, Neuron 2008)

6. References

Aiba A, Kano M, Chen C, Stanton ME, Fox GD, Herrup K, Zwingman TA, Tonegawa S (1994) Deficient cerebellar long-term depression and impaired motor learning in mGluR1 mutant mice. Cell 79:377-388.

Amaral MD, Pozzo-Miller L (2007a) BDNF induces calcium elevations associated with IBDNF, a nonselective cationic current mediated by TRPC channels. J Neurophysiol 98:2476-2482.

Amaral MD, Pozzo-Miller L (2007b) TRPC3 channels are necessary for brain-derived neurotrophic factor to activate a nonselective cationic current and to induce dendritic spine formation. J Neurosci 27:5179-5189.

Ambudkar IS (2006) Ca2+ signaling microdomains:platforms for the assembly and regulation of TRPC channels. Trends Pharmacol Sci 27:25-32.

Ambudkar IS, Bandyopadhyay BC, Liu X, Lockwich TP, Paria B, Ong HL (2006) Functional organization of TRPC-Ca2+ channels and regulation of calcium microdomains. Cell Calcium 40:495-504.

Batchelor AM, Knopfel T, Gasparini F, Garthwaite J (1997) Pharmacological characterization of synaptic transmission through mGluRs in rat cerebellar slices. Neuropharmacology 36:401-403.

Beech DJ, Muraki K, Flemming R (2004) Non-selective cationic channels of smooth muscle and the mammalian homologues of Drosophila TRP. J Physiol 559:685-706.

Beech DJ, Xu SZ, McHugh D, Flemming R (2003) TRPC1 store-operated cationic channel subunit. Cell Calcium 33:433-440.

Berg AP, Sen N, Bayliss DA (2007) TrpC3/C7 and Slo2.1 are molecular targets for metabotropic glutamate receptor signaling in rat striatal cholinergic interneurons. J Neurosci 27:8845-8856.

Bird GS, Aziz O, Lievremont JP, Wedel BJ, Trebak M, Vazquez G, Putney JW, Jr. (2004) Mechanisms of phospholipase C-regulated calcium entry. Curr Mol Med 4:291-301.

Bustin SA (2002) Quantification of mRNA using real-time reverse transcription PCR (RT-PCR): trends and problems. J Mol Endocrinol 29:23-39.

Canepari M, Auger C, Ogden D (2004) Ca2+ ion permeability and single-channel properties of the metabotropic slow EPSC of rat Purkinje neurons. J Neurosci 24:3563-3573.

Canepari M, Papageorgiou G, Corrie JE, Watkins C, Ogden D (2001) The conductance underlying the parallel fibre slow EPSP in rat cerebellar Purkinje neurones studied with photolytic release of L-glutamate. J Physiol 533:765-772.

Chandler DP, Wagnon CA, Bolton H, Jr. (1998) Reverse transcriptase (RT) inhibition of PCR at low concentrations of template and its implications for quantitative RT-PCR. Appl Environ Microbiol 64:669-677.

Chow N, Cox C, Callahan LM, Weimer JM, Guo L, Coleman PD (1998) Expression profiles of multiple genes in single neurons of Alzheimer's disease. Proc Natl Acad Sci U S A 95:9620-9625.

Clapham DE (2003) TRP channels as cellular sensors. Nature 426:517-524.

Clapham DE, Runnels LW, Strubing C (2001) The TRP ion channel family. Nat Rev Neurosci 2:387-396.

Clapham DE, Montell C, Schultz G, Julius D (2003) International Union of Pharmacology. XLIII. Compendium of voltage-gated ion channels: transient receptor potential channels. Pharmacol Rev 55:591-596.

Conquet F, Bashir ZI, Davies CH, Daniel H, Ferraguti F, Bordi F, Franz-Bacon K, Reggiani A, Matarese V, Conde F, et al. (1994) Motor deficit and impairment of synaptic plasticity in mice lacking mGluR1. Nature 372:237-243.

Dietrich A, Kalwa H, Storch U, Mederos YSM, Salanova B, Pinkenburg O, Dubrovska G, Essin K, Gollasch M, Birnbaumer L, Gudermann T (2007) Pressure-induced and store-operated cation influx in vascular smooth muscle cells is independent of TRPC1. Pflugers Arch 455:465-477.

Dietrich A, Mederos YSM, Gollasch M, Gross V, Storch U, Dubrovska G, Obst M, Yildirim E, Salanova B, Kalwa H, Essin K, Pinkenburg O, Luft FC, Gudermann T, Birnbaumer L (2005) Increased vascular smooth muscle contractility in TRPC6-/- mice. Mol Cell Biol 25:6980-6989.

Durand GM, Marandi N, Herberger SD, Blum R, Konnerth A (2006) Quantitative single-cell RT-PCR and Ca(2+) imaging in brain slices. Pflugers Arch 451:716-726.

Eberwine J, Yeh H, Miyashiro K, Cao Y, Nair S, Finnell R, Zettel M, Coleman P (1992) Analysis of gene expression in single live neurons. Proc Natl Acad Sci U S A 89:3010-3014.

Fink L, Seeger W, Ermert L, Hanze J, Stahl U, Grimminger F, Kummer W, Bohle RM (1998) Real-time quantitative RT-PCR after laser-assisted cell picking. Nat Med 4:1329-1333.

Fleige S, Pfaffl MW (2006) RNA integrity and the effect on the real-time qRT-PCR performance. Mol Aspects Med 27:126-139.

Freeman WM, Walker SJ, Vrana KE (1999) Quantitative RT-PCR: pitfalls and potential. Biotechniques 26:112-122, 124-115.

Freichel M, Philipp S, Cavalie A, Flockerzi V (2004a) TRPC4 and TRPC4-deficient mice. Novartis Found Symp 258:189-199; discussion 199-203, 263-186.

Freichel M, Schweig U, Stauffenberger S, Freise D, Schorb W, Flockerzi V (1999) Store-operated cation channels in the heart and cells of the cardiovascular system. Cell Physiol Biochem 9:270-283.

Freichel M, Vennekens R, Olausson J, Hoffmann M, Muller C, Stolz S, Scheunemann J, Weissgerber P, Flockerzi V (2004b) Functional role of TRPC proteins in vivo: lessons from TRPC-deficient mouse models. Biochem Biophys Res Commun 322:1352-1358.

Freichel M, Suh SH, Pfeifer A, Schweig U, Trost C, Weissgerber P, Biel M, Philipp S, Freise D, Droogmans G, Hofmann F, Flockerzi V, Nilius B (2001) Lack of an endothelial store-operated Ca2+ current impairs agonist-dependent vasorelaxation in TRP4-/- mice. Nat Cell Biol 3:121-127.

Futcher B, Latter GI, Monardo P, McLaughlin CS, Garrels JI (1999) A sampling of the yeast proteome. Mol Cell Biol 19:7357-7368.

Garcia RL, Schilling WP (1997) Differential expression of mammalian TRP homologues across tissues and cell lines. Biochem Biophys Res Commun 239:279-283.

Geiger JR, Melcher T, Koh DS, Sakmann B, Seeburg PH, Jonas P, Monyer H (1995) Relative abundance of subunit mRNAs determines gating and Ca2+ permeability of AMPA receptors in principal neurons and interneurons in rat CNS. Neuron 15:193-204.

Goel M, Sinkins WG, Schilling WP (2002) Selective association of TRPC channel subunits in rat brain synaptosomes. J Biol Chem 277:48303-48310.

Greka A, Navarro B, Oancea E, Duggan A, Clapham DE (2003) TRPC5 is a regulator of hippocampal neurite length and growth cone morphology. Nat Neurosci 6:837-845.

Gygi SP, Rochon Y, Franza BR, Aebersold R (1999) Correlation between protein and mRNA abundance in yeast. Mol Cell Biol 19:1720-1730.

Hack CJ (2004) Integrated transcriptome and proteome data: the challenges ahead. Brief Funct Genomic Proteomic 3:212-219.
Halford WP (1999) The essential prerequisites for quantitative RT-PCR. Nat Biotechnol 17:835.
Hartmann J, Konnerth A (2005) Determinants of postsynaptic Ca2+ signaling in Purkinje neurons. Cell Calcium 37:459-466.
Hartmann J, Blum R, Kovalchuk Y, Adelsberger H, Kuner R, Durand GM, Miyata M, Kano M, Offermanns S, Konnerth A (2004) Distinct roles of Galpha(q) and Galpha11 for Purkinje cell signaling and motor behavior. J Neurosci 24:5119-5130.
Hirono M, Konishi S, Yoshioka T (1998) Phospholipase C-independent group I metabotropic glutamate receptor-mediated inward current in mouse purkinje cells. Biochem Biophys Res Commun 251:753-758.
Hofmann T, Schaefer M, Schultz G, Gudermann T (2002) Subunit composition of mammalian transient receptor potential channels in living cells. Proc Natl Acad Sci U S A 99:7461-7466.
Hofmann T, Obukhov AG, Schaefer M, Harteneck C, Gudermann T, Schultz G (1999) Direct activation of human TRPC6 and TRPC3 channels by diacylglycerol. Nature 397:259-263.
Huang WC, Young JS, Glitsch MD (2007) Changes in TRPC channel expression during postnatal development of cerebellar neurons. Cell Calcium 42:1-10.
Inoue R, Morita H, Ito Y (2004) Newly emerging Ca2+ entry channel molecules that regulate the vascular tone. Expert Opin Ther Targets 8:321-334.
Inoue R, Okada T, Onoue H, Hara Y, Shimizu S, Naitoh S, Ito Y, Mori Y (2001) The transient receptor potential protein homologue TRP6 is the essential component of vascular alpha(1)-adrenoceptor-activated Ca(2+)-permeable cation channel. Circ Res 88:325-332.
Ito M (2002) Historical review of the significance of the cerebellum and the role of Purkinje cells in motor learning. Ann N Y Acad Sci 978:273-288.
Jia Y, Zhou J, Tai Y, Wang Y (2007) TRPC channels promote cerebellar granule neuron survival. Nat Neurosci 10:559-567.
Jungnickel MK, Marrero H, Birnbaumer L, Lemos JR, Florman HM (2001) Trp2 regulates entry of Ca2+ into mouse sperm triggered by egg ZP3. Nat Cell Biol 3:499-502.
Kim SJ, Kim YS, Yuan JP, Petralia RS, Worley PF, Linden DJ (2003) Activation of the TRPC1 cation channel by metabotropic glutamate receptor mGluR1. Nature 426:285-291.
Kimchi T, Xu J, Dulac C (2007) A functional circuit underlying male sexual behaviour in the female mouse brain. Nature 448:1009-1014.
Knopfel T, Anchisi D, Alojado ME, Tempia F, Strata P (2000) Elevation of intradendritic sodium concentration mediated by synaptic activation of metabotropic glutamate receptors in cerebellar Purkinje cells. Eur J Neurosci 12:2199-2204.
Kunert-Keil C, Bisping F, Kruger J, Brinkmeier H (2006) Tissue-specific expression of TRP channel genes in the mouse and its variation in three different mouse strains. BMC Genomics 7:159.
Lambolez B, Audinat E, Bochet P, Crepel F, Rossier J (1992) AMPA receptor subunits expressed by single Purkinje cells. Neuron 9:247-258.
Lein ES, Hawrylycz MJ, Ao N, Ayres M, Bensinger A, Bernard A, Boe AF, Boguski MS, Brockway KS, Byrnes EJ, Chen L, Chen L, Chen TM, Chin MC, Chong J, Crook BE, Czaplinska A, Dang CN, Datta S, Dee NR, Desaki AL, Desta T, Diep E, Dolbeare TA, Donelan MJ, Dong HW, Dougherty JG, Duncan BJ, Ebbert AJ, Eichele G, Estin LK, Faber C, Facer BA, Fields R, Fischer SR, Fliss TP, Frensley C, Gates SN, Glattfelder KJ, Halverson KR, Hart MR, Hohmann JG, Howell MP, Jeung DP, Johnson RA, Karr PT, Kawal R, Kidney JM, Knapik RH, Kuan CL, Lake JH, Laramee AR, Larsen KD, Lau C, Lemon TA, Liang AJ, Liu Y, Luong LT, Michaels J, Morgan JJ, Morgan RJ, Mortrud MT, Mosqueda NF, Ng LL, Ng R, Orta

GJ, Overly CC, Pak TH, Parry SE, Pathak SD, Pearson OC, Puchalski RB, Riley ZL, Rockett HR, Rowland SA, Royall JJ, Ruiz MJ, Sarno NR, Schaffnit K, Shapovalova NV, Sivisay T, Slaughterbeck CR, Smith SC, Smith KA, Smith BI, Sodt AJ, Stewart NN, Stumpf KR, Sunkin SM, Sutram M, Tam A, Teemer CD, Thaller C, Thompson CL, Varnam LR, Visel A, Whitlock RM, Wohnoutka PE, Wolkey CK, Wong VY, et al. (2007) Genome-wide atlas of gene expression in the adult mouse brain. Nature 445:168-176.

Li HS, Xu XZ, Montell C (1999) Activation of a TRPC3-dependent cation current through the neurotrophin BDNF. Neuron 24:261-273.

Li Y, Jia YC, Cui K, Li N, Zheng ZY, Wang YZ, Yuan XB (2005) Essential role of TRPC channels in the guidance of nerve growth cones by brain-derived neurotrophic factor. Nature.

Liman ER, Innan H (2003) Relaxed selective pressure on an essential component of pheromone transduction in primate evolution. Proc Natl Acad Sci U S A 100:3328-3332.

Linden DJ, Dickinson MH, Smeyne M, Connor JA (1991) A long-term depression of AMPA currents in cultured cerebellar Purkinje neurons. Neuron 7:81-89.

Lintschinger B, Balzer-Geldsetzer M, Baskaran T, Graier WF, Romanin C, Zhu MX, Groschner K (2000) Coassembly of Trp1 and Trp3 proteins generates diacylglycerol- and Ca2+-sensitive cation channels. J Biol Chem 275:27799-27805.

Liss B (2002) Improved quantitative real-time RT-PCR for expression profiling of individual cells. Nucleic Acids Res 30:e89.

Liss B, Franz O, Sewing S, Bruns R, Neuhoff H, Roeper J (2001) Tuning pacemaker frequency of individual dopaminergic neurons by Kv4.3L and KChip3.1 transcription. Embo J 20:5715-5724.

Liu X, Bandyopadhyay BC, Singh BB, Groschner K, Ambudkar IS (2005) Molecular analysis of a store-operated and 2-acetyl-sn-glycerol-sensitive non-selective cation channel. Heteromeric assembly of TRPC1-TRPC3. J Biol Chem 280:21600-21606.

Liu X, Wang W, Singh BB, Lockwich T, Jadlowiec J, O'Connell B, Wellner R, Zhu MX, Ambudkar IS (2000) Trp1, a candidate protein for the store-operated Ca(2+) influx mechanism in salivary gland cells. J Biol Chem 275:3403-3411.

Minke B (1977) Drosophila mutant with a transducer defect. Biophys Struct Mech 3:59-64.

Mizuno N, Kitayama S, Saishin Y, Shimada S, Morita K, Mitsuhata C, Kurihara H, Dohi T (1999) Molecular cloning and characterization of rat trp homologues from brain. Brain Res Mol Brain Res 64:41-51.

Montell C (2005) The TRP superfamily of cation channels. Sci STKE 2005:re3.

Montell C, Jones K, Hafen E, Rubin G (1985) Rescue of the Drosophila phototransduction mutation trp by germline transformation. Science 230:1040-1043.

Montell C, Birnbaumer L, Flockerzi V, Bindels RJ, Bruford EA, Caterina MJ, Clapham DE, Harteneck C, Heller S, Julius D, Kojima I, Mori Y, Penner R, Prawitt D, Scharenberg AM, Schultz G, Shimizu N, Zhu MX (2002) A unified nomenclature for the superfamily of TRP cation channels. Mol Cell 9:229-231.

Monyer H, Lambolez B (1995) Molecular biology and physiology at the single-cell level. Curr Opin Neurobiol 5:382-387.

Moran MM, Xu H, Clapham DE (2004) TRP ion channels in the nervous system. Curr Opin Neurobiol 14:362-369.

Mori Y, Wakamori M, Miyakawa T, Hermosura M, Hara Y, Nishida M, Hirose K, Mizushima A, Kurosaki M, Mori E, Gotoh K, Okada T, Fleig A, Penner R, Iino M, Kurosaki T (2002) Transient receptor potential 1 regulates capacitative Ca(2+) entry and Ca(2+) release from endoplasmic reticulum in B lymphocytes. J Exp Med 195:673-681.

Munsch T, Freichel M, Flockerzi V, Pape HC (2003) Contribution of transient receptor potential channels to the control of GABA release from dendrites. Proc Natl Acad Sci U S A 100:16065-16070.

Okada T, Inoue R, Yamazaki K, Maeda A, Kurosaki T, Yamakuni T, Tanaka I, Shimizu S, Ikenaka K, Imoto K, Mori Y (1999) Molecular and functional characterization of a novel mouse transient receptor potential protein homologue TRP7. Ca(2+)-permeable cation channel that is constitutively activated and enhanced by stimulation of G protein-coupled receptor. J Biol Chem 274:27359-27370.

Osada T, Uehara H, Kim H, Ikai A (2003) mRNA analysis of single living cells. J Nanobiotechnology 1:2.

Otsuka Y, Sakagami H, Owada Y, Kondo H (1998) Differential localization of mRNAs for mammalian trps, presumptive capacitative calcium entry channels, in the adult mouse brain. Tohoku J Exp Med 185:139-146.

Pavenstadt H, Kriz W, Kretzler M (2003) Cell biology of the glomerular podocyte. Physiol Rev 83:253-307.

Pedersen SF, Owsianik G, Nilius B (2005) TRP channels: an overview. Cell Calcium 38:233-252.

Pfaffl MW (2001) A new mathematical model for relative quantification in real-time RT-PCR. Nucleic Acids Res 29:e45.

Piper M, Holt C (2004) RNA translation in axons. Annu Rev Cell Dev Biol 20:505-523.

Poteser M, Graziani A, Rosker C, Eder P, Derler I, Kahr H, Zhu MX, Romanin C, Groschner K (2006) TRPC3 and TRPC4 associate to form a redox-sensitive cation channel. Evidence for expression of native TRPC3-TRPC4 heteromeric channels in endothelial cells. J Biol Chem 281:13588-13595.

Putney JW (2005) Physiological mechanisms of TRPC activation. Pflugers Arch 451:29-34.

Putney JW, Jr. (2004) The enigmatic TRPCs: multifunctional cation channels. Trends Cell Biol 14:282-286.

Putney JW, Jr., Broad LM, Braun FJ, Lievremont JP, Bird GS (2001) Mechanisms of capacitative calcium entry. J Cell Sci 114:2223-2229.

Rasmussen R (2001) Quantification on the LightCycler. In: Meurer S, Wittwer C, Nakawara K (eds) Rapid cycle real-time PCR, methods and applications. Springer-Verlag, Berlin Heidelberg, pp 21–34

Reiser J, Polu KR, Moller CC, Kenlan P, Altintas MM, Wei C, Faul C, Herbert S, Villegas I, Avila-Casado C, McGee M, Sugimoto H, Brown D, Kalluri R, Mundel P, Smith PL, Clapham DE, Pollak MR (2005) TRPC6 is a glomerular slit diaphragm-associated channel required for normal renal function. Nat Genet 37:739-744.

Riccio A, Medhurst AD, Mattei C, Kelsell RE, Calver AR, Randall AD, Benham CD, Pangalos MN (2002) mRNA distribution analysis of human TRPC family in CNS and peripheral tissues. Brain Res Mol Brain Res 109:95-104.

Shim S, Goh EL, Ge S, Sailor K, Yuan JP, Roderick HL, Bootman MD, Worley PF, Song H, Ming GL (2005) XTRPC1-dependent chemotropic guidance of neuronal growth cones. Nat Neurosci 8:730-735.

Singh BB, Zheng C, Liu X, Lockwich T, Liao D, Zhu MX, Birnbaumer L, Ambudkar IS (2001) Trp1-dependent enhancement of salivary gland fluid secretion: role of store-operated calcium entry. Faseb J 15:1652-1654.

Strubing C, Krapivinsky G, Krapivinsky L, Clapham DE (2001) TRPC1 and TRPC5 form a novel cation channel in mammalian brain. Neuron 29:645-655.

Strubing C, Krapivinsky G, Krapivinsky L, Clapham DE (2003) Formation of novel TRPC channels by complex subunit interactions in embryonic brain. J Biol Chem 278:39014-39019.

Sucher NJ, Deitcher DL (1995) PCR and patch-clamp analysis of single neurons. Neuron 14:1095-1100.

Tabata T, Aiba A, Kano M (2002) Extracellular calcium controls the dynamic range of neuronal metabotropic glutamate receptor responses. Mol Cell Neurosci 20:56-68.
Takechi H, Eilers J, Konnerth A (1998) A new class of synaptic response involving calcium release in dendritic spines. Nature 396:757-760.
Tang Y, Tang J, Chen Z, Trost C, Flockerzi V, Li M, Ramesh V, Zhu MX (2000) Association of mammalian trp4 and phospholipase C isozymes with a PDZ domain-containing protein, NHERF. J Biol Chem 275:37559-37564.
Tempia F, Miniaci MC, Anchisi D, Strata P (1998) Postsynaptic current mediated by metabotropic glutamate receptors in cerebellar Purkinje cells. J Neurophysiol 80:520-528.
Tempia F, Alojado ME, Strata P, Knopfel T (2001) Characterization of the mGluR(1)-mediated electrical and calcium signaling in Purkinje cells of mouse cerebellar slices. J Neurophysiol 86:1389-1397.
Trebak M, Vazquez G, Bird GS, Putney JW, Jr. (2003) The TRPC3/6/7 subfamily of cation channels. Cell Calcium 33:451-461.
Tsuzuki K, Lambolez B, Rossier J, Ozawa S (2001) Absolute quantification of AMPA receptor subunit mRNAs in single hippocampal neurons. J Neurochem 77:1650-1659.
Unwin RD, Whetton AD (2006) Systematic proteome and transcriptome analysis of stem cell populations. Cell Cycle 5:1587-1591.
Vannier B, Zhu X, Brown D, Birnbaumer L (1998) The membrane topology of human transient receptor potential 3 as inferred from glycosylation-scanning mutagenesis and epitope immunocytochemistry. J Biol Chem 273:8675-8679.
Vannier B, Peyton M, Boulay G, Brown D, Qin N, Jiang M, Zhu X, Birnbaumer L (1999) Mouse trp2, the homologue of the human trpc2 pseudogene, encodes mTrp2, a store depletion-activated capacitative Ca2+ entry channel. Proc Natl Acad Sci U S A 96:2060-2064.
Vazquez G, Bird GS, Mori Y, Putney JW, Jr. (2006) Native TRPC7 channel activation by an inositol trisphosphate receptor-dependent mechanism. J Biol Chem 281:25250-25258.
Vazquez G, Wedel BJ, Trebak M, St John Bird G, Putney JW, Jr. (2003) Expression level of the canonical transient receptor potential 3 (TRPC3) channel determines its mechanism of activation. J Biol Chem 278:21649-21654.
Vazquez G, Wedel BJ, Aziz O, Trebak M, Putney JW, Jr. (2004) The mammalian TRPC cation channels. Biochim Biophys Acta 1742:21-36.
Venkatachalam K, Montell C (2007) TRP channels. Annu Rev Biochem 76:387-417.
Venkatachalam K, Zheng F, Gill DL (2003) Regulation of canonical transient receptor potential (TRPC) channel function by diacylglycerol and protein kinase C. J Biol Chem 278:29031-29040.
Venkatachalam K, Ma HT, Ford DL, Gill DL (2001) Expression of functional receptor-coupled TRPC3 channels in DT40 triple receptor InsP3 knockout cells. J Biol Chem 276:33980-33985.
Villereal ML (2006) Mechanism and functional significance of TRPC channel multimerization. Semin Cell Dev Biol 17:618-629.
Wang GX, Poo MM (2005) Requirement of TRPC channels in netrin-1-induced chemotropic turning of nerve growth cones. Nature.
Wes PD, Chevesich J, Jeromin A, Rosenberg C, Stetten G, Montell C (1995) TRPC1, a human homolog of a Drosophila store-operated channel. Proc Natl Acad Sci U S A 92:9652-9656.
Winn MP, Conlon PJ, Lynn KL, Farrington MK, Creazzo T, Hawkins AF, Daskalakis N, Kwan SY, Ebersviller S, Burchette JL, Pericak-Vance MA, Howell DN, Vance JM, Rosenberg PB (2005) A mutation in the TRPC6 cation channel causes familial focal segmental glomerulosclerosis. Science 308:1801-1804.

Wu X, Zagranichnaya TK, Gurda GT, Eves EM, Villereal ML (2004) A TRPC1/TRPC3-mediated increase in store-operated calcium entry is required for differentiation of H19-7 hippocampal neuronal cells. J Biol Chem 279:43392-43402.

Xiao B, Tu JC, Worley PF (2000) Homer: a link between neural activity and glutamate receptor function. Curr Opin Neurobiol 10:370-374.

Xu SZ, Muraki K, Zeng F, Li J, Sukumar P, Shah S, Dedman AM, Flemming PK, McHugh D, Naylor J, Cheong A, Bateson AN, Munsch CM, Porter KE, Beech DJ (2006) A sphingosine-1-phosphate-activated calcium channel controlling vascular smooth muscle cell motility. Circ Res 98:1381-1389.

Xu XZ, Li HS, Guggino WB, Montell C (1997) Coassembly of TRP and TRPL produces a distinct store-operated conductance. Cell 89:1155-1164.

Yu Y, Fantozzi I, Remillard CV, Landsberg JW, Kunichika N, Platoshyn O, Tigno DD, Thistlethwaite PA, Rubin LJ, Yuan JX (2004) Enhanced expression of transient receptor potential channels in idiopathic pulmonary arterial hypertension. Proc Natl Acad Sci U S A 101:13861-13866.

Yuan JP, Kiselyov K, Shin DM, Chen J, Shcheynikov N, Kang SH, Dehoff MH, Schwarz MK, Seeburg PH, Muallem S, Worley PF (2003) Homer binds TRPC family channels and is required for gating of TRPC1 by IP3 receptors. Cell 114:777-789.

Zagranichnaya TK, Wu X, Villereal ML (2005) Endogenous TRPC1, TRPC3, and TRPC7 proteins combine to form native store-operated channels in HEK-293 cells. J Biol Chem 280:29559-29569.

Zhang J, Byrne CD (1999) Differential priming of RNA templates during cDNA synthesis markedly affects both accuracy and reproducibility of quantitative competitive reverse-transcriptase PCR. Biochem J 337 (Pt 2):231-241.

Zhu X, Chu PB, Peyton M, Birnbaumer L (1995) Molecular cloning of a widely expressed human homologue for the Drosophila trp gene. FEBS Lett 373:193-198.

Zhu X, Jiang M, Peyton M, Boulay G, Hurst R, Stefani E, Birnbaumer L (1996) trp, a novel mammalian gene family essential for agonist-activated capacitative Ca2+ entry. Cell 85:661-671.

7. Supplemental material

7.1 Chemicals

Chemical	Supplier
2-Mercaptoethanol, min 98%	Sigma-Aldrich
Agarose SERVA, for DNA electrophoresis, research grade	Serva
Agarose, electrophoresis grade	Invitrogen
Agarose, low melting point	Sigma-Aldrich
Ampiciline sodium salt	Merck
Aqua DeltaSelect, Irrigation Solution	DeltaSelect
Boric acid	Fluka Biochemika
Bromphenolblue sodium salt	Carl Roth, GmbH
Calcium chloride dihydrate approx., 99%	Sigma-Aldrich
D-(+)-Glucose, ≥99,5%, cell culture tested	Sigma-Aldrich
Ethanol, ≥ 99,8%, DAB, pure	Carl Roth, GmbH
Ethidiumbromide 1% (10mg/ml)	Carl Roth, GmbH
Ethylendiamintetraacetic acid (EDTA)	Carl Roth, GmbH
Glicerol, anhydrous for synthesis	Merck
Igepal CA-630, for molecular biology	Sigma-Aldrich
Magnesium chloride hexahydrate, ultra	Fluka Biochemika
N´N´-Dimethylformamid	Merck
Nitrogen 5.0	Sauerstoffwerk
Potassium chloride, ≥95,5%, ultra	Fluka Biochemika
Select Agar, qualified for molecular genetics applications	Gibco BRL
Select Peptone 140, qualified for molecular genetics applications	Gibco BRL
Sodium bicarbonate, 99,7-100,3%	Sigma-Aldrich
Sodium chloride, ultra	Fluka Biochemika
Sodium dihydrogen phosphate monohydrate, ultra	Fluka Biochemika
Tris Base	Boeringer Mannheim
Water, molecular biology reagent	Sigma-Aldrich
X-Gal	Sigma-Aldrich
Yeast extract, for incorporation into microbiological culture media	Difco

7.2 Enzymes and buffers

Enzymes and buffers	Supplier
Bovin Serum Albumin (BSA), 100X	New England Biolabs
Eco R1, 20 000u/ml	New England Biolabs
Hind III, 20 000u/ml	New England Biolabs
M-MLV reverse transcriptase, 200u/µl	Promega
M-MLV RT 5X Buffer, containes 10mM DTT	Promega
NEBuffer 2,10X	New England Biolabs
NEBuffer Eco R1,10X	New England Biolabs
Reaktionspuffer S, 10X	PeqLab
RNasin® Plus, RNase inhibitor, 40u/µl	Promega
Taq-DNA-Polymerase, 5u/µl	PeqLab

7.3 Appliances

Appliances	Manufacturer/Supplier
Centrifuge 5415 C	Eppendorf
Mastercycler gradient	Eppendorf
Thermomixer comfort	Eppendorf
Centrifuge 5415 D	Eppendorf
Centrifuge 5804 R	Eppendorf
GeneQuant, RNA/DNA calculator	Pharmacia Biotech
Gel Doc 2000	Bio Rad
Gel Printer P91	Mitsubishi
LightCycler 1.0	Roche
Personal Cycler	Biometra
BlockThermostat TCR 200	Carl Roth GmbH
Puller, model PC-10	Narishige

7.4 Software

Software	Supplier
Adobe Illustrator 10	Adobe
Adobe Photoshop CS2	Adobe
LightCycler 3.5. software	Roche
Microsoft Office	Microsoft
Oligo Primer Analysis Software, Version 6.57	Molecular Biology Insights, Inc.

Acknowledgements

The presented study was performed under the supervision of Prof. Dr. Arthur Konnerth at Friedrich Schiedel Institute for Neuroscience of the Technical University in Munich. The funding for this study was provided by GRK 333 and GRK 1373.

I wish to thank Prof. Dr. Arthur Konnerth for his excellent scientific support, supervision, and the wonderful opportunity to study in Germany.

To Dr. Robert Blum from the Institute of Physiology of the LMU, Munich and Dr. Jana Hartmann of the Institute for Neuroscience, TUM I owe special thank for their enormous help, scientific advice, training and guidance.

I thank all of my colleagues at the Institute for Neuroscience, TUM and the Institute of Physiology, LMU for support and interest in this study. I would specially like to thank Ines Mühlhahn, Dr. Rosa Maria Karl and Dr. Alexandra Lepier for their practical advices. I am also grateful to Erika Held for her wonderful administrative assistance.

I wish to thank all my friends from all around the world for their help, advices and understanding, and for making my life and work in Germany a great pleasure.

Finally yet importantly, I am deeply grateful to the members of my family for their love, support and encouragement. Without them, this work would not have been done.